2012

Motion of Liquid Drops on Surfaces Induced by Vibration: Role of Contact Angle Hysteresis

Srinivas Mettu
Lehigh University

Motion of Liquid Drops on Surfaces Induced by Vibration: Role of Contact Angle Hysteresis

By

Srinivas Mettu

A Dissertation

Presented to the Graduate and Research Committee

of Lehigh University

in Candidacy for the Degree of

Doctor of Philosophy

in

Chemical Engineering

Lehigh University

September 2012

Approved and recommended for acceptance as a dissertation in partial fulfillment of the requirements for the degree of Doctor of Philosophy.

_____ Date

_____

Prof. Manoj K. Chaudhury, Thesis Advisor

_____

Accepted Date

Committee Members:

_____

Prof. Anand Jagota

_____

Prof. James F Gilchrist

_____

Prof. Jeetain Mittal

_____

Prof. Raymond A Pearson

Acknowledgments

I would like to thank my PhD thesis adviser Prof. Manoj K Chaudhury for his excellent guidance throughout my graduate study. I thoroughly enjoyed working under his guidance and got introduced to his way of working with very simple systems to extract rich and profound scientific information. I think this would help me a lot in my research career ahead. I would also like to thank my PhD thesis committee members Prof. Jagota, Prof. Gilchrist, Prof. Pearson and Prof. Mittal for serving on the committee. I express my sincere gratitude to the Dept of Chemical Engineering and Lehigh University for the initial financial support provided to start my graduate study. I acknowledge the financial support given by Dept of Chemistry at Lehigh University in the form of Teaching Assistantship for Physical Chemistry Lab. I thoroughly enjoyed teaching and evaluating the Physical Chemistry lab reports. I acknowledge all other research funding institutions that directly or indirectly provided financial support for my graduate study.

I am very thankful to all my friends at Lehigh whose company provided constant encouragement to steer through stressful graduate study. I specially thank, Shilpi, Raj, Bhumika, Dadda (Anil Mogha), Ashu, Gautam, KK, Gullu and Shruti, Prady and Mamta (Samudra), Rikhi, Dhruti, Suresh, Sid and Arti, Sap, Chitnis, Kaustubh, Hemant, Jeetu, Ali, Katiyar, Shikha, Alapati, Shomo, Tanuj, Sara, JP, Ratna, Shubham, Dhanesh, Arjun, Valli, Vittal and Sahana, Anil and Jyoti, Bitla and Anupama, Ranjan, Shreya and Animesh, Rajini, Ravi, Gattu, Pradeep, Dhimar, Nazer, Shantanu and Shubra, Shweta Naidu, Rushi and Emily, Rekha and Tony, Venky, Amalraj, Deepak Iyer, Bhaskar Kulkarni, Amol, Bewalkar, Amit Mogha, Kajal, Anand, Apratim, Akshaya, Sonam,

dedicated to my parents

Yashodha

and

Siddiramulu

and

my family and friends

Contents

List of Tables

List of Figures

xiii

xx

Abstract

The role played by contact angle hysteresis during the motion of liquid drops on a solid surface is studied in this thesis by experiments as well as theory. We carried out various experiments in order to achieve this goal. In the first experiment, we demonstrated the combined effect of thermal gradient and external periodic vibration on liquid drops motion on a solid surface. The liquid drops that are stationary on thermal energy gradient surface due to the resistive force arising from contact angle hysteresis show drifted motion when subjected to periodic vibration. We showed that the velocity amplification of liquid drops agrees with the resonance frequencies predicted by Rayleigh's equation. We predicted detailed contact line motions of liquid drops using approximate numerical simulations. We also resolved the velocity dependent slipping of contact line observed in experiments by carrying out simulations using recently developed non-linear contact angle hysteresis model. We carried out numerical simulations of 3-D Navier-Stokes equations in order to understand the detailed development of velocity and temperature profile inside the drop.

In the second experiment, we subjected a liquid drop on an inclined surface to an external white noise vibration. Here, we have drawn analogy between a colloidal particle undergoing Brownian motion in presence of a bias and the drop. We focused on the effect of extra dissipation resulting from threshold contact angle hysteresis force that is not present in the classical Brownian motion of colloidal particle. We found that the drift velocity of drop is found to be a non-linear function of strength of noise. Using experiments and theory we showed that the contact angle hysteresis is not eliminated when the drops are moving under the influence of external vibration. We found that

the displacement distribution of liquid drop is non-Gaussian due to the non-linearity in contact angle hysteresis. We showed that the work done by gravity on the drop does not follow conventional fluctuation theorem due to the presence of contact angle hysteresis.

In the third experiment, the contact line of a liquid drop in non-equilibrium state is subjected to external white noise vibration. The overall relaxation behavior of contact line of drop is found to be exponential with significant stick-slip motion. The stick-slip relaxation behavior is attributed to the presence of metastable equilibrium states in the corrugated parabolic free energy of the drop. The displacement distribution of contact line of drop is found to be non-Gaussian following exponential distribution. We used analogy between a harmonically bound colloidal particle undergoing Brownian motion and contact line of liquid drop in order to theoretically analyze the relaxation behavior. The relaxation time of contact line being much higher than Langevin relaxation time emphasizes that the contact angle hysteresis is not eliminated. Using simulations, we showed that the power required to completely eliminate contact angle hysteresis is so high that it is not easily achieved in usual laboratory conditions.

We also studied at role of contact angle hysteresis in symmetry breaking resulting in rectification of drop motion when subjected to external asymmetric periodic vibrations of zero mean. We carried out systematic drop motion experiments on solid surfaces possessing varying amount of contact angle hysteresis. We observed that drops do not show drifted motion on low hysteresis surfaces but move with high velocity on intermediate hysteresis surfaces. We showed that there needs to be some amount of contact angle hysteresis present on the surface to see drifted motion. We developed a non-linear contact angle hysteresis model to explain such a counterintuitive observation.

2

We studied the height fluctuations of micro liter water drops when subjected to white noise vibration in order to indentify multiple resonance frequencies of drop. The power spectrum plots of height fluctuations of water drops show peaks at the corresponding resonance frequencies. Experimentally identified resonance frequencies of drops on Polystyrene surface and fibrillar PDMS surface agree well with the theoretical models available in literature. The contact line of drop is pinned on polystyrene surface where as it shows huge slippage on fibrillar PDMS surface. We also measured the power spectrum of contact line fluctuations of drops. The lower modes are prominent in the power spectrum of contact line whereas higher modes are damped out and weakly noticeable. The prominent lower modes in contact line power spectrum are in agreement with the modes observed in height fluctuations. We found that the slippage of contact line is mode dependent. The lower modes are affected by contact slip more than higher modes. This is explained by taking slip and no slip of contact line into account in the model. We also studied the effect of viscosity on resonance power spectra using water-glycerol mixtures. The heights of resonance peaks are found decrease with viscosity where as the width increased. The shift in resonance frequencies is accounted by surface tension. The variance of interface fluctuations is found to decrease with increase in viscosity.

Chapter 1: Introduction

1.1. Motivation

The main goal of research presented in this thesis is to elucidate the role played by contact angle hysteresis during the motion of liquid drops on a solid surface. A brief introduction of contact angle hysteresis in the context of stationary drop on a solid surface is provided below. Later, we show how this translates into the context of moving drops. The equilibrium contact angle (θ_e) of a stationary liquid drop on an ideally smooth and homogenous solid substrate is given by Young's equation[1] (Figure 1.1)

$$\gamma_{lv} \cos\theta_e = \gamma_{sv} - \gamma_{sl} \tag{1.1}$$

where, $\gamma_{sv}, \gamma_{sl}, \gamma_{lv}$ are the interfacial tensions of solid-vapor, solid-liquid, and liquid-vapor interfaces respectively. However, when the solid substrate is neither ideally smooth nor homogenous or has other imperfections, the drop can subtend a range of contact angles as opposed to a unique contact angle[2-12]. This is observed when a sessile drop on a solid substrate is inflated by adding more liquid to it (Figure. 1.1). The three phase (vapor-liquid-solid) contact line stays pinned to the solid substrate while more liquid is added to the drop, resulting in the increase of the contact angle until a critical angle is reached. This critical angle is called advancing angle (θ_A). Further addition of liquid to the drop results in movement of contact line maintaining the contact angle constant at advancing angle. Similarly, when such a drop is deflated by removing some liquid from it, the contact line recedes after another critical angle is reached. This critical angle is called receding angle (θ_R). Here, the contact angle remains constant at receding angle while the contact line of drop recedes. With $\theta_A > \theta_R$, the difference of the two angles

4

is called the contact angle hysteresis.
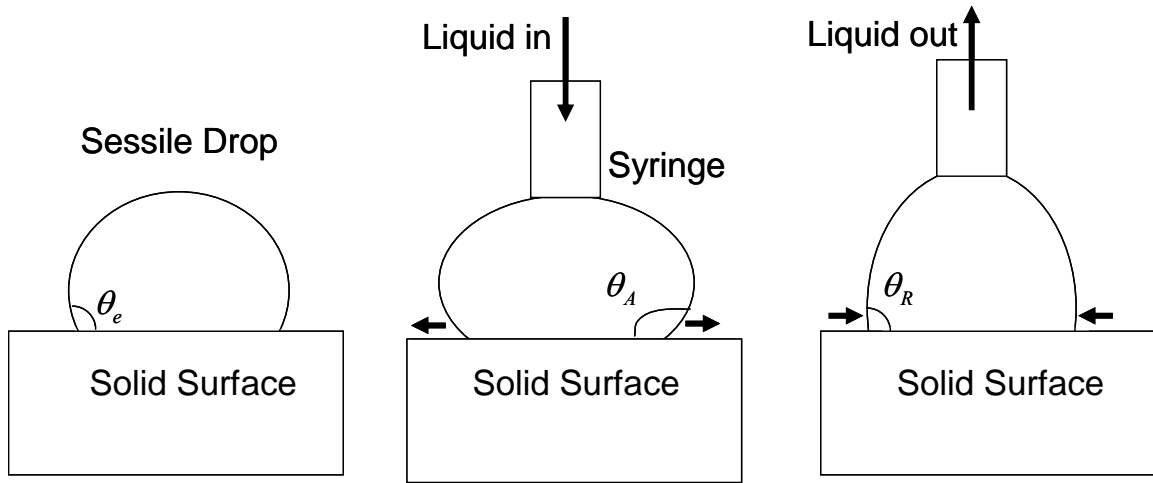
Figure 1.1 (a) Schematic of a sessile water drop on a solid surface (a) stationary drop (b) drop being inflated by pumping more liquid in by a syringe (c) drop being deflated by removing liquid out of the drop. The drop shows three distinct angles in three cases shown above that are called equilibrium (θ_e), advancing (θ_A) and receding (θ_R) angles.

The contact angle hysteresis in the context of moving drops on a solid surface can be explained by a simple experiment. If a small water drop is placed on an inclined solid surface such as a slightly tilted glass plate, the drop gets stuck to it (Figure 1.2). While the gravitational force acting on the drop tries to pull it down, the resistive force due to contact angle hysteresis makes the drop stay pinned to the surface. However, if the glass surface is slowly tilted more, an asymmetry in the shape of the drop develops. Here, contact angle formed by three phase contact line on the bottom side of the drop increases whiles the contact angle on the top side of the drop decreases. The drop slides down on the surface with a constant velocity when the angle of inclination of the glass plate reaches a critical angle. At this critical angle the gravitational force acting on the drop $(mg\sin\theta)$ exceeds the resistance due to contact angle hysteresis $(\gamma_{lv}w(\cos\theta_R - \cos\theta_A))$.

Here, m is the mass of the drop, θ is the tilt angle of the surface to the horizontal and

5

w is the width of the drop. The contact angles formed by the drop at the instant where the drop just starts sliding down the surface define the contact angle hysteresis in this case. The contact angles on bottom and top sides of drop stay at their respective advancing (θ_A) and receding angles (θ_R) while the drop slides down on the surface. Such phenomena can also be observed when water drops get pinned to the windshield of a car or to an inclined glass window of a house when it rains. The water drops get stuck to the windshield or window due to contact angle hysteresis.
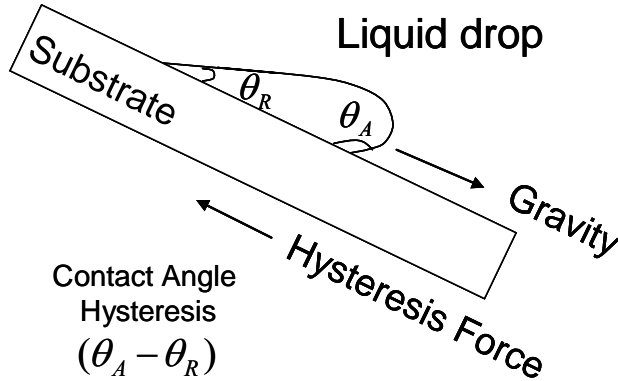
Figure 1.2. Schematic of a water drop sticking to windshield of a car due to contact angle hysteresis. Gravity tries to pull the drop down where as the hysteresis force resists the motion.

Before discussing the fundamental perspective on the origin of contact angle hysteresis, we describe the technological challenges encountered due to the presence of contact angle hysteresis. Pinning of liquid drops on solid surfaces has many practical implications in microfluidic[13-15] and heat transfer devices[16,17]. The drop motion in these devices is generally induced by utilizing forces that arise due to surface energy gradient[18-20] or thermal energy gradient[16,17,21,22]. Among these methods of inducing liquid drops motion on surfaces, Marangoni flow induced by thermal energy gradient has been

6

very popular in the development of microfluidic devices[16,17,23,24,27]. The popularity of thermal Marangoni flow is attributed to two factors, the first being, flexibility in fabricating the devices with programmable patterns as well as magnitudes of thermal gradients. The second being the reversibility of liquid drops motion by simply reversing the directions of gradients. As the liquid drop contacts a thermal gradient surface, the surface tension of liquid on hotter side of drop is smaller than its other part that contacts the cold region. At thermal steady state due to higher tension acting on the molecules of liquid on cold side, the molecules on hot side of drop get pulled towards cold side resulting in surface flow from hot side to cold side. This surface flow in turn causes a bulk flow with thin the drop resulting in liquid drop migration towards the cooler part of the surface. There have been many experimental and theoretical studies that have looked at thermal Marangoni flow of low surface tension organic liquids[16,17,21-30]. These organic liquids have low contact angles $(\theta_e < 90^0)$ and easily move on solid surfaces due to large change in surface tension with small change in temperatures as well as low contact angle hysteresis. However, major problem encountered very often in microfluidic devices is that drops get pinned to underlying solid surface due to resistance from contact angle hysteresis. Such a pinning is observed when dealing with high surface tension liquids such as water $(\theta_e > 90^0)$. Therefore, there is a need to develop a simple technique that moves pinned high surface tension liquids. There have been many studies in that literature that have looked at the ways to move liquid drops that are pinned on solid surfaces[31,32,43-45]. Among the many techniques developed, applying external vibration to drops has been proved very effective. The effect of vibration on pinned liquid drops is studied experimentally by several investigators[33-52]. It is well established that

hysteresis is mitigated by vibration resulting in increasing speed of drop motion. Here we used external vibration to move water drops pinned to a thermal energy gradient surface. A liquid drop stuck to thermal gradient energy surface due to contact angle hysteresis moves rapidly when subjected to periodic vibration.

From the fundamental point of view, a general conclusion arrived in the literature about drops showing contact angle ranging from receding to advancing angle is that roughness and other imperfections of a solid substrate modify the ideal parabolic free energy of drop to a corrugated profile[2-12] (Figure 1.3). As mentioned earlier, if a liquid drop is sitting on an ideally smooth and homogenous solid substrate, the contact angle formed by the drop would be equal to the Young's equilibrium contact angle (θ_e). If such a drop is deformed by applying some external force, the drop would be in non equilibrium state. This is because of the restoring spring force due to the surface tension of liquid (spring constant, $k_s \sim 2\pi\gamma_{lv}$) that tries to bring back the drop to equilibrium state. However, if the solid surface is non ideal, the drop gets stuck to any of the metastable states of the corrugated parabolic potential (Figure 1.3). In order for the drop to escape from metastable state to reach global equilibrium state, some amount of vibrational energy has to be supplied to the drop[5-7]. There have been many theoretical and experimental studies in the literature that have looked at contact angle hysteresis in the context of equilibrium thermodynamics[31-39]. Here, the conclusions that have been drawn about contact angle hysteresis so far are based on equilibrium measurements such as contact angle after the drop has reached steady state. The usual procedure of such experiments is to place a drop on a non ideal surface possessing some amount of contact angle hysteresis and then subject the drop to external vibration of some form until the

8

contact angle of drop reaches a certain equilibrium value. Then, the equilibrium contact angles are used to draw conclusions about contact angle hysteresis. But, it is not clear whether contact angle hysteresis plays any important role while the contact line of drop is in non equilibrium state. This information is very useful in understanding the motion of a drop on a surface assisted by vibrations[41-51]. Here, when a drop is moving on solid surface under the influence of external vibration, it is always in non equilibrium state. Hence, it is not justifiable to use equilibrium information to explain non equilibrium phenomena and draw definitive conclusions.
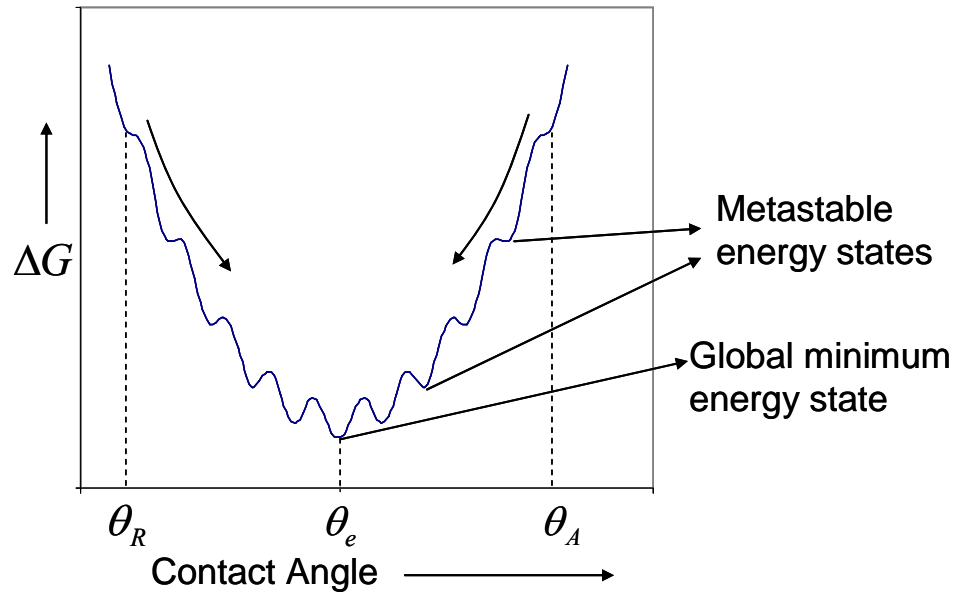
Figure 1.3: Schematic of corrugated free energy (ΔG) profile of drop showing metastable equilibrium states along with global minimum energy state corresponding to equilibrium contact angle (θ_e). The arrows at advancing and receding angles indicate that the restoring spring force arising from surface tension acts to relax the drop to equilibrium.

In order to overcome the short comings of equilibrium methods, we devised novel ways of studying contact angle hysteresis using non equilibrium thermodynamics[54-64]. The non equilibrium methods that include information of fluctuations around the

equilibrium give much more fruitful understanding of the system than equilibrium methods because they provide dynamic information about the system. In order to use recently developed principles of non equilibrium thermodynamics, we have drawn parallels between a drop undergoing external vibrations and a colloidal particle undergoing Brownian motion due to thermal fluctuations in viscous medium. Such a comparison has two fold uses, first being, theory of Brownian motion of colloidal particle is well developed[65-72] which facilitates in the ease of analysis of the current problem. The second being, any anomalies observed in the current system would help in elucidating the role of a contact angle hysteresis that is not present in the Brownian motion of colloidal particle. Another unresolved issue in the context of vibration assisted motion of liquid drop on a solid surface is whether the contact angle hysteresis is completely eliminated or not while the drop is moving[41-49]. There have been several reports[45-47] in the literature that claim without any solid experimental or theoretical proof that when a liquid drop is moving on a solid surface under the influence of external vibrations, the contact angle hysteresis is totally eliminated. Contrary to this argument, our hypothesis is that contact angle hysteresis is not completely eliminated and it plays a crucial role when a liquid drop is moving on the solid surface. We also use the analogy between the Brownian motion of colloidal particle and liquid drop undergoing Brownian-like motion under the influence external white noise vibration to probe this issue.
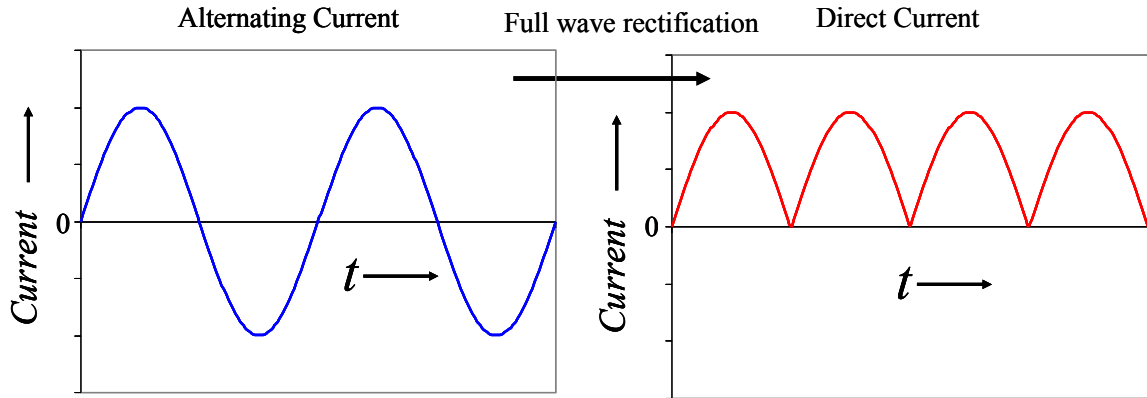
Figure 1.4: Rectification of alternating electrical current to direct current in electrical devices using full wave rectifier.

Another important aspect of contact angle hysteresis that is not resolved so far is its role in rectification of drops when subjected external periodic vibrations[41-49]. It is well known that resistive force arising due to contact angle hysteresis is responsible for pinning of liquid drops on a solid substrate. The liquid drops have to overcome this threshold hysteresis force before they start moving on solid surface. Recently, it is shown that motion of liquid drops that are pinned on a solid substrate possessing gradients of surface energy[41,43] or thermal energy[51] can be induced by external vibration. A common feature in above mentioned methods is that there is an externally applied bias such as surface energy gradient and thermal energy gradient acting on the drop. However, there have been new techniques developed recently where the rectification of liquid drops[43-50,52,53,] or solid object[73-77] is achieved even without any external applied bias acting on the drop. Such a rectified motion of liquid drops in the absence of external bias has received considerable attention due to its significant implications in the potential applications like microfluidics. Before discussing the details of how such a rectification can be achieved, we discuss rectification in electrical and physical terms in order to

11

understand it in a simplistic manner. In electrical devices, rectifiers are used to convert alternating current (AC) that changes direction of electrical current periodically, to direct current (DC) in which electrical current always flows in one direction (Figure 1.4). In physical terms, rectification is achieving motion of an object in a preferred direction when the object is subjected to some form of periodic driving with zero mean. So the rectification analogy can be drawn between electrical current and drop oscillating on a surface. When a liquid drop sitting on a smooth solid surface is subjected to external symmetric periodic vibrations, the drop oscillates back and forth without showing any net motion. However, if the underlying solid surface has asymmetric structure (Figure 1.5), oscillations of drop get rectified resulting in drop translating in one direction[52,53]. Here the asymmetric structure amounts to having slope of grooves on the surface not equal in both the directions. This kind of ratcheting mechanism has been discussed extensively in the literature and it is well understood[52,53,78].
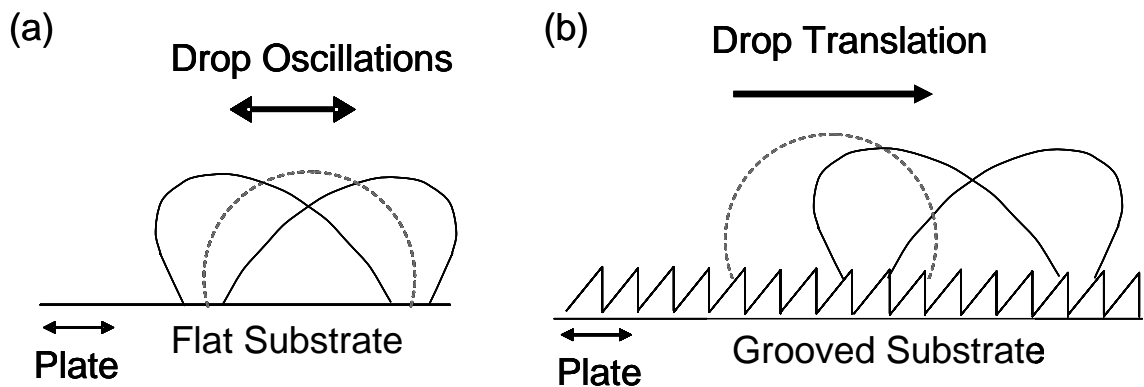
Figure 1.5: (a) Oscillations of liquid drops on a flat solid substrate (b) asymmetrically structured solid substrate. The drop on a flat substrate oscillates back and forth where as drop on asymmetrically structured surface shows translation when subjected to symmetric periodic vibration.
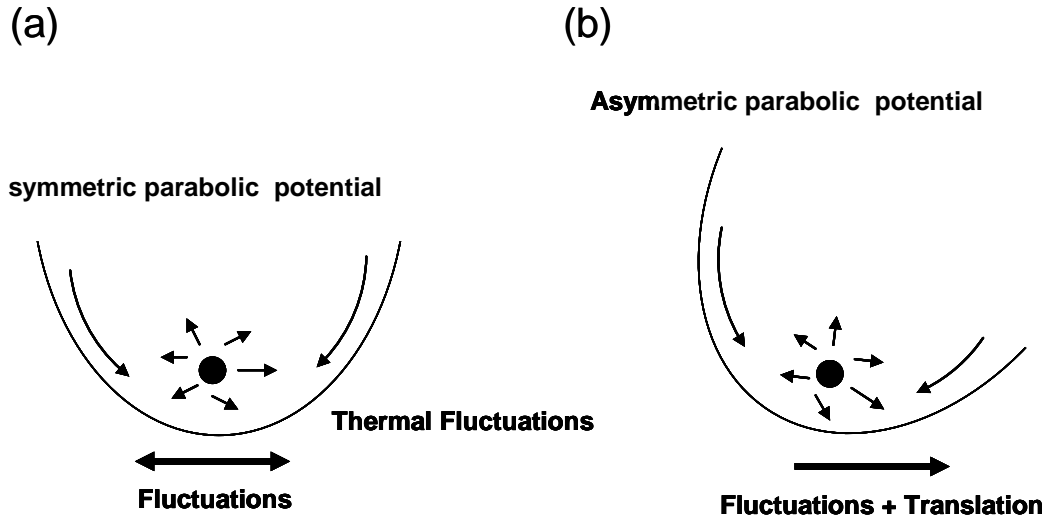
Figure 1.6: (left) A Brownian particle in symmetric parabolic potential fluctuates around the minimum of potential due to thermal fluctuations. (Right) When the parabolic potential is asymmetric the particle shows fluctuations and translation.

Another simple example of such a ratchet is a microscopic particle that is undergoing Brownian motion due to thermal fluctuations in an asymmetric potential instead of classical symmetric parabolic potential[78-83] (Figure 1.6). In case of particle in parabolic potential, position of the particle fluctuates around the minimum of potential where as in asymmetric potential the position of the particle fluctuates as well as showing a net translation in one preferred direction. Therefore, for any time symmetric system to achieve rectification there needs to be a mechanism that breaks the symmetry resulting in motion in one direction. Recently, Daniel et al[43] have achieved such a rectification of liquid drops on a solid surface by subjecting them to asymmetric periodic vibrations of zero mean. The asymmetry in periodic vibration is the result of fast acceleration followed by slow deceleration with zero mean in one period of vibration (Figure 1.7). For a drop to move in presence of an asymmetric vibration of zero mean, some kind of non-linearity is needed in order to break periodic symmetry. The drop would simply exhibit an

13

asymmetrical oscillation without net motion in the absence of symmetry breaking mechanism. There have been several arguments[43-50] in the literature about the origin of non-linearity. However, there has been no definitive answer to question of the origin of non-linearity required for symmetry breaking in this case. Daniel et al[43] have suggested that contact angle hysteresis provides the required non-linearity. Similarly, in a related theoretical analysis, Fleishman et al[74] have also argued that static friction between two contacting solids that is analogous to contact angle hysteresis is responsible symmetry breaking.

However, some other mechanisms for symmetry breaking have been presented recently in the context of drop oscillated with periodic vibration on inclined surface that results in upward motion of drop[45-47]. These authors have suggested that hysteresis would be eliminated with a strong vibration[45]. They have attributed the rectification of drops to non-linear friction force between the drop and substrate. Recently, another interesting possibility of asymmetric shape fluctuation[46,47] resulting in such an upward motion of drops has also been suggested. In wake of such contrasting theories available in the literature about the non-linearity that is responsible for symmetry breaking, there is a need to analyze the phenomena systematically using experiments and theory.

Symmetric Vibration

Asymmetric Vibration
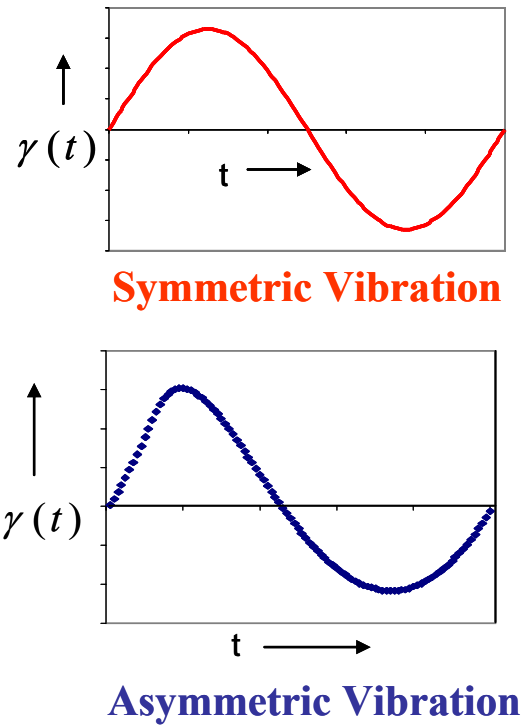
Figure 1.7: Typical profiles of symmetric and asymmetric vibrations.

Another important aspect of drop motion on a solid surface when subjected to external vibration is the resonance frequency of drop since it significantly affects the velocity. It is well known from the works of Kelvin[84], Rayleigh[85], Lamb[86] and Chandrasekhar[87] that the drop exhibits multiple resonance modes that depend on mass, and surface tension of liquid. The viscosity of liquid also has an effect on resonance frequencies which is minor compared the effect of mass and surface tension. The resonant properties of liquid drops are crucial to many technological processes such as crystallization[88,89], spray coating[90], inkjet printing[91], vibration induced motion of drops on surfaces[41-44,92] and microscale heat transfer involving drop wise condensation[19]. Estimation of multiple resonance modes of liquid drops would greatly enhance the design of microfluidic devices. Also, from the fundamental point of view, oscillating bubbles and drops are useful

in estimating surface tension of liquids[93-95]. Hence, we used white noise vibration to identify resonance frequencies of liquid drops.

Here is the outline of thesis. In Chapter 2, we discuss the motion of liquid drops on a thermal gradient surface induced by harmonic vibration. We discuss Brownian like motion of drop a surface induced by white noise vibration in presence of a bias in Chapter 3. In Chapter 4, we discuss relaxation dynamics of contact line of liquid drop when subjected to external white noise vibration. We discuss motion liquid drops on surface induced by asymmetric vibrations in Chapter 5 where as we discuss estimation of resonance frequencies of liquid drops when subjected to white noise vibration in Chapter 6. We conclude the thesis in Chapter 7 along with providing recommendations for future research based on the present thesis.

1.2. References

1. Young,T. *Trans. Roy. Soc* **1803**, *95*, 65.

2. Good, R. J. *J. Am. Chem. Soc*. **1952**, *74*, 5041.

3. Neumann, A. W.; Good, R. J. J. *Colloid Interface Sci.* **1972**, *38*, 341.

4. Eick, J. D.; Good, R. J.; Neumann, A. W. *J. Colloid Interface Sci.* **1975**, *53*, 235.

5. Johnson, R. E.; Dettre, R. H. *Contact Angle, Wettability and Adhesion, Adv. Chem.* Ser. No 43, 112, American Chemical Society, Washington, DC (1964).

6. Johnson, R. E.; Dettre, R. H. *J. Phys. Chem*. **1964**, *68*, 1744.

7. Dettre, R. H.; Johnson, R. E. *J. Phys. Chem*. **1965**, *69*, 1507.

8. Wenzel, R. N. J. *Ind. Eng. Chem.* **1936**, *28*, 988.

9. Cassie, A. B. D.; Baxter, S. *Trans.   Faraday Soc.* **1944**, *40*, 546.

10. Marmur, A. *Adv. Colloid Interface Sci*. **1994**, *50*, 121.

11. Marmur, A. *J. Colloid Interface Sci*. **1994**, *168*, 40.

12. Marmur, A. *J. Colloid Interface Sci*. **1996**, *183*, 351. De Gennes, P.-G. *Rev. Mod. Phys.* **1985**, *57*, 827.

13. Oulette, *J. Ind. Phys.* **2003**,9,14.

14. Wu, H.; Wheeler, A.; Zare, R. N. *Proc. Natl. Acad. Sci. U.S.A.* **2004**, *101*, 12809.

15. Northrup, M. A. *Anal. Chem.* **1998**, *70*, 918.

16. Darhuber, A. A.; Davis, J. M.; Troian, S. M.; Reisner, W. W. *Phys. Fluids* **2003**, *15*, 1295.

17. Darhuber, A. A.; Valentino, J. P.; Davis, J. M.; Troian, S. M.; Wagner, S. *Appl. Phys. Lett*. **2003**, *82*, 657.

18. Chaudhary, M. K.; Whitesides, G. M. *Science* **1992**, *256*, 1539-1541

19. Daniel, S.; Chaudhury, M. K. Chen, J. C. *Science* **2001**, *291*, 633-636.

20. Petrie, R. J.; Bailey, T.; Gorman, C. B.; Genzer, J. *Langmuir* **2004**, *20*, 8993.

21. Brochard, F. *Langmuir* **1989**, *5*, 432-438.

22. Brzoska, J. B.; Brochard-Wyart, F.; Rondelez, F. *Langmuir* **1993**, *9*, 2220.

23. Burns, M. A.; Mastrangelo, C. H.; Sammarco, T. S.; Man, F. P.; Webster, J. R.; Johnson, B. N.; Foerster, B.; Jones, D.; Fields, Y.; Kaiser, A. R.; Burke, D. T. *Proc. Natl. Acad. Sci. USA* **1996**, *93*, 5556.

24. Burns, M. A.; Johnson, B. N.; Brahmasandra, S. N.; Handique, K.; Webster, J.; Krishnan, R. M.; Sammarco, T. S.; Man, P. M.; Jones, D.; Helsinger, D.; Mastrangelo, C. H.; Burke, D. T. *Science* **1998**, *282*,484.

25. Ford, M. L.; Nadim, A.; *Phys. Fluids*   **1994**, *6* ,3183.

26. Smith MK. *J. Fluid Mech* **1995**, *294*, 209.

27. Sammarco T. S.; Burns, M. A. *AIChE. J* **1999**,*45*,350.

28. Yarin, A. L.; Liu, W.; Reneker, D. H. *J. Appl. Phys* **2002**, *91*, 4751.

29. Chen, J. G.; Troin, S. M.; Wagner, S. *J. Appl. Phys* **2005**, 97 , 014906.

30. Pratap, V.; Moumen, N.; Subramanian R. S. *Langmuir,* **2008**, *24*, 5185.

31. Smith, T.; Lindberg, G.; *J. Colloid Interface Sci.* **1978**, *66*, 363.

32. Andrieu, C.; Sykes, C.; Brochard, F. *Langmuir* **1994**, *10*, 2077.

33. Nadkarni, G. D.; Garoff, S. *Langmuir* **1994**, *10*, 1618.

34. Decker, E. L.; Garoff, S. *Langmuir* **1996**, *12*, 2100.

35. Meiron, T.S.; Marmur, A.; Saguy, I.S. *J. Colloid Interface Sci.* **2004**, *274*, 637.

36. Bormashenko, E.; Pogreb, R.; Whyman, G.; Erlich, M. *Langmui* **2007**, *23*, 6501.

37. Bormashenko, E.; Pogreb, R.; Whyman, G.; Erlich, M. *Langmuir* **2007**, *23*, 12217.

38. Bormashenko, E.; Pogreb, R.; Whyman, G.; Bormashenko, E.; Erlich, M. *Appl. Phys. Lett.* **2007**, *90*, 201917.

39. Noblin, X.; Buguin, A.; Brochard, F. *Eur. Phys. J. E* **2004**, *14*, 395.

40. Noblin, X.; Buguin, A.; Brochard, F. *Eur. Phys. J. Special Topics* **2009**, *166*, 7.

41. Daniel, S.; Chaudhury, M. K. *Langmuir* **2002**, *18*, 3404.

42. Daniel, S.; Sircar, S.; Gliem, J.; Chaudhury, M. K. *Langmuir* **2004**, *20*, 4085.

43. Daniel, S.; Chaudhury, M. K.; De Gennes, P.-G. *Langmuir* **2005**, *21*, 4240

44. Dong, L.; Chaudhury, A.; Chaudhury, M. K. *Eur. Phys. J.E* **2006**, *21*, 231.

45. Brunet, P.; Eggers, J.; Deegan, R. D. *Phys. Rev. Lett.* **2007**, *99*, 144501.

46. John, K.; Hanggi, P.; Thiele, U. *Soft Matter* **2009**, *4*, 1183.

47. Thiele, U.; John, K. *Chem. Phys* **2010**, *375*, 578.

48. Benilov, E. S. *Phys. Rev. E* **2010**, *82*, 026320.

49. Benilov, E. S.; Billingham, J.; *J. Fluid. Mech* **2011**, *674*, 93.

50. Noblin, X.; Kofman, R.; Celestini, F. *Phys. Rev. Lett.* **2009**, *102*, 194504.

51. Mettu, S. ; Chaudhury, M. K. *Langmuir* **2008**, *24*, 10833.

52. Sandre, O.; Gorre-Talini, L.; Ajdari, A.; Prost, J.; Silberzan, P. *Phys. Rev. E* **1999**, *60*, 2964.

53. Buguin, A.; Talini, L.; Silberzan, P. *Appl. Phys. A* **2002**, *75*, 207.

54. Gallavotti, G.; Cohen, E.G.D. *Phys. Rev. Lett* **1995**, *74*, 2694.

55. Gallavotti, G.; Cohen, E. G. D. *J. Stat. Phys* **1995**, *80*, 931.

56. Evans, D. J.; Cohen, E.G.D.; Morriss, G.P. *Phys. Rev. Lett* **1993**, *71*, 2401.

57. Evans, D. J.; Searles, D. J. *Phys. Rev. E* **1994**, *50*, 1645.

58. Evans, D. J.; Searles D. J. *Adv. Phys* **2002**, *51*, 1529.

59. van Zon, R.; Cohen, E.G.D. *Phys. Rev. E* **2003**, *67*, 046102.

60. van Zon, R.; Cohen, E.G.D. *Phys. Rev. Lett* **2003**, *91*, 110601.

61. Wang, G.M.; Sevick, E. M.; Mittag, E.; Searles D. J.; Evans, D. J. *Phys. Rev. Lett* **2002**, *89*, 050601.

62. Imparato, A.; Peliti, L.; Pesce, G.; Rusciano, G.; and Sasso, A.; *Phys. Rev. E* **2007**, *76*, 050101.

63. Douarche, F.; Joubaud, S. ; Garnier, N. ; Petrosyan, A.; Ciliberto, S. *Phys. Rev. Lett.* **2006,** *97*,140603.

64. Feitosa, K.; Menon, N. *Phys. Rev. Lett.* **2004**, *92*, 164301.

65. Brown, R. *Phil. Mag.* **1828**, *4*, 161.

66. Sutherland, W. *Phil. Mag*. **1902**, *3*,   161.

67. Einstein, A. *Ann. Phys.* **1905**, 17, 549, Edited by R. Furth, translated by A.D. Cowper, Dover Publications Inc., **1956,** pp. 1-18.

68. Smoluchowski, M. V. *Ann. Phys. (Leipzig).* **1906**, *21*, 756.

69. Langevin, P. *C. R. Acad. Sci. (Paris).* **1908**, *146*, 530. Translated by Lemons, D. S. and Gythiel, A. *Am. J. Phys.* **1997**, 65, 1079.

70. Chandrasekhar, S. *Rev. Mod. Phys.* **1943**, *15*, 1.

71. Chandrasekhar, S. Rev. *Mod. Phys.* **1949**, *21*, 383.

72. Kubo, R. *Rep. Prog. Phys.* **1966**, *29*, 255.

73. Mahadevan, L.; Daniel, S.; Chaudhury, M. K. *Proc. Natl. Acad. Sci. U.S.A.* **2004**, *101*,

74. Fleishman, D.; Asscher, Y.; Urbakh, M. *J. Phys.: Condens. Matter.* **2007**, *19*, 096004.

75. Buguin, A.; Brochard, F.; De Gennes, P.-G. *Eur. Phys. J.E* **2006**, *19*, 31.

76. Eglin, M.; Eriksson M, A.; Carpick R, W. *J. Appl. Phys* **2006**, *88*, 091913.

77. Fleishman, D.; Klafter, J.; Porto, M.; Urbakh, M. *Nano Lett.* **2007**, *7*, 837.

78. Marquet, C. ; Buguin, A.; Talini, L.; Silberzan, P. *Phys. Rev. Lett.* **2002**, *88*, 168301.

79. Gorre, L.; Ioannidis, E.; Silberzan, P. *Eur. Phys. Lett* **1996**, *33*, 267.

80. Ajdari, A.; Prost, J. ; Mukamel, D.; Peliti, L. ; *J. Phys. I France* **1994**, *4*, 1551.

81. Julicher, F .; Ajdari, A.; Prost, J. *Rev. Mod. Phys.* **1997**, *69*, 1269.

82. Kettner, C.; Reimann, P.; Hanggi, P.; Muller, F. *Phys. Rev. E* **2000**, 61, 312.

83. Hanggi, P.; Marchesoni, F. *Rev. Mod. Phys.* **2009**, *81*, 38.

84. Lord Kelvin, Mathematical and Physical Papers **1890**, *3*, 384 ,

85. Lord Rayleigh, The Theory of Sound (Macmillan, **1894**).

86. Lamb, H. Hydrodynamics; Cambridge University Press: Cambridge, U.K., **1932**.

87. Chandrasekhar, S. *Proc. London Math. Soc.* **1959**,*9*,141. Chandrasekhar, S. Hydrodynamic and Hydromagnetic Stability; Clarendon: Oxford, **1961**. Page: 466.

88. Rodot, H.; Bisch, C.; Lasek. A. *Acta Astronaut*. **1979**, *6*, 1083

89. Strani, M.; Sabetta, F, *J. Fluid Mech*. **1984**, *14*, 23.

90. Harris, M. T.; Scott, T. C.; Byers, C. H. U.S. Patent 5,122,360 (June 16, l992).

91. Chaudhary, K.C.; Maxworthy, T. *J. Fluid Mech*., **1980**, *96*, 275.

92. Sekeroglu, K.; Gurkan, U. A.; Demirci, U.; Demirel, M. C. *Appl. Phys. Lett.* **2011**, *99*, 063703.

93. Basaran, O. A.; DePaoli, D. W. *Phys. Fluids* **1994**, *6*, 2923.

94. Wilkes, E. D.; Basaran, O. A. *Phys. Fluids* **1997**, *9*, 1512.

95. Chang, C. H.; Coltharp, K. A.; Park, S. Y.; Franses, E. I. *Colloid Sur A*. **1996**, *114*, 185.

Chapter 2: Motion of liquid drops on a thermal gradient surface induced by vibration

2.1. Introduction:

The motion of a liquid drop on a solid surface has many practical implications in microfluidic devices which are currently being used in applications like drug screening, cell cytometry studies and DNA analysis[1-5]. The liquid drop can be moved on a solid substrate by utilizing physical forces that arise due to surface energy gradient[6-9], vibration of solid surface [10-14] and thermal energy gradient[15-27]. Among these various methods of moving liquid drops on surfaces, Marangoni flow induced by thermal gradients on solid substrates has received considerable attention recently. The flexibility in fabricating devices with programmable patterns as well as magnitudes of thermal gradients, and the reversibility of liquid drops motion by simply reversing the directions of gradients resulted in using this technique in many microfluidic devices[4,5,14,21-23]. As the liquid drop contacts a thermal gradient surface, the surface tension of liquid on hotter side of drop is smaller than its other part that contacts the cold region. When thermal steady state is reached, due to higher tension acting on the molecules of liquid on cold side, the molecules on hot side of drop get pulled towards cold side resulting in surface flow from hot side to cold side. This surface flow in turn causes a bulk flow within the drop resulting in liquid drop migration towards the cooler part of the surface. Thermal or concentration gradients at the interface can be observed in many natural phenomenon like tears of wine effect, suppression of capillary waves in the wake of ship and dance of camphor ball on water surface. The first comprehensive theoretical work on motion of drops on a thermal gradient surface was carried out by Brochard[15] using lubrication

22

approximation in the limit of low contact angles ($\theta_e \ll 90^\circ$). An approximate analytical expression for velocity of drops was obtained by equating the mechanical force exerted by solid on liquid due to surface tension gradient to contact angle hysteresis force with Marangoni contribution included[15]. It was found that the liquid drop has to be larger than a critical size before it moves on a solid surface. This critical size is related to the threshold force due to contact angle hysteresis. The authors suggested a force balance of the following form:

$$mD_c\left(\frac{dS}{dT} + \frac{3}{2}\frac{d\gamma_{lv}}{dT}\right)\frac{dT}{dx} \sim \gamma_{lv}\left(\cos\theta_r - \cos\theta_a\right) \qquad (2.1)$$

where, where m is a numerical constant related to geometrical configuration, D_c is the critical droplet size, dS/dT is gradient of spreading coefficient, $d\gamma_{lv}/dT$ is the gradient of surface tension, dT/dx is the thermal gradient on the surface and $\gamma_{lv}\left(\cos\theta_r - \cos\theta_a\right)$ is the hysteresis force per unit length due to the difference in the advancing and receding contact angles. The gradient in spreading coefficient results in capillary force on the drop that propels it towards higher temperatures regions there by reducing the surface energy. However, the Marangoni flow developed due to the surface tension gradient results in the motion of the drop towards colder regions[15,16]. If the Marangoni effect supersedes the spreading energy effect, the drop would move from the hotter to the cooler side of the drop as observed by Brzoska et al[16]. The hysteresis force due to the difference in the advancing and receding contact angles of the drop on the surface pins the drop resisting its motion. Hence the drop sitting on a solid surface with spatial thermal gradient has to overcome threshold hysteresis force apart from the viscous force before it sets into motion, the direction of which depends on magnitudes of capillary and Marangoni

flows.

Subsequently many theoretical[17,18] and experimental studies[19-23] have been carried out to elucidate thermal Marangoni flow of a drop on a solid surface. Most of the theoretical results available in the literature[17,18] are obtained by using lubrication theory that is applicable only in the limit of low contact angles. Ford and Nadim[17] used lubrication approximation to estimate velocity and pressure profiles inside a drop that is moving under the influence of temperature gradient. They also studied the effect of dynamic boundary condition near the contact line that allows for slip at the contact line on migration velocity of drop. Smith[18] also analyzed thermocapillary migration of a liquid drop using lubrication approximation as carried out by Ford and Nadim[17], however including the effect of contact angle. The relation between contact line speed and apparent contact angle of drop is used to show that it affects drop migration velocity considerably.

In the context of experimental studies on thermocapillary migration of drop, Sammarco and Burns[19] developed a thermocapillary pumping mechanism to pump nano and pico liter volume drops in microfluidic channels. Yarin et al[20] looked at droplets migration on a thin fiber possessing temperature gradient. Darhuber et al[21] carried out experiments to demonstrate that very small drops can also be moved on temperature gradient surfaces. They studied the effect of the magnitude of temperature gradient as well as volume of drop on migration velocity of drops. In subsequent experiments Darhuber et al[22] have also shown that by combining spatially varying chemical, thermal energy gradients liquid drops can be split, turned, moved and mixed on solid surfaces. The importance of these operations in healthcare diagnostics is emphasized. Chen

et al[23] have carried out experiments to analyze the effect of contact angle hysteresis on migration velocity of liquid drops on temperature gradient surfaces. Recently, Pratap et al[24] carried out experiments to determine the effect of drop size, temperature gradient and contact angle hysteresis on velocities of drops moving on temperature gradient surfaces. They also presented theoretical analysis using spherical cap approximation.

Recently, Daniel et al[7] have reported a new type of surface tension induced flow where radial surface tension gradient on hydrophobic surface increases the speed of condensing drops by two to three orders of magnitudes of typical Marangoni flows. Low speeds of Marangoni flows can be enhanced by application external energy to overcome the hysteresis force that suppresses motion. The use of vibration force to overcome hysteresis force has also been demonstrated by Daniel and Chaudhury[12]. The effect of vibration on wetting hysteresis has been studied experimentally by several other investigators[25-29]. It is well known that hysteresis, a retentive force that hinders the drop motion on solid surface, is overcome by vibration resulting in increase in speed of drop motion. Daniel and Chaudhury[12] obtained rectification of motion of drop on a surface through vibration of the solid surface. A liquid drop, placed on an energy gradient surface, which moves at low speeds of 1-2 mm/sec, due to retentive force by hysteresis, moves with increased speeds of 5-10 mm/sec when a periodic force is applied to the drop through vibration of the solid surface. There was significant enhancement in the velocity of drops when the frequency of vibration of surface matches the natural frequency of vibration of drops[13]. This basic observation has been used to demonstrate the potential of vibration induced motion of drops on surface for the application in batch microfluidic processes[14].

25

While considerable amount of work is done on the motion of low surface tension liquid drops with thermal gradient, similar studies do not exist for liquid drops of large contact angles (>90°). When we attempted such an experiment by placing water drops on a silanized silicon wafer with a preformed thermal gradient, no drop movement could be observed. The lack of motion is due to the pinning of the drop by contact angle hysteresis. However, when the stage containing the silicon wafer is vibrated with a periodic noise, drops were found to move towards the regions of lower temperature. The interesting and useful phenomena of motion of drops on horizontal surface subjected to either surface energy gradient or thermal gradient has also motivated us to investigate the effect of vibration force combined with thermal gradient on the motion of drop on a hydrophobic surface.

2. 2. Preparation of hydrocarbon monolayer coated silicon wafer

The solid surface used in the experiments is a silicon wafer coated with self assembled mono layer (SAM) of decyltrichlorosilane that is prepared using vapor deposition method. Here, we briefly describe the vapor deposition method. The hydrocarbon monolayer was prepared by reacting plasma cleaned silicon wafer (Silicon Quest International) to the vapor of decyltrichlorosilane (CH_3-$(CH_2)_9$-$SiCl_3$, Gelest Inc.). Before the vapor deposition is carried out, the silicon wafer is thoroughly cleaned as described below. The silicon wafer was placed in Piranha solution (20% Hydrogen Peroxide and 80% Sulfuric Acid by volume) for 30 min followed by rinsing with copious amount of distilled deionized (DI) water. After drying with ultra purified nitrogen gas (Praxair Inc.), the silicon wafer was treated with oxygen plasma (model PDC-32G; Harrick Plasma) at 0.2Torr for 45s. Before the vapor deposition is carried out,

the silane is degassed for two hours in vacuum to remove any trapped air bubbles. The plasma treated silicon wafer was immediately transferred to a vapor deposition chamber containing decyltrichlorosilane. The vapor deposition of silane onto silicon wafer was carried for 1h in vacuum. After deposition, the silicon wafer was baked in oven for 15 min at 75°C. After cooling the samples to room temperature, it is rinsed with DI water followed by drying with ultra purified nitrogen gas (Praxair Inc.). Advancing and receding angles on this surface are measured by adding and withdrawing liquid to a water drop lying on the surface using a microsyringe in contact. The wetting hysteresis on the silicon wafer thus measured was ~ 7° with advancing and receding angles of 109.7±0.6^o and 102.5±1.6^o respectively.

2. 3. Experimental Setup

Schematic of the experimental setup is shown in Figure 2. 1(a). A brief description of the apparatus used to induce symmetrical sinusoidal vibration of the hydrophobic substrate is given here. The silicon wafer is attached firmly to an aluminum plate that is connected to the stem of a mechanical oscillator (Pasco Scientific, Model SF-9324). The symmetric sinusoidal wave generated by a wave form generator (Agilent, model 33120A) is fed to the oscillator via a power amplifier (Sherwood Model No: RX-4105). The entire setup is placed on a vibration isolation table (Micro-g, TMC) to eliminate the effect of ground vibration. The motion of drops has been recorded by a low speed camera (Sony Model No: DCR-HC65) operating at 30 frames/sec. The test liquid used is distilled, deionized water. Linear temperature gradient on hydrophobic substrate is maintained by circulating hot water and cold water/ethylene glycol mixture through the hollow aluminum plate on which substrate is supported. The hot stream

maintained at a constant temperature is fed to the support on one end where as the cold stream enters and leaves on the other end. The temperature profile on the substrate, measured using a K-type thermocouple, is found to be linear with temperature varying from about 69° C to 12° C over a distance of 7cm as shown in Figure 2. 1 (b).
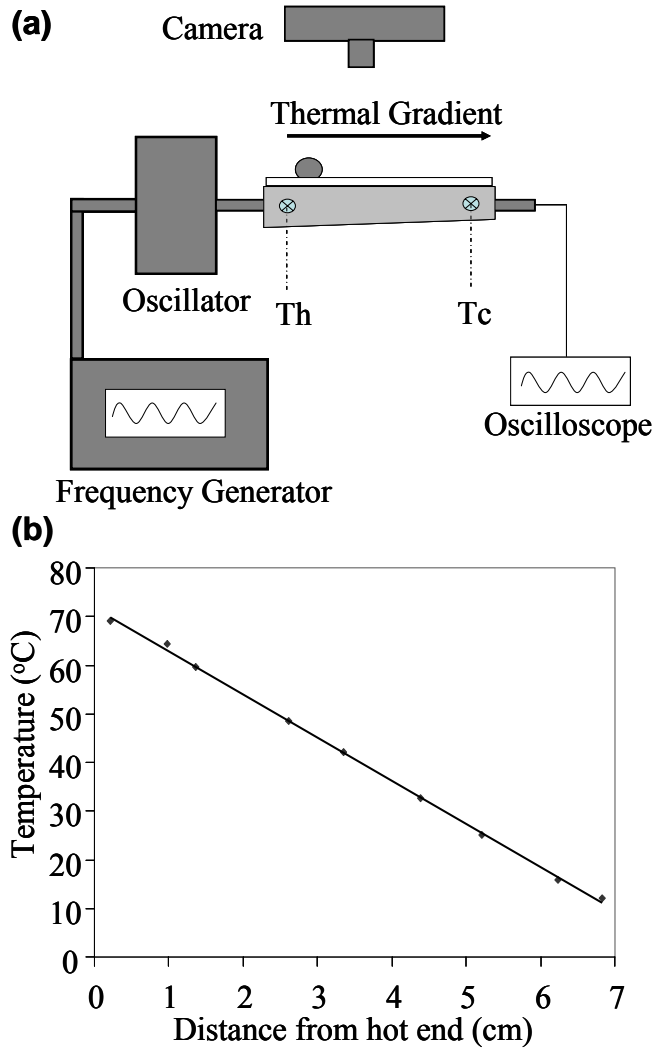
Figure 2. 1. (a) Schematic of the experimental setup. The silicon substrate is firmly attached to an aluminum plate using plastic clips (not shown in the figure) on which linear temperature gradient is maintained by circulation hot (T_h) and cold (T_c) streams of water/ethylene glycol mixtures. The symmetric harmonic wave generated by frequency generator is fed to the aluminum plate through the oscillator via a power amplifier. The acceleration is measured by an oscilloscope and the high speed camera used to analyze the motion of drops. (b) A typical temperature gradient on the surface of silicon wafer is shown.

2. 4. Results and Discussion

The deionized water drops of volume ranging from 1 to $20\mu L$ are deposited on hot side of surface using a microsyringe and their motion towards colder side is recorded from top view using a video camera. Position of center of mass of the drop is tracked using image analysis software to determine velocity. The effect of thermal energy gradient in conjunction with vibration on motion of drop on hydrophobic surface is investigated using three different sets of experiments. The first set of experiments consisted of studying the motion of drop on the surface having only thermal energy gradient with no symmetrical sinusoidal vibration of surface. The second set of experiments was carried out on an isothermal hydrophobic surface subjected to symmetrical sinusoidal vibration. The third set consisted of studying the combined effect thermal energy gradient and symmetrical sinusoidal vibration on the motion of drop.

The liquid drops deposited on the substrate having a linear temperature gradient (dT/dx~0.78^{o}C/mm) have been observed to remain stationary in the absence of vibration of the substrate. As first analyzed by Brochard[15] for the case of thermal energy gradient driven motion of droplet on a solid surface, the relative magnitude of the forces acting on the drop determines the direction of the drop movement. Force due to solid acting on the liquid at contact line drives drop towards region of high temperature in order to lower surface energy. Marangoni flow generated due to imbalance of surface tension forces drives drops towards the region of lower temperature (high surface tension) where as hysteresis force pins drops to solid surface there by hindering the drop motion. The approximate analytical solution for drop velocity obtained by Brochard[15] using lubrication approximation gives the estimate of critical droplet size required to

overcome the hysteresis force as following

$$mD_c\left(\frac{dS}{dT} + \frac{3}{2}\frac{d\gamma_{lv}}{dT}\right)\frac{dT}{dx} \sim \gamma_{lv}\left(\cos\theta_r - \cos\theta_a\right) \qquad (2.2)$$

where m is a numerical constant related to geometrical configuration, D_c is the critical droplet size and S is spreading coefficient. Neglecting the variation of spreading coefficient with temperature ($dS/dT\sim0$) and plugging in the parameters from experimental conditions ($d\gamma_{lv}/dT \sim 0.1818\times10^{-3}$ N/m^{0}C, $dT/dx\sim0.78^o$C/mm, $\gamma_{lv}\left(\cos\theta_r - \cos\theta_a\right)\sim0.008$ N/m) in the above equation gives critical drop size $D_c \sim$90mm. The large critical drop size signifies that the drop has to overcome a huge hysteresis force before it sets into motion which is in agreement with our experimental results. On the other hand, temperature gradient (dT/dx) required for the largest drop (D$\sim$7mm) to overcome hysteresis estimated using (2.2) is approximately 10°C/mm. It is impractical to maintain such a large temperature gradient in reference to heat sensitive microfluidic devices where temperature sensitive reactants (DNA analysis) are present. This restriction necessitates for an alternate way to overcome hysteresis force.

Similarly, liquid drops deposited on isothermal substrate subjected to symmetrical sinusoidal vibration (amplitude 0.12 mm, frequency 100Hz) have been observed to remain stationary in the absence of temperature gradient ($dT/dx\sim0$). As observed by Daniel and Chaudhury[12] for case of vibrating drop on an energy gradient surface, unequal body force experienced by drop during forward and backward pulse, due to asymmetry in surface energy, results in the rectification of drop motion there by resulting in unidirectional motion of drop. Our experiments with vibrating drop on isothermal substrate are similar to Daniel and Chaudhury[12] except that there is no gradient

30

of any transport property which if present would provide the required rectification for unidirectional motion.

However, the drops deposited on thermal energy gradient surface subjected to symmetrical sinusoidal vibration (amplitude 0.12 mm, frequency 100 Hz) have been observed to move towards the regions of low temperatures with enhanced velocities. The hysteresis force hindering the motion of drops is overcome in the presence of vibration. In order to check whether the observed motion is genuine and it is result of vibration combined with temperature gradient, we carried out few other experiments. In the first set of experiments, we tilted the solid substrate slightly (~3 deg) upwards towards the cold side in order to check whether the drops climb upwards. When subjected to vibrations, the drops moved uphill. In the second set of experiments, we switched off the cold bath supply, while the drop was moving under the influence temperature gradient and vibration. As soon as the cold bath is switched off, the temperature on the substrate reaches uniform temperature and the liquid drop that was previously moving towards cold side does not move showing symmetrical oscillations back and forth without any net drift. The drop again moves towards cold side as soon as the cold bath is switched on and the temperature gradient on the surface is resumed. We also checked the effect of contact time of drop on the surface by subjecting the drops that are equilibrated on surface for 10 and 180 sec. Both the drops show drift towards cold side of substrate without any appreciable change (~2%) in velocity. We have used 10 sec as the equilibration time for the drops before vibration is applied in all the experiments. We have varied the mass of liquid drops at given amplitude (0.12 mm) and frequency (100 Hz) of symmetrical sinusoidal vibration to see the effect of resonance modes of liquid drops on drift

velocities.
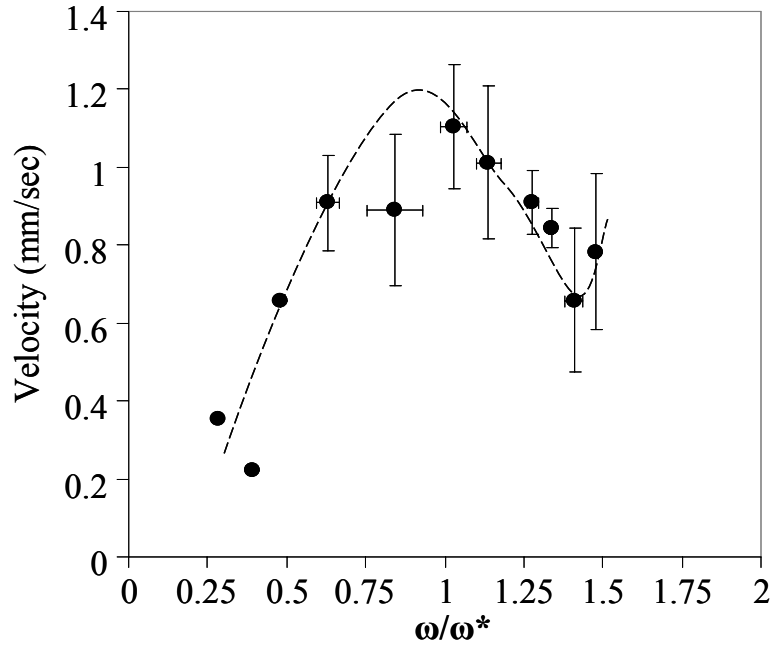
Figure 2.2. Velocity as a function of non-dimensional frequency for water drops of volume ranging from 1 to 20μL. The wetting hysteresis on the silicon wafer was ~ 7° with advancing and receding angles of 109.7±0.6^o and 102.5±1.6^o respectively. The dashed line is provided as a guide to the eye.). Th peak at ω/ω^* ~0.9 corresponds to the natural frequency (ω/ω^*) as predicted by Raleigh's equation (2.3) for the first mode.

2.5. Resonance Modes of Liquid Drops

It is well known that a vibrating spherical liquid drop shows different vibration modes as predicted by Rayleigh's eqaution[30-32]. The resonance frequencies corresponding to such vibration modes can be obtained by equation 2.3 for n = 2(first), 3 (second), 4(third).

$$\frac{\omega}{\omega^*} = \sqrt{\frac{1}{3\pi}n(n-1)(n+2)} \tag{2.3}$$

In order to check whether the velocity amplification corresponds to the resonance frequency of the vibrating drop or not, we plotted velocity of drops as a function of

ratio of forcing frequency (ω) to the natural frequency ($\omega^* = \sqrt{\gamma_{lv}/m}$) of the drop in

Figure. 2.2. Here, γ_{lv} is surface tension of liquid and m is the mass of the drop. When

deformed from its equilibrium position, the drop readily retracts to equilibrium. Such a

restoring force is due to the surface tension of liquid. Here the drop acts like linear spring

with spring constant proportional to the surface tension. For the first mode (n = 2), the

ratio of forcing frequency to the natural frequency (ω/ω^*) as predicted by Rayleigh's

equation[30-32] is ~0.9 where as interpolation from Figure 2.2 shows that the velocity shows

a peak at ω/ω^* ~0.9.
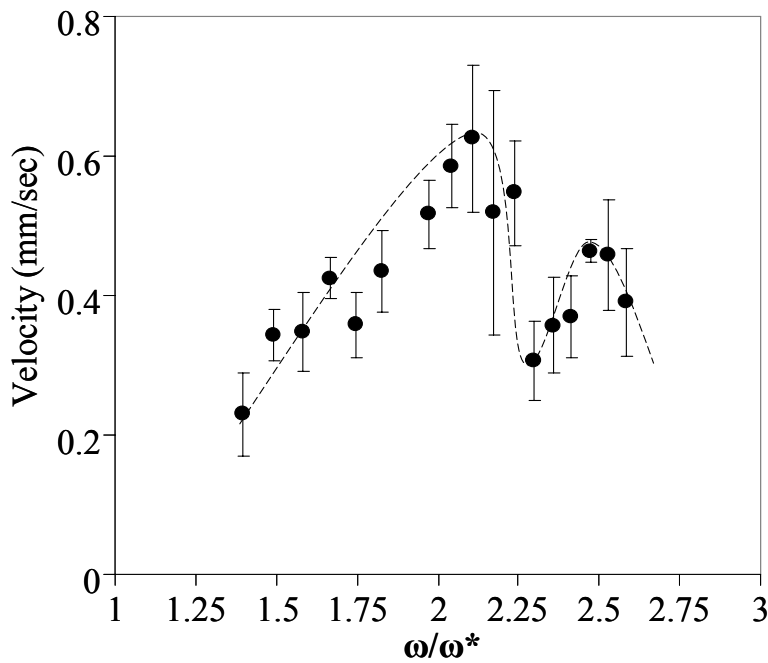
Figure 2.3. Velocity as a function of non-dimensional frequency for water drops of
volume ranging from 14 to 50μL. These experiments are carried out on different

surface coated with the monolayer of decyltrichlorosilane that had slightly different amount of hysteresis. The wetting hysteresis on this surface was ~10° with advancing and receding angles of 108.9±0.5° and 99.6±1.1° respectively. The dashed line is provided as a guide to the eye. Th peaks observed here approximately correspond to the natural frequency (ω/ω^*) as predicted by Raleigh's equation (2.3) for the second and third modes.

We carried out experiments on a different decyltrichlorosilane monolayer coated silicon wafer with a slightly different hysteresis. The wetting hysteresis on this surface was ~10° with advancing and receding angles of 108.9±0.5° and 99.6±1.1° respectively. We plotted drift velocities of drops of volumes ranging from 14 to 50μL obtained on this surface as a function of the ratio of forcing frequency to the natural frequency (ω/ω^*) in Figure 2.3. As observed from figure, even though there is significant scatter in the data, there are two resonance peaks that approximately correspond to second (n = 3) and third (n = 4) Rayleigh modes[30-32] as given by equation 2.3 for n=3 ($\omega/\omega^* \sim 1.78$) and n= 4 ($\omega/\omega^* \sim 2.76$) respectively. Daniel et al[13], Dong and Chaudhury[33] have already identified such a resonance modes of drops oscillating on a solid substrate when subjected to symmetrical sinusoidal vibration. They used a method that is slightly different though both essentially point out the same conclusions.
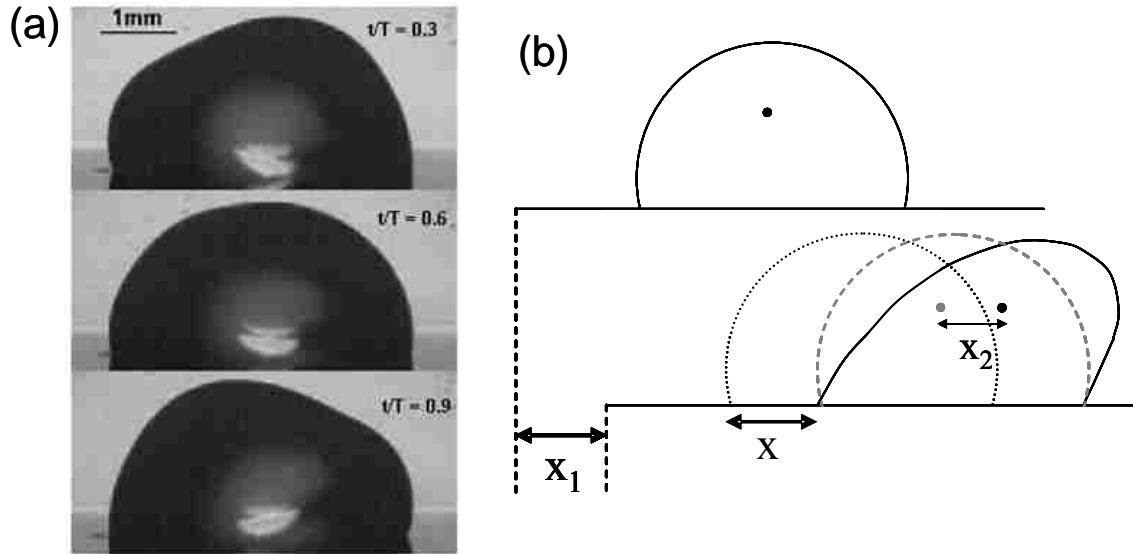
Figure 2.4. (Left) Snapshots of a 30 μL drop on a temperature gradient surface vibrating at a frequency of 100 Hz. (Right) Schematic defining the coordinates in the analysis of drop motion during vibration. The upper diagram shows the static drop profile before the substrate moves. In the lower diagram, the undisturbed profile of the drop is shown by the dashed gray line, and the new profile and position of the drop during vibration are shown by the solid line. x_1 indicates the displacement of the substrate during oscillation with x being the displacement, or slippage, of the contact line, and x_2 is the displacement of the center of mass of the drop.

2.6. Effect of Hysteresis

Here we attempt to understand the above experimental observations using a simple model where the drop is approximated as a harmonic oscillator. The schematic of a drop vibrating on a solid substrate is shown in Figure 2.4. Previously, Daniel et al[14] analyzed the problem of the horizontal oscillation of a drop on a surface due to asymmetric vibration. Daniel et al[14] derived Lagragian equation of motion for the drop ignoring the dissipation due to contact angle hysteresis. They considered the dissipation in the contact line of drop as well as in the bulk of drop. Later Buguin et al[34] have analyzed the asymmetric vibration of solid or liquid drop taking either threshold static

friction or contact angle hysteresis into consideration. A modification of the equations of motion of the drop presented by Daniel et al[14] along with the effect of hysteresis by De Gennes[35] and Buguin et al[34] lead to the following equations of motion for the displacement of plate (x_1), contact line (x) and center of mass of the drop (x_2).

$$\frac{d^2}{dt^2}(x_1 + x + x_2) = -\frac{k_s}{m}x_2 - \frac{1}{\tau_2}\frac{dx_2}{dt} \qquad (2.4)$$

$$\frac{d^2}{dt^2}(x_1 + x + x_2) = \bar{\gamma} - \sigma(V)\Delta - \frac{1}{\tau_1}\frac{dx}{dt} \qquad (2.5)$$

Here, τ_1 and τ_2 are relaxation times (ratio of mass to friction coefficient) due to the relative displacement of the drop with respect to the plate and that due to bulk deformation of the drop respectively. m is the mass of the drop and k_s is its spring constant, which is related to the its resonance frequency and is proportional to the surface tension of liquid. $\bar{\gamma}$ is the ratio of the applied force to mass and Δ is the hysteresis force divided by the mass of the drop. The applied force arises due to the surface tension gradient existing on the drop surface. $\sigma(V)$ is the signum function of velocity. Usually, hysteresis term enters in the equation of motion as a jump discontinuity, $\sigma(V)\Delta$ with $\sigma(V) = V/|V|$ providing the sign of velocity of the contact line. $\sigma(V)$ takes the values of -1, 0, +1 when $V < 0$, $V = 0$, $V > 0$ respectively that ensures that the resistance due to contact angle hysteresis always acts against the motion of contact line of drop. Rearranging of equation 2.4 and 2.5 and ignoring the inertia of contact line of drop results in the following two equations for the center of mass (x_2) and contact line (x) of drop

$$\frac{d^2x_2}{dt^2} + \frac{k_s}{m}x_2 + \frac{1}{\tau_2}\frac{dx_2}{dt} = \gamma(t) \tag{2.6}$$

$$\frac{1}{\tau_1}\frac{dx}{dt} = \bar{\gamma} + \frac{k_s}{m}x_2 + \frac{1}{\tau_2}\frac{dx_2}{dt} - \sigma(V)\Delta \tag{2.7}$$

Here $\gamma(t)$ is the acceleration of the liquid drop due to the sinusoidal vibration of the plate. Ignoring the initial transient due to dissipation in the bulk of the drop, since $\gamma(t)$ is periodic, the solution of equation 2.6 for the center of mass of drop is also periodic. This periodic motion of center of mass combined with bias $(\bar{\gamma})$ due to temperature gradient results in net drift of the contact line of drop towards cold side of the surface. However, the resistance due to contact angle hysteresis $(\sigma(V)\Delta)$ impedes this motion.

Taking average of equation 2.7 over a cycle, as was done by de Gennes[35] and Buguin et al.[34], we obtain the drift velocity of contact line as follows* (*This analysis is by Prof. Chaudhury*):

$$V_{drift} = \bar{\gamma}\tau_1 - \langle\sigma(V)\rangle\Delta\tau_1 \tag{2.8}$$

when there is no external vibration, $\langle\sigma(V)\rangle=+1$. However, in the presence of vibration, $\langle\sigma(V)\rangle<1$. We describe the procedure used to calculate the average value $\langle\sigma\rangle$ using Figure 2.5.
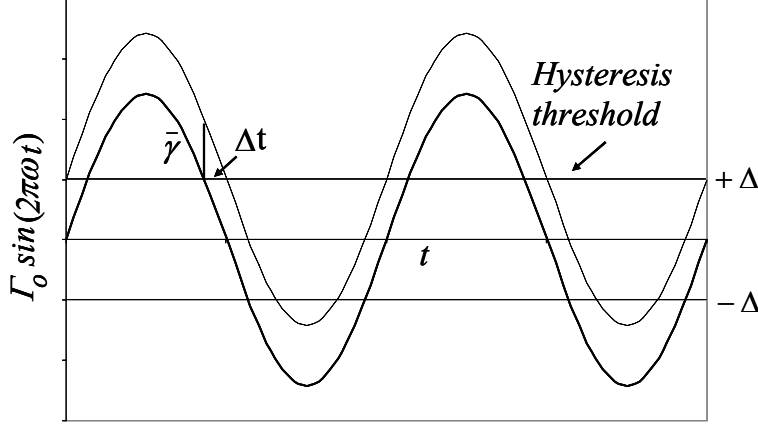
Figure 2.5. A schematic illustrating the estimation of $\langle\sigma\rangle$ for drop vibrating under external bias ($\bar{\gamma}$).

The dark solid curve ($\Gamma = \Gamma_o \sin(2\pi\omega t)$) in Figure 2.5 indicates the acceleration of the drop due to the periodic vibration of the center of mass of a drop in the absence of any external force. The solid lines above and below the X-axis indicate the hysteresis threshold acceleration $(\pm\Delta)$. When subjected to external vibration, contact line of drop gets stuck to the surface if acceleration amplitude of vibration (Γ_0) is less than threshold contact angle hysteresis present on the surface. The contact line shows motion only when $\Gamma_0 > \Delta$. In the absence of any external bias $(\bar{\gamma})$, the drop shows symmetrical oscillations about its stationary position without showing any net drift. However, in presence of external bias, the solid curve shifts upward to the dashed curve, thus creating an asymmetry above the hysteresis threshold. Lower part of the curve is reduced by $2\Delta t$ and the upper curve is expanded by the same amount horizontally. Hence, the signum function $\sigma(V)$ is slightly biased upward. Using simple geometry we find that

$$\frac{\bar{\gamma}}{\Delta t} \approx \frac{d\Gamma}{dt} = 2\pi\Gamma_o\omega\cos(2\pi\omega t) \qquad\qquad (2.9)$$

38

However, at $\Gamma = \Delta$, $\Delta = \Gamma_o \sin(2\pi\omega t)$, this leads to $cos(2\pi\omega t) = \sqrt{1 - \dfrac{\Delta^2}{\Gamma_o^2}}$. Substitution of

this expression in equation 2.9 leads to

$$\Delta t = \frac{\bar{\gamma}}{2\pi\Gamma_o\omega\sqrt{1 - \Delta^2/\Gamma_o^2}} \tag{2.10}$$

The average value of the $\langle\sigma(V)\rangle$ can now be estimated approximately as follows:

$$\langle\sigma\rangle = \left[\left(\frac{1}{\omega} - 2\Delta t - 2t\right)(-1) + \left(\frac{1}{\omega} + 2\Delta t - 2t\right)(+1)\right] / \left(\frac{1}{\omega}\right) \tag{2.11}$$

where t is the amount of time the drop remains pinned on the surface due to hysteresis.

Substituting the expression of Δt from equation 2.10 into equation 2.11 results in

equation 2.12:

$$\langle\sigma\rangle = \left(\frac{2\bar{\gamma}}{\pi\Gamma_o\sqrt{1 - \Delta^2/\Gamma_o^2}}\right) \tag{2.12}$$

Based on a derivation given in Daneil et al[14], we have

$$\Gamma_o = k_2 x_{2o}/m \tag{2.13}$$

where, x_{2o} is the amplitude of the oscillation of the center of mass of the drop. k_2/m is

related to its resonance frequency $2\pi\omega_o$. Substitution of the equations 2.12 and 2.13 in

equation 2.8 now leads to an expression for the drift velocity of the drop as:

$$V_{drift} = \bar{\gamma}\tau_1\left(1 - \frac{\Delta}{2\pi^3\omega_o^2 x_{2o}\sqrt{1 - \left[\dfrac{\Delta}{4\pi^2\omega_o^2 x_{20}}\right]^2}}\right) \tag{2.14}$$

where,

$$x_{2o} = \frac{A\omega^2}{\left[\left(\omega_o^2 - \omega^2\right)^2 + \left(2\pi\tau_1\omega\omega_o^2\right)^2\right]^{0.5}} \qquad (2.15)$$

From equation 2.14, when $\Delta = 0$ velocity of a drop is maximum which is equal to $\bar{\gamma}\tau_1$. However, when $\Delta > 0$, the velocity of drop decreases reaching zero when $\Delta > \bar{\gamma}$. Here, the drop gets stuck to the surface. The velocity of drop can be increased either by increasing the amplitude of vibration (A) or by oscillating the drop close to the resonance frequency of drop that maximizes the oscillation of center of mass (x_{2o}). It can be observed from equation 2.15 that when $\omega \approx \omega_o$, center of mass oscillation (x_{2o}) is maximized. This effect of velocity amplification close to the resonance frequencies of drop is observed in Figures 2.2 and 2.3.
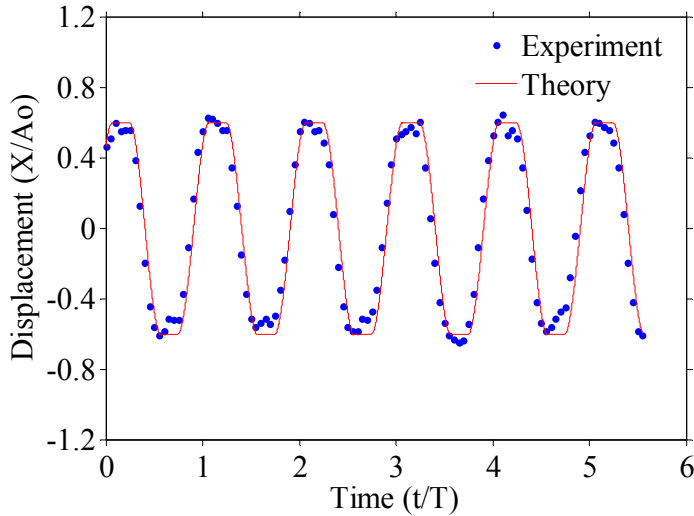
Figure 2.6. Non-dimensional displacement of contact line of a $30\mu L$ water drop relative to the plate at a vibration frequency of 100 Hz on an isothermal surface. Ao is amplitude (0.12 mm) and T is time period (0.01 sec) of oscillation. The acceleration of amplitude of the vibration is 47 m/s². Blue circles represent displacement of contact line relative to the plate. Red line represents the displacement of contact line obtained from numerical simulation of equation 2.7 without $\bar{\gamma}$. Static wetting hysteresis on the surface is ~10° with advancing and receding angles of 108.9 ± 0.5^o and 99.6 ± 1.1^o respectively. Advancing and receding edges were tracked using a high speed camera (Redlake, MotionPro, Model 2000) at 2000 frames/sec. In this case, there is no drift as the contact lines exhibit symmetric stick-slip behavior.

2.7. Periodic Rectification of Drop

In order to better understand the periodic rectification resulting from vibration and thermal gradient, we have recorded a high speed video (2000 frames/sec) of a $30\mu L$ water drop on an isothermal and a temperature gradient surface subjected to symmetric sinusoidal vibration. We have tracked the detailed contact line motion using image analysis software MIDAS. We have also carried out numerical simulations to predict the contact line motion observed in the experiments.

Here we briefly describe the procedure used to predict contact line motion based on the theory presented in section 2.6. We tracked the motion of centre of mass of the drop from experimental data and fitted it with a sine curve, which is then substituted in equation 2.7. The relaxation time ($\tau_1 = 0.02$ sec) and hysteresis threshold acceleration ($\Delta = 3.3$ m/sec^2) that are required in equation 2.7 are approximate values. We used the fact that $V_{drift} = \bar{\gamma}\tau_1$ (0.0018 m/sec) in the absence of hysteresis to eliminate $\bar{\gamma}\tau_1$ from

equation 2.7. The term $\dfrac{1}{\tau_2}\dfrac{dx_2}{dt}$ in equation 2.7 represents dissipation in the bulk of the drop due to the motion of centre of mass. The contribution of this dissipation in bulk of the drop to motion of contact line is to introduce a phase shift between oscillations of the plate and contact line. We needed to use a phase shift of 52 deg to account for the above dissipation. Another adjustable parameter in the simulations is the spring constant k_s, which has been varied till a good match between contact line motion in simulations and the experiments is obtained. The spring constant (k_s) used in the simulations is 2.0 N/m. The drift velocity, as calculated from equation 2.7, is then integrated to obtain the

displacement of contact line as a function of time. The red solid lines in Figures 2.6 and 2.7 show the motion of the contact line motion as obtained from the procedure described above. For the case of a drop vibrating on an isothermal and temperature gradient surfaces respectively, theory predicts (figures 2.6 and 2.7) a stick slip behavior of the contact line, which is qualitatively observed in experiments as well. However, while the theory predicts a complete arrest of the contact line in the stick phase, very slow movement of the contact line is observed in experiments. In the next section we describe how we resolve this issue of complete sticking of contact line observed in the simulations.
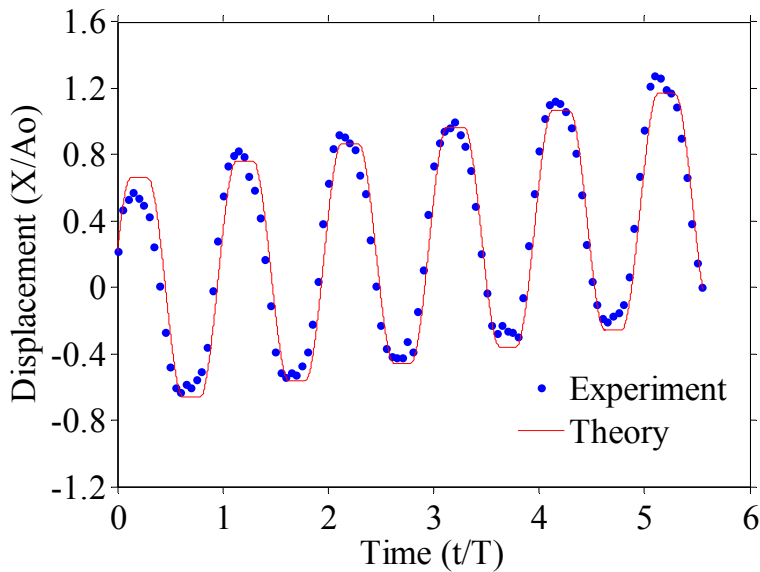
Figure 2.7. The experiment as described in figure 6 is repeated on a thermal energy gradient surface with temperature gradient of dT/dx~0.78^{o}C/mm. Blue circles represent experimental data for the displacement of contact line relative to the plate. Red line represents the displacement of contact line obtained from numerical simulation of equation 2.7 with $\bar{\gamma}$ included. Note that contact line exhibits stick-slip behavior, which is evident from the relative displacement of contact line with respect to plate (blue closed circles). In this case of drop vibrating on a temperature gradient wafer, a net drift results from the asymmetric slipping of contact line.

2.8. Simulations with Non-linear Contact Angle Hysteresis Model

Even though the simulation procedure described in the section above predicts the contact line motion of drop well, it also predicts complete sticking of the contact line. Such a complete sticking of contact line does not match with the experiments where there is some amount of velocity dependent slipping of contact line. We have recently used a non-linear contact angle hysteresis model to explain the detailed contact line motions of small liquid drops subjected to asymmetric vibration on a horizontal solid surface[36]. Apart from predicting detailed contact line motions of drops of various volumes, we could also predict the directions of drops motion accurately. We wanted to check whether this new non-linear contact angle hysteresis model explains the contact line motion observed in current experiments. In order to predict the contact line motion very accurately we replace the discontinuous $\sigma(V)$ with a continuous non-linear function $\tanh(\alpha V)$. The equation of motions for the center of mass and contact line of the drop are modified as below.

$$\frac{d^2 x_2}{dt^2} + \frac{k_s}{m} x_2 + \frac{1}{\tau_2} \frac{dx_2}{dt} = \gamma(t) \tag{2.16}$$

$$\frac{1}{\tau_1} \frac{dx}{dt} = \bar{\gamma} + \frac{k_s}{m} x_2 + \frac{1}{\tau_2} \frac{dx_2}{dt} - \Delta \tanh\left(\alpha \frac{dx}{dt}\right) \tag{2.17}$$

Here, unlike in the previous section where the spring constant of liquid drop was used as a fitting parameter, it is proportional to the surface tension of the liquid, γ_{lv} given by $k_s = 2\pi\gamma_{lv}$. $\Delta \tanh(\alpha V)$ is the hysteresis force divided by the mass of the drop, where

$V = dx/dt$ is the velocity of the contact line. As described earlier, hysteresis term $\sigma(V)\Delta$ enters in the equation of motion as a jump discontinuity. The difficulty associated with such a term is that the signum function is discontinuous at $V = 0$ which results in the discontinuity in force versus velocity relationship. We replaced the signum function with a non-linear function $\tanh(\alpha V)$ which is widely used in tribology literature[37] involving Coulombic dry friction that has a jump discontinuity similar to that of the wetting hysteresis at $V=0$. Here, α is a parameter that signifies how fast the resistive force (acceleration) due to contact angle hysteresis reaches the threshold force (acceleration, Δ) as a function of velocity of contact line. In the limit of $\alpha \to \infty$, hyperbolic tangent function is a good approximation to signum function.
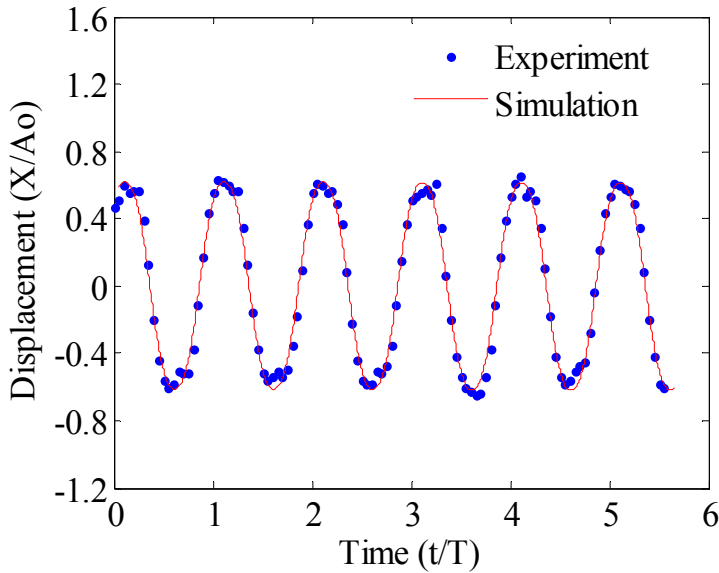
Figure 2.8. Non-dimensional displacement of contact line of a $30\mu L$ water drop relative to the plate at a vibration frequency of 100Hz on an isothermal surface. Ao is amplitude (0.12 mm) and T is time period (0.01 sec) of oscillation. The acceleration of amplitude of the vibration is 47 m/s². Blue circles represent displacement of contact line relative to the plate. Red line represents the displacement of contact line obtained from numerical simulation of simultaneous equations 2.16 and 2.17 without $\bar{\gamma}$. We carried out numerical simulations of equations 2.16 and 2.17 using commercial software Mathematica®.

The unknown parameters in the simulations are Δ, τ_1 and τ_2. Below we describe the procedure used to estimate approximate values for Δ, τ_1 and τ_2. Langevin relaxation time (the ratio of the mass to kinematic friction coefficient, $\tau_1 = M / \zeta$) scales with the volume (V) of the drop as $\tau_1 \sim V^{2/3}$. We found that τ_1 for a 4μL drop on a decyltrichlorosilane monolayer coated silicon wafer with similar hysteresis as the current surface to be approximately 0.01 sec[36]. The scaling law predicts approximate τ_1 for a 30μL drop to be $0.01*(30/4)^{2/3} \sim 0.038\,\text{sec}$. However, we had to use 0.02sec which approximately half of the predicted value. We also found from our previous simulations of drops subjected to asymmetric vibration that relaxation time due to dissipation in the bulk of the drop (τ_2) is approximately equal to relaxation time due to dissipation at the contact line (τ_1). So we have used $\tau_2 \sim 0.018$ sec in the simulations. We also found that Δ for a 4μL drop on a decyltrichlorosilane monolayer coated silicon wafer to be $10 m/s^2$. The scaling law for contact angle hysteresis is $\Delta \sim V^{-2/3}$. This scaling law predicts approximate Δ for a 30μL drop to be $10*(30/4)^{-2/3} \sim 2.6 m/s^2$. We had to use $\Delta = 2m/s^2$ in the simulations to match the contact lines as observed in the experiments. We carried out numerical simulations of equations 2.16 and 2.17 in order to obtain displacement of contact line (x) of drop and thus the velocity of the drop, which are compared with the experimental data. We used commercial software Mathematica® to numerically solve the simultaneous differential equations 2.16 and 2.17. The integration time step is $\Delta t = T/200$ where $T = 0.01\text{sec}$ is time period corresponding to frequency ($\omega = 100 Hz$) of oscillations. The amplitude of acceleration of vibrations is

$\Gamma_o \sim 4\pi^2\omega^2 A \sim 47m/s^2$. The displacement of contact lines as obtained from the simulations are shown in Figure 2.8 and 2.9 for drop moving on an isothermal and thermal gradient surface respectively. These simulations carried out using non-linear contact angle hysteresis model predicts the details of contact line motions very accurately along with predicting the exact drift velocity on thermal gradient surface (Figure 2.9). Unlike the simulations in the previous section, the new model predicts the velocity dependent contact line slipping accurately.
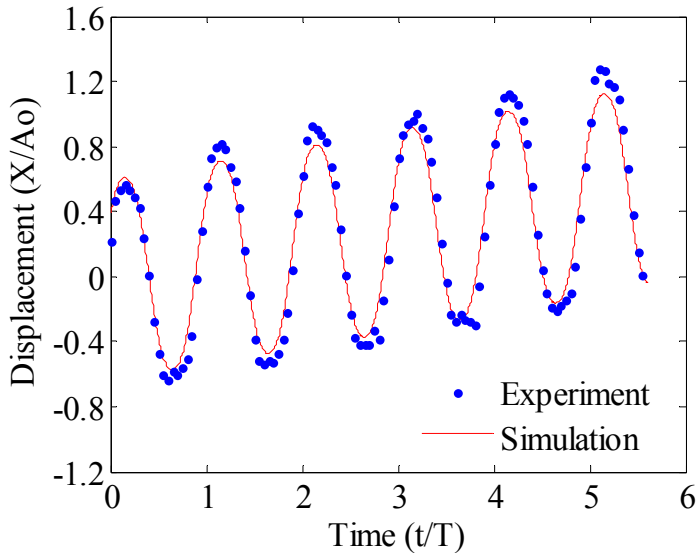
Figure 2.9. The experiment as described in figure 8 is repeated on a thermal energy gradient surface with temperature gradient of $dT/dx \sim 0.78°C/mm$. Blue circles represent displacement of contact line relative to the plate. Red line represents the displacement of contact line obtained from numerical simulation of simultaneous equations 2.16 and 2.17 with $\bar{\gamma} = 0.09m/s^2$ included. We carried out numerical simulations of equations 2.16 and 2.17 using commercial software Mathematica[®].

2.9. Conclusions

The motion of liquid drops placed on a hydrophobic surface having thermal energy gradient subjected to periodic vibration force has been studied to elucidate

46

the combined effect of thermal energy gradient and vibration. The liquid drop placed on a thermal energy gradient surface is observed to remain stationary in the absence of vibration force. This pinning of liquid drops is attributed to the presence of large hysteresis force. The drop requires overcoming the hysteresis force before it sets into motion. High temperature gradient required for given size of a drop to overcome hysteresis force is highly impractical especially while dealing with temperature sensitive reactants in microfluidic devices. Application of external energy through vibration of solid surface shows a promising way of overcoming hysteresis. Liquid drops placed on an isothermal surface subjected to symmetrical sinusoidal vibration force are observed to remain stationary due to the absence of asymmetry in any of the transport property which if present would have resulted in the rectification of drop motion there by resulting in unidirectional motion of drop. However, the effect of thermal energy gradient when combined with symmetrical sinusoidal vibration force results in the unidirectional motion of the drop. The velocity amplification shown by moving liquid drops corresponds to the resonance frequencies predicted by Rayleigh's equation. Using a simple model we could explain the velocity amplification when the frequency of oscillations is close to the resonance frequency of liquid drops. Approximate numerical simulations predict the detailed contact line motions well except that they predict completely sticking of the drop that is contrary to the experimental observation. Such a velocity dependent slipping of contact line observed in experiments is reproduced by simulations incorporating recently developed non-linear contact angle hysteresis model. However, for the detailed understanding of the dynamics of the flow phenomena and to analyze the development of temperature, velocity and pressure profiles inside the drop we need to resort to

47

numerical simulation of 3-D Navier-Stokes equations. To this end, we have solved the 3-D Navier-Stokes equations numerically for a small drop of radius 1 mm using the commercial Computational Fluid Dynamics (CFD) software code FLUENT by simultaneously solving heat and momentum transfer equations inside the drop with and without vibration the details of which are described below.

2.10. Computational Fluid Dynamics Simulations using FLUENT

Most of the theoretical results on thermocapillary migration of drop available in the literature are obtained by using lubrication theory that is applicable only in the limit of low contact angles. Also, scope of the results obtained using lubrication approximation is limited as very little information like drop migration velocity is extracted from it. However, for the detailed understanding of the dynamics of the flow phenomena and to analyze the development of temperature, velocity and pressure profiles inside the drop we need to resort to numerical simulation of 3-D Navier-Stokes equations. The 3-D simulation results are also very useful in understanding the dynamic variation in the contact angles on both sides of the drop as it migrates towards colder side. The rich information obtained using these simulation results will considerably advance the field of microfluidics to design, build and operate microfluidic devices with enhanced efficiency. Recent paper by Tseng et al[38] seems to be the only paper where 3-D numerical simulations of Navier-Stokes equations are carried out for a drop sitting on a thermal gradient (dT/dx~100°C/mm) solid surface by taking into consideration the heat and momentum transfer effects. These authors have also found the drops of contact angle ~ 50° to move to the region of colder temperature that confirms the analytical

prediction of Brochard[15]. Recently Nguyen and Chen[39,40] have looked at the thermocapillary migration of liquid drops using finite element analysis.

The main aim of this numerical study is to obtain an understanding of the phenomenon of motion of drops on thermal gradient surface subjected lateral vibration by carrying out numerical simulation of 3D Navier-Stokes equations and energy equation. Here, we look at how the velocity field develops inside the drop due to thermal gradient on the surface. We do not attempt to compare the simulations results with the experiments as many details like dynamic contact angle and contact angle hysteresis are not taken into account. We only look at the simulations in a qualitative way. Development of accurate contact angle hysteresis model that needs to be incorporated into FLUENT simulations is left for the future work.
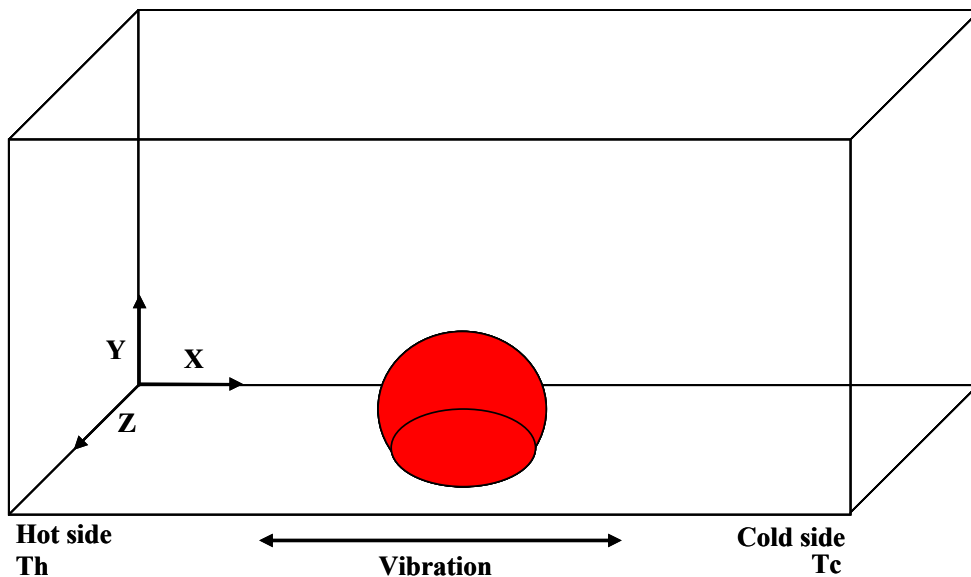
Figure 2.10. Schematic geometry for a liquid drop on vibrating hydrophobic surface with linear thermal energy gradient on it.

2.11. Problem Statement

Consider a water droplet surrounded by air on a temperature gradient surface that is undergoing sinusoidal lateral vibration as shown schematically in Figure 2.10. The geometry used in the model is a rectangular brick with dimensions of 5mm×2.5mm×2.5mm where a drop of radius 1mm is placed at center of the domain. The use of smaller computational domain with Lx/R=5, Ly/R=Lz/R=2.5 where Lx, Ly, and Lz are the computational domain lengths in x,y,z directions and R is the radius of drop, is justified by the fact that symmetry boundary conditions used on the boundaries in x-direction minimize the effect of boundaries on the numerical solution. The computational domain is descretized with uniform rectangular mesh of size $50\mu m \times 50\mu m \times 50\mu m$. In a similar study of liquid drop vibrating on isothermal solid surface, Dong et al[33] arrived at a mesh size of $40\mu m \times 40\mu m \times 40\mu m$ after experimenting with various mesh sizes in decreasing order until the simulation results became independent of grid size used. Therefore we also used a mesh size comparable to Dong et al[33]. Bussmann et al[41] have also studied the effect of grid resolution on the dynamics of a drop spreading on an inclined surface and found that solution obtained with 10 computational cells per radius of drop accurately predicts the dynamics. We have used 20 computational cells per radius of drop which is sufficient enough to give grid independent results. Numerical simulations have been carried out using the commercial Computational Fluid Dynamics (CFD) software code FLUENT in which the 3-D Navier-Stokes, energy and continuity equations are solved using Volume of Fluid (VOF) model[42]. In VOF model a single momentum and a single energy equation are solved throughout the domain and the resulting field variables are shared by two phases. The momentum and energy equations are solved along with an extra VOF advection

equation; where α, the volume fraction of one of the phases is introduced as an extra variable to keep track of whether a given computational cell is at the interface or in one of the phases. When α = 1, a given cell is completely filled with one of the phases (i.e. water), whereas α = 0 implies that the cell is completely filled with the other phase (air). The cells that are present at the interface satisfy the condition that: 0 < α < 1. The 3-D Navier-Stokes, energy, continuity, and VOF advection equations used to solve the problem of the oscillating drop on temperature gradient surface are shown below:

$$\frac{\partial}{\partial t}(\rho \mathbf{v}) + \nabla \cdot (\rho \mathbf{v} \mathbf{v}) = -\nabla p + \nabla \cdot \left[\eta \left(\nabla \mathbf{v} + \nabla \mathbf{v}^T \right) \right] + \rho g \mathbf{k} + f \qquad (2.18)$$

$$\frac{\partial}{\partial t}(\rho E) + \nabla \cdot (\mathbf{v}(\rho E + p)) = \nabla \cdot \left[K_{eff} (\nabla T) \right] \qquad (2.19)$$

$$\frac{\partial \rho}{\partial t} + \nabla \cdot (\rho \mathbf{v}) = 0 \qquad (2.20)$$

$$\frac{\partial \alpha}{\partial t} + \mathbf{v} \cdot \nabla \alpha = 0 \qquad (2.21)$$

where $\mathbf{v} = (u, v, w)$ and p are velocity vector and pressure. $\rho = \rho^w \alpha + \rho^a (1-\alpha)$ is the density in the computational cell, ρ^w and ρ^a being the density of water and air, respectively. $\eta = \eta^w \alpha + \eta^a (1-\alpha)$ is the viscosity in the computational cell, where η^w and η^a are the viscosity of water and air, respectively. Energy (E) and temperature (T) are mass averaged values in VOF model.

$$E = \frac{\sum\limits_{q=1}^{q=2} \alpha_q \rho_q E_q}{\sum\limits_{q=1}^{q=2} \alpha_q \rho_q} \qquad (2.22)$$

where E_q for each phase is based on specific heat and temperature shared by that particular phase. $\mathbf{k} = (0, -1, 0)$ is a unit vector in the negative y-direction. The continuum surface

force (CSF) model developed by Brackbill et al[43] has been used to account for the volume forces resulting due to the surface tension and curvature of the interface. CSF model is implemented by adding a volume force term f on the right side of equation 2.18 which is defined as below:

$$f = \gamma_{lv} \, \kappa \nabla \alpha \tag{2.23}$$

where γ_{lv} is the surface tension and κ is the curvature of the interface. The curvature at the interface is calculated as follows

$$\kappa = -\nabla \cdot \boldsymbol{n}; \qquad \boldsymbol{n} = \frac{\nabla \alpha}{|\nabla \alpha|} \tag{2.24}$$

Where **n** is the outward unit normal vector. The volume force f is finite near interface and vanishes in the computational cells that are far away from interface. We used implicit interpolation with geometric reconstruction scheme for interface tracking. In our model a second order upwinding scheme is used for the descretization of convective terms in momentum equation and energy equation with a PISO (Pressure Implicit with Splitting of Operator) algorithm for pressure-velocity coupling. The time step used for temporal descretization was in the order of 10^{-5} sec which is small enough to capture the transient behavior of the system.

2.12. Boundary Conditions

The momentum boundary conditions applied on the solid surface at y = 0 are no-slip and no-penetration with sinusoidal periodic vibration $U_p = 2\pi\omega A Cos(2\pi\omega t)$ in x-direction i.e. the direction of vibration is perpendicular to that of gravity where A, ω are the amplitude and frequency of vibration respectively.

$$u = U_p = 2\pi\omega A Cos(2\pi\omega t), v = 0 \text{ and } w = 0 \tag{2.25}$$

The thermal boundary condition applied on the solid surface at y = 0 is a linear temperature gradient in positive x-direction with a gradient of 0.78° C/mm as follows.

$$T(x) = T_o - 0.78x \tag{2.26}$$

The thickness of the solid boundary is taken to be very small and the thermal conductivity to be very high to ensure that there is no temperature gradient within the solid boundary due to conduction. The wall adhesion boundary condition applied on the solid surface to specify the equilibrium contact angle (θ_e) is to set the normal $(\hat{n})$ to the interface at all points on the wall as follows[44]

$$\hat{n} = \hat{n}_{wall} Cos\theta_e + \hat{n}_t Sin\theta_e \tag{2.27}$$

where $\hat{n}_{wall}$ and $\hat{n}_t$ are unit vectors normal and tangential to the wall. An equilibrium contact angle (θ_e) of ranging from 45° to 110° is specified on the solid surface using the above boundary condition. Temperature dependence of contact angle is neglected since the dependence is negligible as elucidated by Newmann[45] that the contact angle varies approximately by 2° over a range of temperature from 10°C to 50°C. The surface tension of water is specified as a linear function of temperature[46] in the model to account for the thermal Marangoni flow for the range of T from 283°K to 353°K as follows

$$\gamma_{lv}(T) = 0.12121 - 0.0001653\,T \tag{2.28}$$
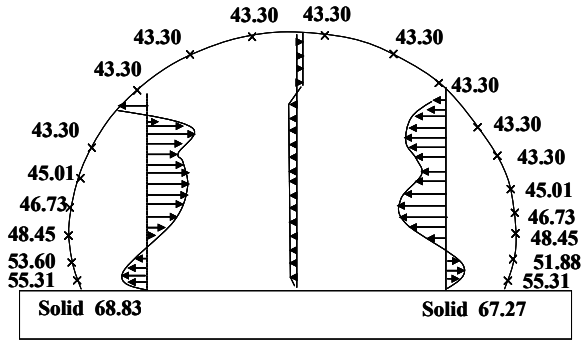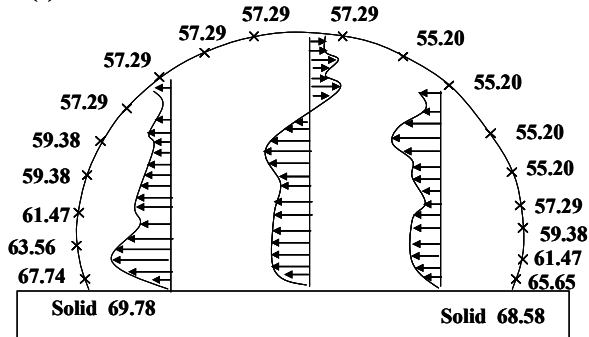
Figure 2.11. Instantaneous velocity profiles inside a drop sitting on thermal energy gradient surface (dT/dx~0.78°C/mm) along with surface temperature profile (°C) obtained from CFD simulations (a) and (b) drop with an equilibrium contact angle of 110° at t=0.01 and 0.4323 sec respectively.

Figure 2.11 (a) and (b) show instantaneous velocity vectors at center plane of the drop and temperature profile on the surface of the drop sitting on a temperature gradient surface (dT/dx~0.78°C/mm). Initially (t~0.01 sec), the thermal diffusion is confined to a thin layer adjacent to the solid. As the temperature profile on the surface of the drop is nearly symmetric about the center line, the surface flow results in two convection cells of equal magnitude on the both halves of the drop. Here the left half of the drop has a velocity profile with net average velocity in positive x-direction where as the right half of the drop has a velocity profile with net average velocity in negative x-direction. There is no net motion of the drop in this case as the convection cells negate the flow developed. As time proceeds (t~0.4323 sec), an asymmetry in the surface temperature profile is

54

developed and strengthened thus resulting in higher temperature on the left half and lower temperature on the right half of the drop. The convection cells are also asymmetric, the consequence of which is that the drop moves towards hotter side. Such a development asymmetric convection cell within the drop is in agreement with recent finite element simulations carried out by Nguyen and Chen[39,40]. However, in the simulation as shown in Figure 2.11 (a) and (b), drops with contact angles greater than 90° show movement towards hotter side where as in the experiments with vibration the drops have moved towards colder side. On the other hand, when we performed similar computations for drops of contact angles 90° or less, we have found that the drops movement is towards the colder region, in agreement with the original prediction of Brochard[15] and with the CFD simulations of Tseng et al[38]. The asymmetric temperature profiles and velocity profiles inside the drop are shown in Fig. 2.12 (a) and (b) for drops with equilibrium contact angles of 90° and 45° respectively.
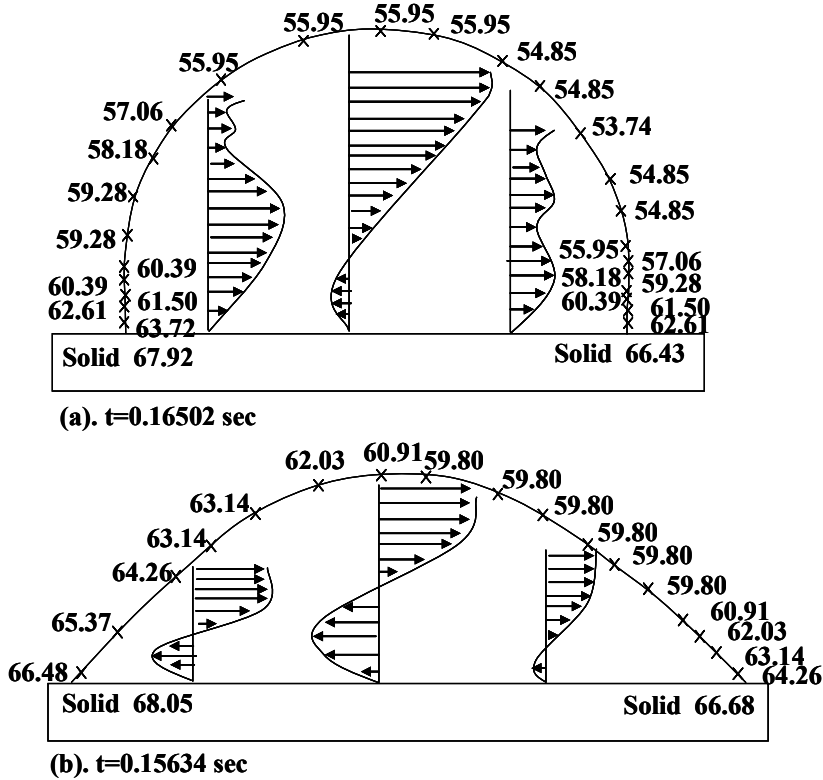
Figure 2.12. Instantaneous velocity profiles inside a drop sitting on thermal energy gradient surface ($dT/dx \sim 0.78^\circ$C/mm) along with surface temperature profile ($^\circ$C). (a) drop with an equilibrium contact angle of 90° at t=0.16502 sec, (b) drop with an equilibrium contact angle of 45° at t=0.15634 sec.

As observed from Fig. 2.11 (b), Fig. 2. 12 (a) and (b), the convection cell pattern resulting from asymmetry in temperature profile on surface is quite similar in all cases with the left convection cell dominating. It is also interesting to note that in case of θ_e=110° from Fig. 2.11 (b), the velocity profile pattern in the upper half portion of the drop is similar to the velocity profile pattern in the whole portion of drops of θ_e=90° and 45°. However, the velocity profile in the lower half portion of drop with θ_e=110° is similar to the plug flow velocity profile with opposite direction (towards hotter side). Hence the drops with θ_e>90° have shown movement towards hotter side in the simulation. Since the

56

drops with $\theta_e > 90^o$ have shown movement towards hotter side and drops with $\theta_e \leq 90^o$ have shown movement towards colder side, there may be a transition region where the direction of drop motion changes sign.

(a). t=0.49052 sec

(b). t=0.49252 sec

(c). t=0.49572 sec
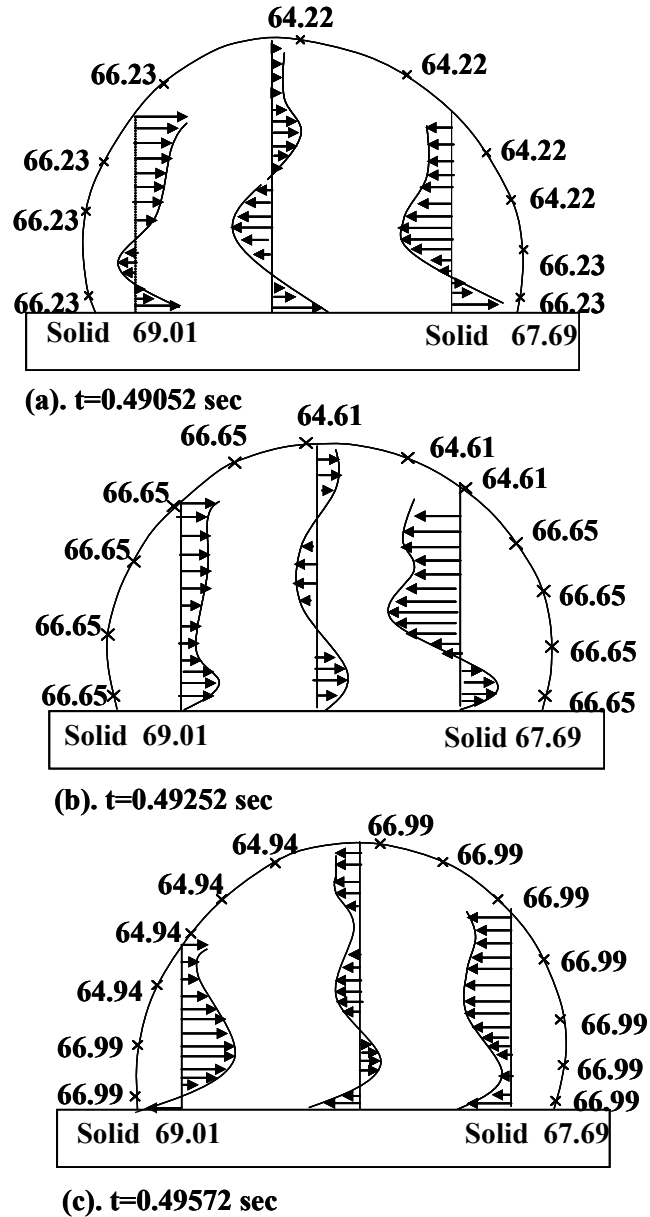
Figure 2.13. Instantaneous velocity profiles inside a drop sitting on thermal energy gradient surface (dT/dx~0.78^{o}C/mm) subjected to vibration (Frequency 100Hz, Amplitude 1.33mm): (c) drop at maximum swing to the left, (d) drop at middle of the swing, (e) drop at maximum swing to the right. Temperature profiles (^{o}C) on the surface of the drop are also shown.

In order to elucidate the effect of vibration on motion of drop, we next subjected the plate to a sinusoidal vibration with a horizontal velocity of the drop being $u = U_p = 2\pi\omega A Cos(2\pi\omega t)$. The temperature and velocity profiles in a drop subjected to vibration are shown in Fig. 2.13 (a), (b) and (c) for three different time steps in one cycle of oscillation. While the surface temperature increases faster with vibration, the drop was still found to move first towards the colder region and then ultimately towards the warmer region. Asymmetric convection of liquid was again evident inside the drop with vibration in conjunction with a thermal gradient. After the initial movement towards colder side, the drop has shown an asymmetric motion with the movement towards hotter side being higher than the movement towards the colder side in each cycle of the oscillation. This is contrary to the experimental observation that drops with contact angles greater than 90° show movement towards colder side with applied vibration force. However, when we performed simulations with drops of $\theta_e \leq 90^o$, the drops have shown movement towards colder side when vibration force is applied.

2.13. Conclusions from CFD Simulations

The motion of liquid drops placed on a silanized silicon wafer having thermal energy gradient subjected to periodic vibration force has been studied by solving 3D numerical simulation to elucidate the combined effect of thermal energy gradient and vibration. The CFD simulations have also shown the asymmetric motion of the drop on thermal energy gradient surface subjected to periodic vibration. However, the direction predicted by simulation is in contrary to the experimental observations for $\theta_e > 90^o$ which

58

needs to be resolved by taking change of dynamic contact angles during motion of drop into account. Here, we looked at the simulations in qualitative way to observe how the flow field develops inside the drop. We suggest the future work in conclusions section of this thesis.

2.14. References

1. Oulette, *J. Ind. Phys.* **2003**,9,14.

2. Wu, H.; Wheeler, A.; Zare, R. N. *Proc. Natl. Acad. Sci. U.S.A.* **2004**, *101*, 12809.

3. Northrup, M. A. *Anal. Chem.* **1998**, *70*, 918.

4. Burns, M. A.; Mastrangelo, C. H.; Sammarco, T. S.; Man, F. P.; Webster, J. R.; Johnson, B. N.; Foerster, B.; Jones, D.; Fields, Y.; Kaiser, A. R.; Burke, D. T. *Proc. Natl. Acad. Sci. USA* **1996**, *93*, 5556.

5. Burns, M. A.; Johnson, B. N.; Brahmasandra, S. N.; Handique, K.; Webster, J.; Krishnan, R. M.; Sammarco, T. S.; Man, P. M.; Jones, D.; Helsinger, D.; Mastrangelo, C. H.; Burke, D. T. *Science* **1998**, *282*,484.

6. Chaudhury, M. K.; Whitesides, G. M. *Science* **1992**, *256*, 1539-1541

7. Daniel, S.; Chaudhury, M. K. Chen, J. C. *Science* **2001**, *291*, 633-636.

8. Petrie, R. J.; Bailey, T.; Gorman, C. B.; Genzer, J. *Langmuir* **2004**, *20,* 8993.

9. Ichimura, K.; Oh, S.-K.; Nakagawa, M. *Science* **2000**, *288*, 1624

10. Sandre, O.; Gore-Talini, L.; Ajdari, A.; Prost, J.; Silberzan, P. *Phys. Rev. E* **1999**, *60*, 2964

11. Buguin, A.; Talini, L.; Silberzan, P. *Appl. Phys. A* **2002**, *75*, 207.

12. Daniel, S.; Chaudhury, M. K. *Langmuir* **2002**, *18*, 3404.

13. Daniel, S.; Sircar, S.; Gliem, J.;   Chaudhury, M. K. *Langmuir* **2004**, *20*,

4085

14. Daniel, S.; Chaudhury, M. K.; De Gennes, P.-G. *Langmuir* **2005**, *21*, 4240.

15. Brochard, F. *Langmuir* **1989**, *5*, 432-438.

16. Brzoska, J. B.; Brochard-Wyart, F.; Rondelez, F. *Langmuir* **1993**, *9*, 2220.

17. Ford, M. L.; Nadim, A.; *Phys. Fluids* **1994**, *6* ,3183.

18. Smith, M. K. *J. Fluid Mech* **1995**, *294*, 209.

19. Sammarco T. S.; Burns, M. A. *AIChE. J* **1999**,*45*,350.

20. Yarin, A. L.; Liu, W.; Reneker, D. H. *J. Appl. Phys* **2002**, *91*, 4751.

21. Darhuber, A. A.; Davis, J. M.; Troian, S. M.; Reisner, W. W. *Phys. Fluids* **2003**, *15*, 1295.

22. Darhuber, A. A.; Valentino, J. P.; Davis, J. M.; Troian, S. M.; Wagner, S. *Appl. Phys. Lett* **2003**, *82*, 657.

23. Chen, J. G.; Troin, S. M.; Wagner, S. *J. Appl. Phys* **2005**, 97 , 014906

24. Pratap, V.; Moumen, N.; Subramanian R. S. *Langmuir*, **2008**, *24*, 5185.

25. Smith, T.; Lindberg, G.; *J. Colloid Interface Sci.* **1978**, *66*, 363.

26. Andrieu, C.; Sykes, C.; Brochard, F. *Langmuir* **1994**, *10*, 2077.

27. Nadkarni, G. D.; Garoff, S. *Langmuir* **1994**, *10*, 1618.

28. Decker, E. L.; Garoff, S. *Langmuir* **1996**, *12*, 2100.

29. Meiron, T.S.; Marmur, A.; Saguy, I.S. *J. Colloid Interface Sci.* **2004**, *274*, 637.

30. Lord Rayleigh, The Theory of Sound (Macmillan, 1894).

31. Lamb, H. Hydrodynamics, Cambridge University Press: Cambridge, U.K., 1932.

32. Chandrasekhar, S. Hydrodynamic and Hydromagnetic Stability; Dover: Mineola, NY, 1961.

33. Dong, A. L.; Chaudhury, A.; Chaudhury, M. K. *Eur. Phys. J.E* **2006**, *21*, 231.

34. Buguin, A.; Brochard, F.; De Gennes, P.-G. *Eur. Phys. J.E* **2006**, *19*, 31.

35. De Gennes, P. -G. *J. Stat. Phy*s **2005,** *119*, 953.

36. Mettu, S.; Chaudhury, M. K. *Langmuir* **2011**, *27*, 10327.

37. Andersson, S.; Soderberg,A.; Bjorklund, S. *Tribol. Int* **2007**, *40*, 580.

38. Tseng, Y.; Tseng, F. N.; Chen, Y. F.; Chieng, C. C. *Sensors and Actuators A* **2004**, *114*, 292.

39. Nguyen, H. B.; Chen, J. C. *Phys. Fluids* **2010**, *22*, 062102.

40. Nguyen, H. B.; Chen, J. C. *Phys. Fluids* **2010**, *22*, 122101.

41. Bussmann, M., Mostaghimi, J., Chandra, S., *Phys. Fluids* **1999**, *11*, 1406.

42. Hirt, C. W.; Nichols, B. D. *J. Comput. Phys* **1981**, *39*, 201.

43. Brackbill, J. U.; Kothe, D. B.; Zemach, C. *J. Comput. Phys.* **1992**, *100*, 335.

44. Fluent 6.2 User's Guide, Fluent Inc., 2003.

45. Neumann, A.W. *Adv. Colloid Interface Sci* **1974**, *4*, 105.

46. Pellicer, J.; Garcia-Morales, V.; Gaunter, L.; Hernandez, M. J.; Dolz, M. *Am. J. Phys* **2002**, *70*, 705.

47. Nichita, B. A.; Zun, I.; Thome, J. R. 7th Int. Conf. on Multi Phase Flow. **2010**, Tampa, FL, USA.

48. Fang, C.; Hidrovo, C.; Wang, F. M.; Eaton, J.; Good, K. Int. J. of Multiphase Flow **2008**, *34*, 690.

49. Sikalo, S.; Wilhelm, H. D.; Roisman, I. V.; Jakirlic, S.; Tropea, C. *Physics of Fluids* **2005**, *17*, 062103.

50. ChrisM, Bachelors ofEngineering Thesis, University of Victoria, 2007.

Chapter 3: Brownian Motion of a Liquid Drop with Dissipation due to Contact Angle Hysteresis

3.1. Introduction

Brownian motion of a colloidal particle in a solvent is a well known phenomenon[1-8]. The colloidal particle shows random motion due to thermal fluctuations (Gaussian Noise) while dissipating energy by kinematic friction due to interaction with surrounding molecules. This system is studied extensively with well developed theory[2-8] to describe the relation between diffusivity and system parameters such as temperature and friction coefficient. Here, the Fluctuation-Dissipation theorem[2,3,8] states that the ratio of diffusivity to mobility is $k_B T$. Also, the displacement or velocity distribution of colloidal particle is Gaussian due to the linear nature of kinematic friction. Recently, Daniel and Chaudhury[9] have observed similar random motion of water drops condensing on a solid substrate. The solid substrate used in the experiments was a circular silicon wafer having surface energy gradient in radial direction. The condensing water drops coalesce randomly on the surface and drift away from hydrophobic end of the substrate towards hydrophilic end showing drifted Brownian like motion. They observed that when rate of condensation was high, drops were moving with high velocities and when rate of condensation was low drops were moving slowly. Analogous to thermal fluctuations that the colloidal particle experiences, water drops also experience fluctuations from random coalescence as well as from thermal fluctuations of contact line. However, in case of water drop under going random motion on a surface, apart from the kinematic frictional dissipation at the contact line there is also an additional mechanism for energy dissipation

due to threshold contact angle hysteresis force. Contact angle hysteresis resulting either from physical or chemical heterogeneity on the surface resists the motion of drops on a surface. When a drop moves on solid substrate (Figure. 3.1), its front side attempts to reach the advancing angle, whereas its rear side tries to achieve receding angle. This leads to a threshold force of the magnitude: $\gamma_{lv} w(\cos\theta_r - \cos\theta_a)$ acting on the drop, where γ_{lv} is the surface tension of liquid, w is width of drop, θ_a and θ_r are the advancing and receding contact angles respectively. Resistive force due to contact angle hysteresis that always acts against the direction of motion of the drop must be overcome before the drop moves on the surface. The presence of threshold hysteresis force significantly modifies the dynamics of drop motion.
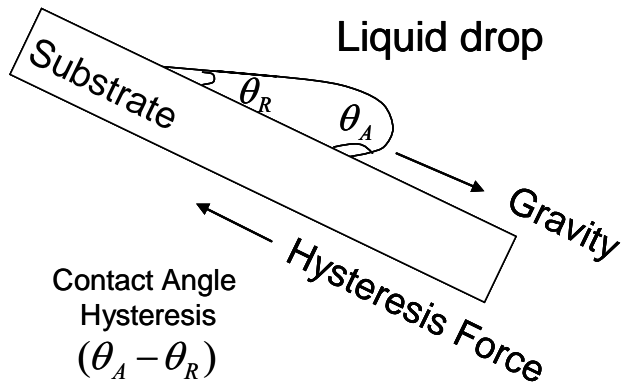
Figure 3.1. Schematic of a water drop sticking to windshield of a car due to contact angle hysteresis. Gravity tries to pull the drop down where as the hysteresis force resists the motion.

In the case of a colloidal particle diffusing under the influence of thermal noise, velocity autocorrelation function is exponential ($\langle V(0)V(t)\rangle = \langle V_L^2 \rangle e^{-t/\tau_L}$) in which $\langle V_L^2 \rangle = K\tau_L / 2$ where V_L is Langevin velocity, τ_L is Langevin relaxation time. In

63

this case, one dimensional diffusivity of colloidal particle can be calculated using Green-Kubo relation[8], $D = \int_0^\infty \langle V(0)V(t) \rangle dt$, that gives diffusivity as a function of power of external noise as $D = K\tau_L^2 / 2$. Here, the power of noise (K) is proportional to the temperature of the system. Hence, the diffusivity in presence of only kinematic friction scales linearly with the strength of the noise (K). Also, the drift velocity of colloidal particle in presence of a bias of magnitude $\bar{\gamma}$ is equal to the Stokes-Einstein limit $\bar{\gamma}\tau_L$ which does not depend of the strength of the noise.

However, presence of contact angle hysteresis significantly modifies the behavior of contact line of drop resulting non-exponential velocity correlation. There is also an important and fundamental distinction between colloidal particle undergoing Brownian motion and water drop undergoing Brownian like motion. The colloidal particle diffuses under the influence of thermal noise due to molecular collisions. Here, both of the noise acting on colloidal particle and the diffusive behavior of particle are result of the same molecular process namely molecular collisions. However, diffusive behavior of a liquid drop is dependent on two dissimilar mechanisms. The noise acting on the liquid drop is external that has no relation to the molecular process occurring at the interface of the liquid-solid contact which is being affected by contact angle hysteresis. This intern affects the Stokes-Einstein relation that states that the ratio of diffusivity to mobility is equal to $k_B T$. Hence the diffusivity of liquid drop on a solid surface may not follow the usual Stokes-Einstein equation. An interesting question that arises at this juncture is whether there exists any Fluctuation-Dissipation like relation when the friction and noise are decoupled which is the case for liquid   drop that is diffusing on solid in presence of

64

external noise. Another interesting question that we ask is how the drift velocity of drop depends on the strength of the noise.

Other important issue in this system is that the presence of threshold resistive force due to contact angle hysteresis introduces non-linearity into the system. There have been quite a few studies in recent literature[10-18] that looked at the behavior of a non-linear system subjected to white noise excitation. Caughey and Dienes[10,11] studied a similar non-linear system subjected to white noise excitation. Here, they analyzed velocity distribution of a Coulombic system where there is a non-linear threshold static friction between two contacting solids. They have shown using the solution of Fokker-Planck equation that the velocity distribution is non-Gaussian following exponential distribution. Unaware of the work of Caughey and Dienes[10,11] where kinematic friction is completely ignored, de Gennes[15], Kawarada and Hayakawa[16], Hayakawa[17] and Mauger[18] studied the combined effect Coulombic and kinematic friction on the velocity distribution for the case of a solid-solid contact subjected to a white noise vibration. In this case, the Coulombic dry friction at the interface gives rise to a non-Gaussian velocity distribution leading to a non-classical Brownian like motion. In the case of drop subjected to external white noise vibration which is studied here, contact angle hysteresis plays the role of Coulombic friction.

3.2. Theory

Inspired by the work of Daniel and Chaudhury[9], de Gennes[15] has developed a theory for Brownian like motion of a small objects on a solid substrate subjected to Gaussian white noise vibration. When a water drop on a solid substrate is subjected to white noise vibration, it experiences pulses of random accelerations $(\gamma(t))$ lasting

over a finite time width τ_c. The drop exhibits one dimensional random motion that can be described by modified Langevin equation[15-17].

$$\frac{dV}{dt} + \frac{1}{\tau_L}V = \bar{\gamma} + \gamma(t) - \sigma(V)\Delta \qquad (3.1)$$

Here, V is the velocity of the drop, τ_L is the Langevin relaxation time (ratio of the mass M of the drop and its hydrodynamic friction coefficient ζ), Δ is the hysteresis force divided by the mass of the drop. $\sigma(V) = V/|V|$ is signum function of velocity of contact line with $\sigma(0) = 0$ when drop is stationary $(V = 0)$. $\sigma(V) = -1$ when $V < 0$ and $\sigma(V) = +1$ when $V > 0$. Therefore, $\sigma(V)$ ensures that the resistive force due to contact angle hysteresis always acts against the motion of contact line of drop. $\gamma(t)$ is the time dependent acceleration that the drop experiences from the white noise source. The acceleration $\gamma(t)$ of white noise is ideally delta correlated with zero mean value. However, due to finite width and heights of the acceleration pulses in the experiments, the following approximation introduced by de Gennes[15] is used:

$$\langle \gamma(t_1)\gamma(t_2)\rangle = \Gamma^2 \qquad \text{for } |t_1 - t_2| < \tau_c$$

$$\langle \gamma(t_1)\gamma(t_2)\rangle = 0 \qquad \text{for } |t_1 - t_2| > \tau_c \qquad (3.2)$$

Here, Γ is the root mean square acceleration and τ_c is the time duration of a pulse. Here, K is the power of noise which is defined as $\Gamma^2\tau_c$. Following Chaudhury[16] equation 3.1 can be integrated as follows

$$V_{drift} = \int_{-\infty}^{t} dt' \{\langle \gamma(t')\rangle + \bar{\gamma} - \Delta\langle\sigma(V(t'))\rangle\}\exp\left\{-\frac{t-t'}{\tau_L}\right\} \qquad (3.3)$$

66

Carrying out the integration and noting that $\langle \gamma(t') \rangle = 0$ since the external noise is of zero mean results in

$$V_{drift} = \tau_L \left[\bar{\gamma} - \Delta \langle \sigma(V) \rangle \right] \qquad (3.4)$$

In case of noise free sliding of drop $\langle \sigma(V) \rangle = 1$, hence the drift velocity in this case is $V_{drift} = \tau_L \left[\bar{\gamma} - \Delta \right]$. However, in presence of external noise $\langle \sigma(V) \rangle \neq 1$. Chaudhury[16] approximated the value of $\langle \sigma(V) \rangle$ in presence of noise as

$$\langle \sigma(V) \rangle \sim \frac{\left(\sqrt{V_A^2 + V_{drift}^2} - V_A \right)}{V_{drift}} \qquad (3.5)$$

Here V_A is velocity amplitude in presence of hysteresis. Using first two terms in binomial expansion of $\sqrt{V_A^2 + V_{drift}^2}$ results in

$$\langle \sigma(V) \rangle \sim \frac{V_{drift}}{c_1 V_A} \qquad (3.6)$$

Following Chaudhury[16], it can be shown that

$$V_A \sim \frac{K}{\Delta} \qquad (3.7)$$

Omitting numerical constant c_1 and substituting equation 3.7 in equation 3.6 results in

$$\langle \sigma(V) \rangle \sim \frac{\Delta V_{drift}}{K} \qquad (3.8)$$

Substituting $\langle \sigma(V) \rangle$ from equation 3.8 in equation 3.4 results in

$$V_{drift} = \tau_L \left[\bar{\gamma} - \frac{\Delta^2 V_{drift}}{K} \right] \qquad (3.9)$$

Rewriting equation 3.9, the approximate expression for drift velocity of drop is as

follows

$$V_{drift} = \frac{\bar{\gamma}\tau_L}{1 + \Delta^2\tau_L / K}$$ (3.10)

When $\Delta = 0$, $V_{drift} = \bar{\gamma}\tau_L$ is Stokes-Einstein limit as mentioned earlier independent of the power of noise K. On the other hand, in presence of some amount of hysteresis ($\Delta \neq 0$, and $K << \Delta^2\tau_L$), drift velocity is a nonlinear function of K.

In order to elucidate the effect of hysteresis force on dynamics of drop motion; we studied Brownian like motion of a drop on a solid when it is subjected to an external Gaussian white noise by systematically varying the strength of noise (K).
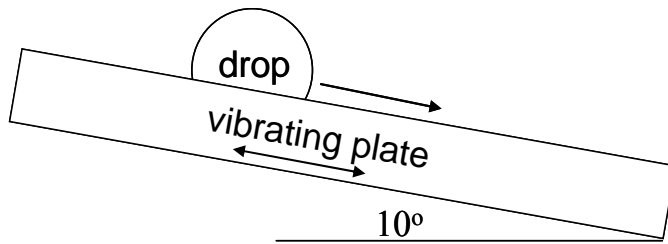
Figure 3.2. Schematic of experimental set up of a water drop on a tilted (10º) hydrophobic surface subjected to a white noise vibration.

3.3. Experiment

The schematic of the experiment is shown in Figure 3.2. The substrate is firmly attached to aluminum platform (not shown here, for the details of the complete setup refer to Figure 2.1(a) in Chapter 2) connected to a mechanical oscillator (Pasco Scientific, Model No: SF-9324). The substrate used in the experiments is a silicon wafer coated with monolayer of decyltrichlorosilane the preparation of which is described in Chapter 2. White noise generated by signal generator (Agilent, Model 33120A) is sent to the

oscillator after it is being amplified by a power amplifier (Sherwood, Model No: RX-4105). A calibrated accelerometer (PCB Peizotronics, Model No: 353B17) driven by Signal Conditioner (PCB Peizotronics, Model No: 482) connected to an oscilloscope (Tektronix, Model No. TDS 3012B) is used to measure the acceleration of the supporting aluminum plate. The acceleration of the plate is found to follow Gaussian distribution as shown in Figure 3.3. The whole set-up is placed on a vibration isolation table (Micro-g, TMC) to eliminate the effect of ground vibration. We used a constant volume (V=10μL, Mass=10^{-5} kg) of drop in all the experiments. The test liquid used in the experiments is water that is de-ionized using Barnstead NanopureII water purifying system. The purified water used in the experiments had a resistivity of 18 Ω Ohm-cm and a surface tension of 72.8 mN/m. The substrate is kept at a tilt angle of 10° to the horizontal shown in Figure 3.2. When placed on this inclined surface, $10\mu L$ drop does not spontaneously slide due to resistive force arising from contact angle hysteresis $(\gamma_{lv} w(\cos\theta_r - \cos\theta_a))$; however when external white noise acceleration of sufficient power is applied to the supporting plate the drop shows stochastic drifted Brownian like motion. Since the externally applied noise is white, there is always a finite probability of having vibration pulses whose accelerations are greater than the threshold acceleration ($\gamma_{lv} w(\cos\theta_r - \cos\theta_a)/m$) required to overcome contact angle hysteresis. Here m is the mass of drop. However, when it encounters acceleration pulses whose magnitude is less than the threshold acceleration, the drop relaxes to stationary state finally coming to a complete stop. The drop thus exhibits random motion with net drift in the direction of applied bias ($mg\sin\alpha$) analogous to a colloidal particle moving in a tilted potential.

In order to verify the effect of the power of vibration on drift velocity, bands of

white noise of root mean square acceleration ranging from 12 m/s^2 to 250 m/s^2 and

$\tau_c \sim 40 \ \mu s$ were used. We used a low speed camera operating at 30frames/sec to record

the drop motion and subsequently measure the drift velocity of drop as function of

strength of noise. We also recorded the high time resolution motion of the contact line of

drop that is moving under the influence of external white noise vibration of power $K =$

0.022 m^2/s^3. Here, we recorded the motion of drop at 2000 frames/sec. First we discuss

the results of drift velocities obtained as a function of strength of white noise vibration.

Later we focus on detailed contact line motion along with fluctuations obtained at higher

time resolution.
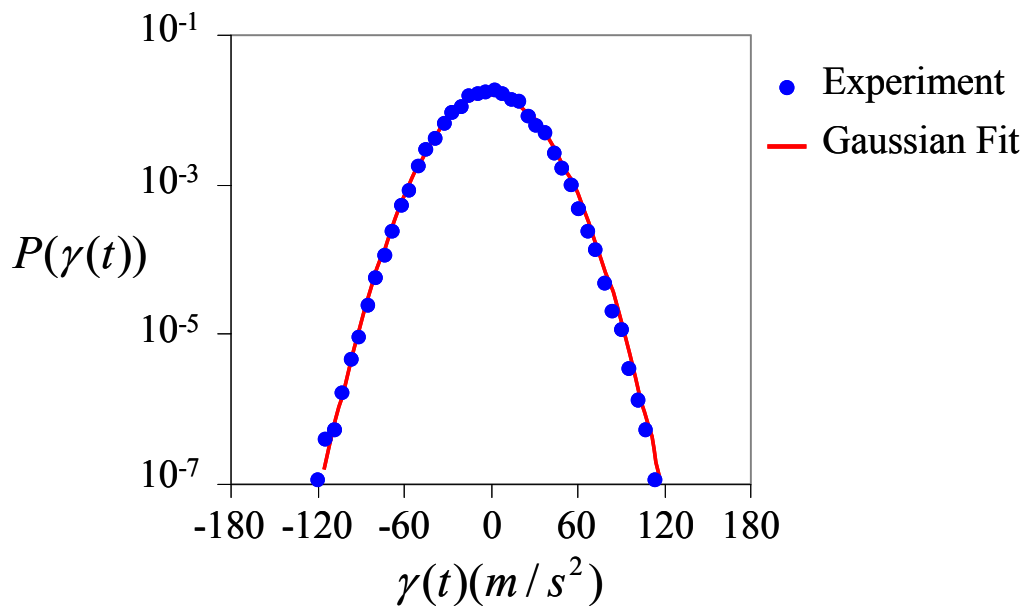
Figure 3.3. Log-linear plot of output acceleration obtained from accelerometer at a noise power of 0.022 m²/s³. Blue Circles represent experimental data and the solid line is a Gaussian fit to the data.

3.4. Drift Velocity of Drops

We plotted the drift velocities of small drop (10^{-5} kg) water as function of strength

of noise in Figure 3. 4. As the power of the noise increases, the drift velocity increases non-linearly with K tending to saturate at large power of noise from as also observed from equation 3.10. Experimental data could be fitted to the equation 3.10 with the values of Δ and τ_L as 3 m/s^2 and $0.01s$ respectively.
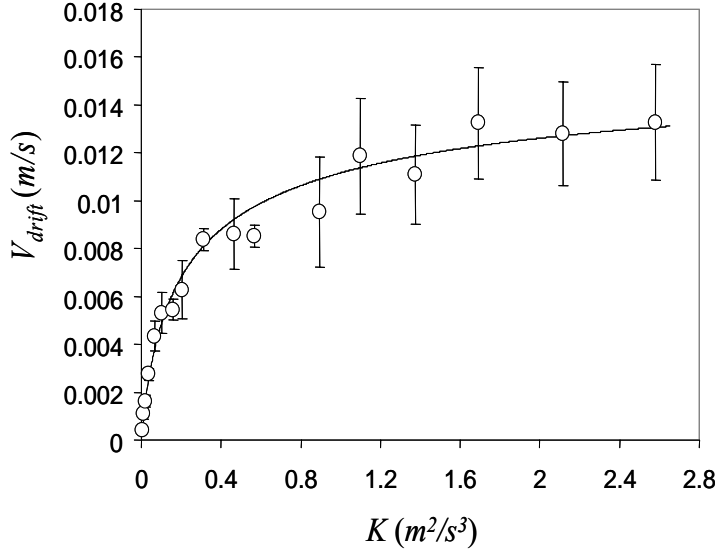
Figure 3.4. Drifted motion of small drops of water on a tilted (10°) hydrophobic silicon wafer in response to Gaussian white noises of root mean square acceleration ranging from 12 m/s^2 to 250 m/s^2. Circles represent experimental data and the solid line is generated using equation 3.10.

3.5. Estimation of Approximate Langevin Relaxation Time of Drop

Apart from fitting the drift velocity data, we also used another simple experiment to estimate the approximate Langevin relaxation time for a $10\mu L$ drop on the same surface. In this experiment, noise free drift velocity of a $10\mu L$ drop sliding on the surface is measured at various inclination angles of the substrate to the horizontal. As mentioned earlier, noise free sliding velocity of drop is given by $V_{drift} = \tau_L[\bar{\gamma} - \Delta]$. Here, the limiting velocity of drop is $V_s = \bar{\gamma}\tau_L$ where $\bar{\gamma} = g \sin\alpha$. Here g is acceleration due to gravity and

71

α is angle of inclination the substrate to the horizontal. As shown in Figure 3.5, the slope of drift velocity versus $g \sin \alpha$ gives an approximate value of Langevin relaxation time to be 0.005s which is in the same order of 0.01s estimated from drift velocity fitting.
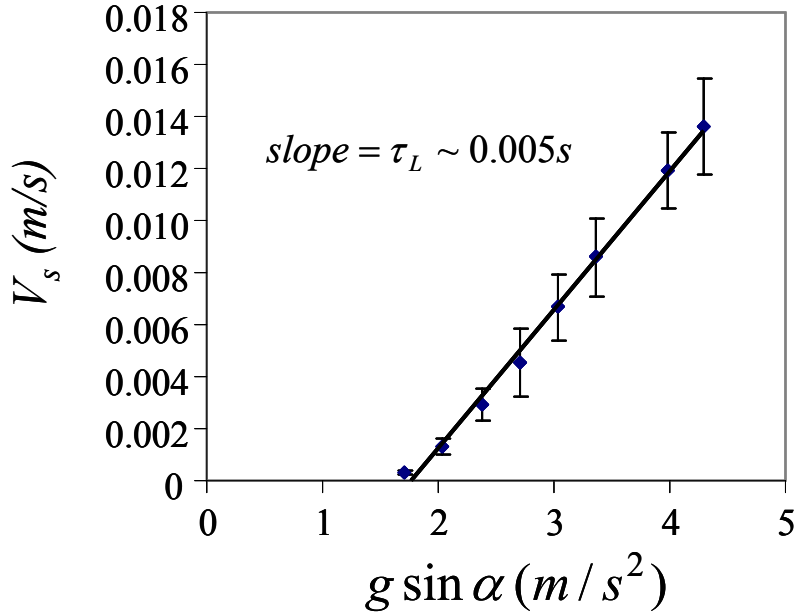
Figure 3.5. Velocity of the sliding of a $10\mu L$ water drop on a silanized (decyltrichlorosilane) silicon wafer as a function of the angle of inclination α. Here, g is the gravitational acceleration.

3.6. Effect of Contact Angle Hysteresis on Drift Velocities

We also studied the effect of contact angle hysteresis on drift velocities of drop subjected to white noise vibration. We carried out the experiments on two different silanized silicon wafers having hysteresis of different magnitudes. The magnitude of hysteresis can also specified by the critical angle of inclination of the solid substrate at which drop starts sliding on its own without applying any external noise. We measured the critical angle for these two substrates which are approximately found to be 10° and 18°. The drift velocities of drops moving on an inclined substrate subjected to white noise

vibration are measured as a function of power of noise are shown in Figure 3.6. As expected from equation 3.10, drift velocity increases non-linearly as a function of power of noise showing a tendency to saturate at higher powers of noise. Also, as expected, the drift velocities of drops on the substrate with higher hysteresis are lower compared to drift velocities on substrate with lower hysteresis. The experimental data is fitted with solid lines obtained using equation 3.10.
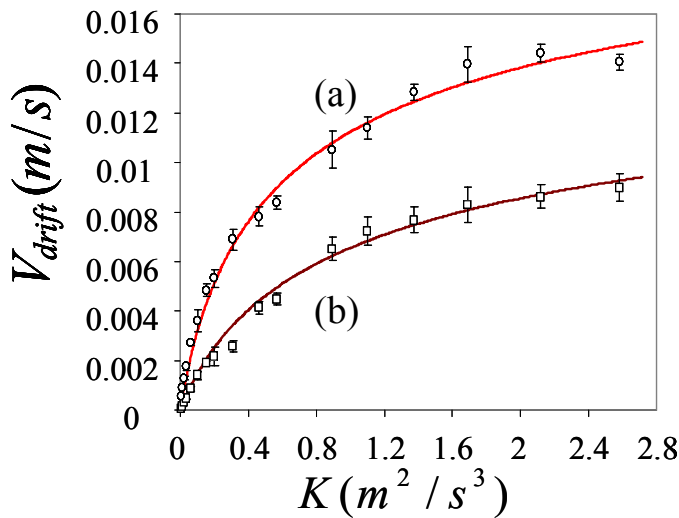
Figure 3.6. Drift velocities of a small water drop (10^{-5} kg) on a hydrophobic (silanized) silicon wafer. These measurements were conducted with an inclined (10°) substrate with low (a) and high (b) hysteresis surface. The experimental data is fitted with solid lines obtained using equation 3.10.

3.7. Effect of External Vibration on Contact Angle Hysteresis

As discussed in the Chapter 1, it is not clear from the previous experimental studies on vibration assisted motion of liquid drop on a solid surface whether the contact angle hysteresis is completely eliminated or not while the drop is moving. There have been several reports[20-22] in the literature that claim that when a liquid drop is moving on a solid surface under the influence of external vibrations, the contact angle

hysteresis is totally eliminated. Contrary to this argument, our hypothesis is that contact angle hysteresis is not completely eliminated and it plays a crucial role when a liquid drop is moving on the solid surface. We use the analogy between the Brownian motion of colloidal particle and liquid drop undergoing Brownian-like motion under the influence external white noise vibration to probe this issue.

As discussed earlier, the drift velocity of a colloidal particle in presence of a bias of magnitude $\bar{\gamma}$ is equal to the Stokes-Einstein limit $\bar{\gamma}\tau_L$ which does not depend of the strength of the noise. Here, in the case of colloidal particle there is only one dissipation mechanism that is due to kinematic friction. However, in the case of water drop moving on a solid surface, there is an additional dissipation mechanism that is due to threshold contact angle hysteresis. As argued by few authors in literature, if contact angle hysteresis is completely eliminated during the vibration induced motion of drop, the drift velocity of drop should be equal to the Stokes-Einstein limit of $\bar{\gamma}\tau_L$. However, as observed from the drift velocities as function of strength of noise plotted in Figures 3. 4 and 3. 6, the drift velocity is not constant and it strongly depends on the strength of noise. Also, the drift velocity at higher strengths of noise did not saturate to the Stokes-Einstein limit of $\bar{\gamma}\tau_L$ in all the experimental data shown. The trends observed from experimental data Figures 3.4 and 3.6 as well as from the prediction of drift velocity from equation 3.10 indicate that the drift velocity of drop saturates asymptotically to hysteresis free drift velocity of Stokes-Einstein limit ($\bar{\gamma}\tau_L$) only in the limit of infinitely high strength of noise (K). Such a high strengths of noise may be impractical to generate in the usual laboratory conditions. These experimental and theoretical observations clearly prove that the contact angle hysteresis is not eliminated when a liquid drop is moving on a

solid surface under the influence of external vibration.

3.8. Motion of Drops on an Energy Gradient Surface

So far we discussed the drift velocities of drops when the external bias applied to the drop is due to gravity. We also carried out experiments of drop motion on an energy gradient surface subjected to external white noise vibration. As schematically shown in Figure 3.7, in this case solid substrate is kept horizontal without any inclination. However, the silicon wafer has a gradient of surface energy i.e. the contact angle on the surface is position dependent. This surface is prepared by coating silicon wafer with gradient of monolayer of decyltrichlorosilane as described below.

surface energy gradient

drop

Vibrating plate ⟷
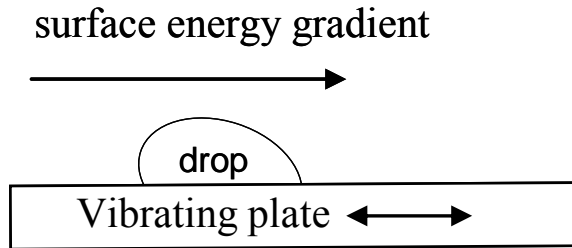
Figure 3.7. Schematic of experimental set up of a water drop on an energy gradient surface (0° inclination) subjected to a white noise vibration.

3.9. Preparation of Energy Gradient Surface

The solid surface used in the experiments is a silicon wafer coated with gradient of self assembled monolayer (SAM) of decyltrichlorosilane (CH_3-$(CH_2)_9$-$SiCl_3$, Gelest Inc.). This surface is prepared using a deposition method used by Daniel and Chaudhury[23] which is described below. Before deposition is carried out, the silicon wafer was thoroughly cleaned as described below. The silicon wafer was placed in Piranha solution (20% Hydrogen Peroxide and 80% Sulfuric Acid by volume) for 30

minutes followed by rinsing with copious amount of distilled deionized (DI) water. After drying with ultra purified nitrogen gas (Praxair Inc.), the silicon wafer was treated with oxygen plasma (model PDC-32G; Harrick Plasma) at 0.2Torr for 45s. The oxygen plasma cleaned silicon wafers are immediately transferred to a Petri dish where a polyester thread soaked in decyltrichlorosilane is stretched rigidly and placed above one end of the silicon wafer. The deposition of silane onto silicon wafer takes place for few minutes. The silane diffuses and deposits non-uniformly onto the silicon wafer. The end of the silicon wafer close to polyester thread has higher concentration of silane where as the far end of the silicon wafer has lower concentration of silane. Such a non-uniform deposition results in gradient of surface energy on the surface. The end of silicon wafer close to the source of silane has high contact angle. The contact angle decreases towards the far end of the silicon wafer. After deposition, the silicon wafer was baked in oven for 15 minutes at $75^{o}C$. After cooling the samples to room temperature, they are rinsed with DI water followed by drying with ultra purified nitrogen gas (Praxair Inc.). The surface is characterized by measuring the static contact angle of deionized liquid drops at various positions on the surface. We plot static contact angles thus obtained as a function of displacement from the end that was close to the polyester thread in Figure 3.8 (a). We also plot cosine of contact angle in Figure 3.8 (b) as a function of displacement which shows that the surface energy gradient is linear.
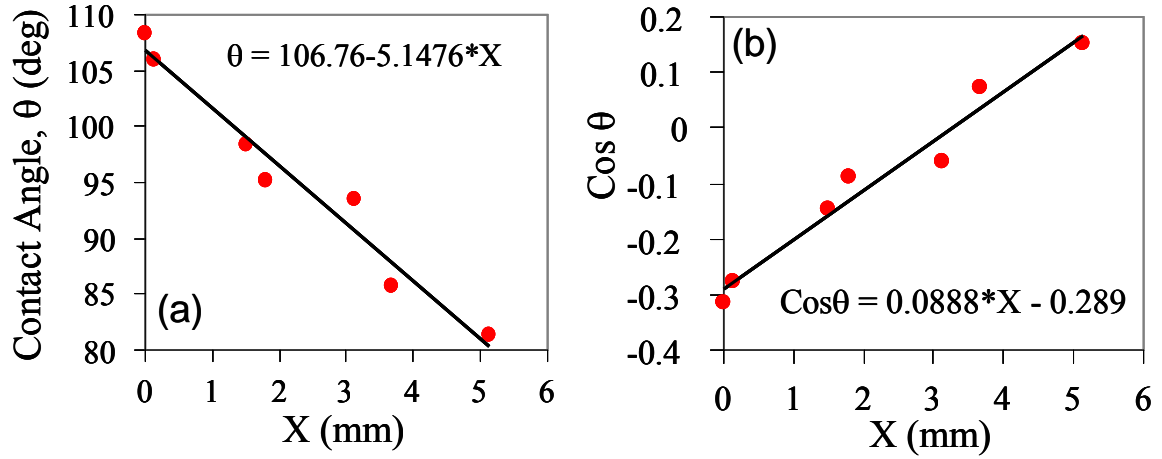
Figure 3.8. Details of contact angle gradient on the surface. (a) Contact angle (θ) as a function of distance (X). (b) $Cos\theta$ as a function of distance (X).

For a liquid drop on a surface energy gradient substrate the driving acceleration for movement is due to change in the free energy of adhesion ($\Delta G = -A\gamma_{lv}(1+\cos\theta))^{23}$ given by

$$\bar{\gamma} = -\frac{1}{m}\left(\frac{d(\Delta G)}{dx}\right) \approx \frac{A\gamma_{lv}}{m}(d\cos\theta/dx) \qquad (3.11)$$

Where A is the base area of the drop and γ_{lv} is the surface tension of water drop. When a water drop of 10^{-5} kg was deposited on the substrate, it shows a very slow movement. However, when a white noise vibration of finite power is applied, the drop drifts down the surface with high velocities. Similar to the drops drifting on an inclined substrate, drift velocity of drops increases non-linearly as a function of power of noise as shown in Figure 3.9. The solid line shown in the figure is a fit to the equation 3.10 with the values of Δ and τ_L as 4.8 m/s^2 and 0.0076 sec respectively.
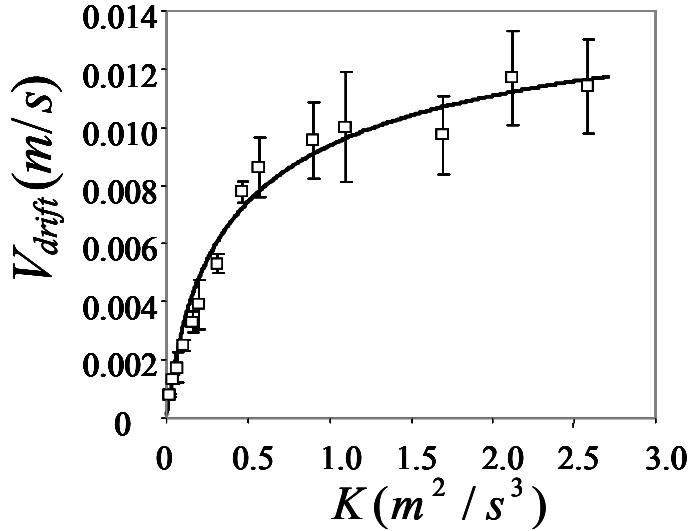
Figure 3.9. Drift velocities of a small water drop (10^{-5} kg) on an energy gradient surface (0° inclination) for which $d\cos\theta/dx \approx 88 \ m^{-1}$. The experimental data is fitted with solid lines obtained using equation 3.10 with the values of Δ and τ_L as 4.8m/s^2 and 0.0076s respectively.

3.10. Displacement Fluctuation Analysis of Drop on Inclined Surface Subjected to White Noise Vibration

So far we looked at the drift velocity of drop as a function of strength of noise and showed that unlike the case of Brownian motion of colloidal particle where drift velocity is independent of strength of noise, the drift velocity of drop is a non-liner function of strength of noise due to the presence of contact angle hysteresis. We also presented an evidence to show that contact angle hysteresis is not eliminated when the drops are moving on a solid surface under the influence of external vibration in usual laboratory conditions where low powers are used. In this section we look at the detailed contact line motion of drop with high speed video recording. Similar to the colloidal particle driven out of equilibrium by thermal fluctuations, the water drop also experiences

fluctuating forces due to white noise. Hence it is driven out of its equilibrium by white noise as well as by applied bias due to gravity. As described earlier, the drop exhibits one dimensional random motion (Figure 3.10) on the surface behaving like a dragged colloidal particle. We recorded the high resolution motion of the contact line of such a drop at 2000 frames/sec. We have examined the fluctuations of contact line of drop at a low power (0.022 m^2/s^3) vibration. Before discussing the experimental results, we focus on theoretical basis for studying the detailed contact line motion of drop. In order to proceed in this direction we look at the Klein-Kramers form of the Fokker-Planck equation[15-18,24] corresponding to equation 3.1 for the transition probability density of velocity $P(V,t)$ as follows:

$$\frac{\partial P(V,t)}{\partial t} = \left[\frac{1}{\tau_L} \frac{\partial(VP)}{\partial V} + \Delta \frac{\partial P(V/|V|)}{\partial V} + \frac{K}{2} \frac{\partial^2 P}{\partial V^2} \right]$$
(3.12)

Steady state solution of the above Fokker-Planck equation has an exponential term as shown below[16].

$$P(V) = P_o \exp\left(-\frac{V^2}{K\tau_L} - \frac{2|V|\Delta}{K} + \frac{2V\bar{\gamma}}{K} \right)$$
(3.13)

If we replace $V = x/\tau*$ where $\tau* = 0.0005\,\sec$ corresponding to time resolution of high speed video recording, we get

$$P(x) = P_o \exp\left(-\frac{x^2}{K\tau_L\tau*^2} - \frac{2|x|\Delta}{K\tau*} + \frac{2x\bar{\gamma}}{K\tau*} \right)$$
(3.14)

This steady state solution for the probability distribution of displacement has a Gaussian term $\left(\exp\left(-x^2/K\tau_L\tau*^2\right)\right)$, an exponential term $\left(\exp\left(-2|x|\Delta/K\tau*\right)\right)$ and a bias

79

term $\left(\exp\left(2x\bar{\gamma}/K\tau^{*}\right)\right)$. This shows that in the absence of contact angle hysteresis $(\Delta=0)$, the displacement distribution is Gaussian with non-zero mean. However, in presence of contact angle hysteresis $(\Delta\neq 0)$, displacement distribution is non-Gaussian with non-zero mean. Here, the displacement distribution is Gaussian at $x\sim 0$, with exponential tails at $x\gg 0$. Also, the distribution is asymmetric. We expect that the distribution of displacement obtained in the experiments would be asymmetric non-Gaussian with exponential tails. Here, we use five experimental realizations each lasting about 1.8 seconds for this analysis. An example of such an experimental realization is shown in Figure 3.10.
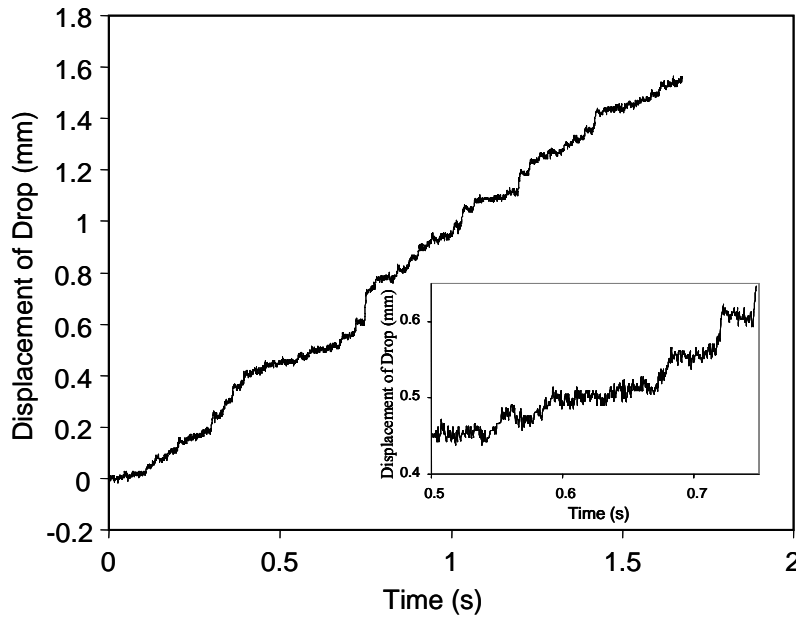
Figure 3.10. Displacement of a water drop on a silanized silicon wafer subjected to a white noise vibration of power 0.022 m^2/s^3.

In order to see whether the experimental displacement distribution is Gaussian or not, we plot (Figure 3.11) the probability distributions x_T by non-dimensionalizing it as follows: $(x_T - x_p)/\sigma_{x_T}$, σ_{x_T} being the standard deviation of x_T and x_p is the

80

displacement value at the peak of the distribution function, which is not all that different from the mean displacement x_m. The distribution is more Gaussian near the center, but then it becomes exponential as we move away from the center of the distribution. However, for these Gaussian noise induced displacement fluctuations, an asymmetry can be observed.

Here, the evidence that the displacement distribution is asymmetric and non-Gaussian clearly disproves several reports in the literature which suggest that the hysteresis itself may disappear with the vibration of a drop[20-22]. If this were the case, i.e. $\Delta = 0$, the displacement distribution would be symmetric and Gaussian. This is clearly not the situation in our case as we obtain an asymmetric and non-Gaussian distribution. However, this observation opens up a new question as to how the displacement fluctuation behaves if the hysteresis truly disappear, which may be the case at a very high power of noise.
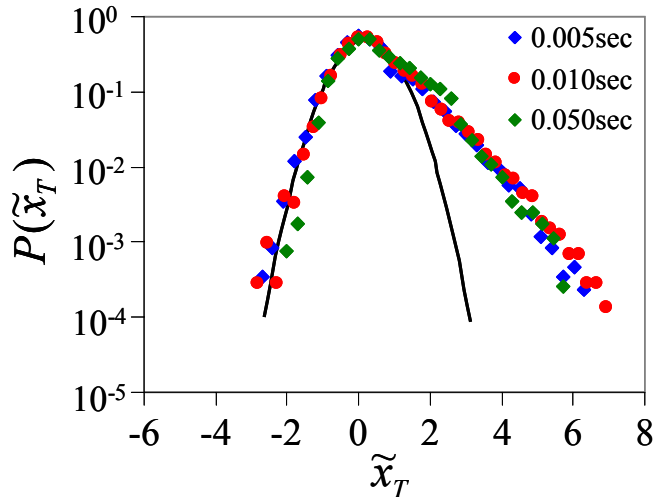
Figure 3.11. Probability distribution of normalized displacement $\left(\tilde{x}_T = \left(x_T - x_p\right)/\sigma_{x_T}\right)$ of a water drop moving on an inclined surface. The drop is subjected to Gaussian noise of power 0.022 m^2/s^3. The solid symbols are experimental data. Solid black line is a Gaussian fit to the data. The displacement distribution at all the time steps shown in the figure is asymmetric and non-Gaussian.

3.11. Quantifying the non-Gaussianity of Displacement Distributions

In order to quantitatively show the non-Gaussianity and asymmetry of the displacement distributions, we approximated the tails of distribution by a stretched exponential function as shown below.

$$P(\tilde{x}_T) = P_o \exp\left(-|\tilde{x}_T|^n + C\right) \qquad (3.15)$$

Here C is a numerical constant and n is the exponent of stretched exponential fit to the tails of the distribution. If the displacement distribution is symmetric and Gaussian, the exponent n for the left and right tails of the distribution would be equal to 2. Also, if the exponents of right and left arms are not equal to each other, then the distribution is asymmetric. We plot the tails of distributions at various 'T' values using the following expression and calculate n for left and right arms of the distributions.

$$\ln\left(-\ln(P/P_o)\right) = n \ln\left(|\tilde{x}_T|\right) + C_1 \qquad (3.16)$$

As observed from Figure 3.12, which shows stretched exponential fits to the displacement distribution at various times, the exponents are not equal to 2. This observation quantitatively shows that displacements distributions are non-Gaussian. Also, except for very short time (*T=0.001sec*) the exponents of the fits are not the same for right and left arms which also quantitatively shows that the displacement distributions are asymmetric. These quantitative observations clearly point out the contact angle hysteresis is not eliminated when the drops are moving on a surface under the influence of external vibration.
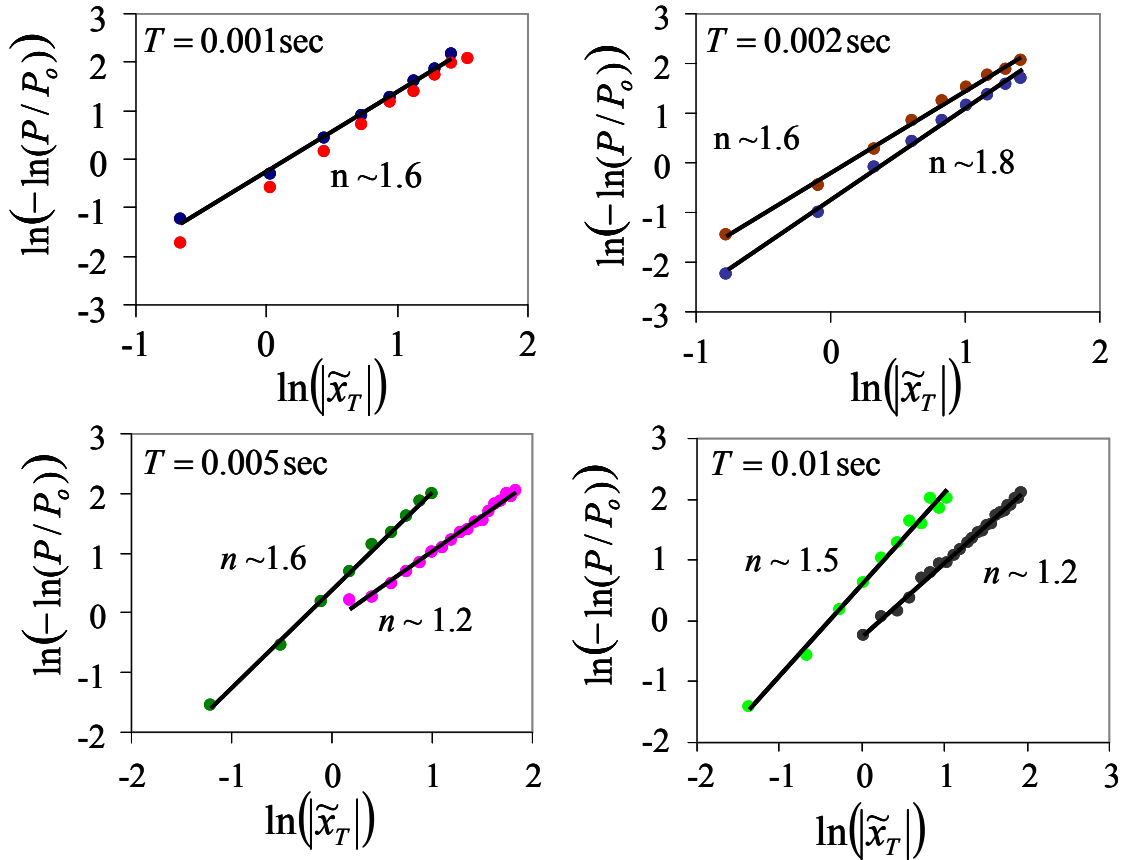
Figure 3.12. Stretched exponential fits to the right and left arms of experimental displacement distributions at various times for a water drop moving on an inclined surface subjected to Gaussian noise of power 0.022 m^2/s^3.

3.12. Displacement Fluctuation Analysis of Drop on an Energy Gradient Substrate Subjected to White Noise Vibration

We also analyzed the displacement fluctuation of water drop on the gradient surface (Figure 3.7) when subjected to a low power ($0.022 m^2/s^3$) vibration. We recorded the high resolution motion of the contact line of such a drop at 2000 frames/sec. We examined the fluctuations of contact line of drop by studying the stochastic movements of drop relative to a plate. A total of five tracks, each lasting about 3 seconds, were used for this analysis.
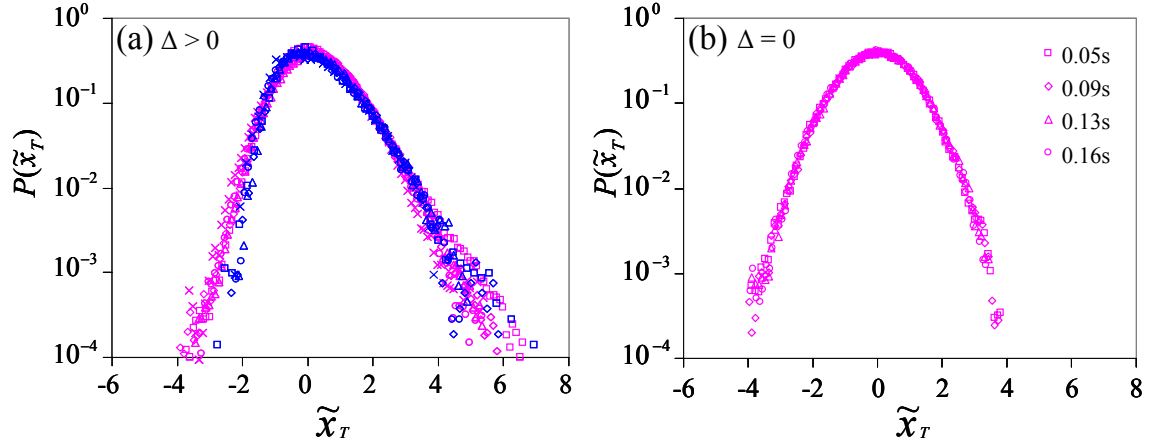
Figure 3.13. (a) Probability distribution of normalized displacement $\left(\tilde{x}_T = (x_T - x_p)/\sigma_{x_T}\right)$ of a water drop moving on an energy gradient surface at time intervals: 0.02s (□), 0.05s (◊), 0.08s (Δ), 0.12s (o) and 0.2s (×). The drop is subjected to Gaussian noise of power 0.022 m²/s³. The blue and pink colors indicate experimental data and simulation results respectively. (b) In the absence of hysteresis ($\Delta = 0$) from the simulations, the distribution is purely Gaussian.

We also attempted to understand how the displacement fluctuations should behave by solving equation 3.1 numerically. Numerical integration of the modified Langevin equation (equation 3.1) is carried out using a generalized integration method for stochastic differential equations as outlined by Gillespie[25]. The update formula for the stochastic output variable (velocity or displacement) consists of rescaling stochastic input (acceleration, $\gamma(t)$) to simulations in order to match strength of noise (K) in simulations to strength of noise in experiments. We generated zero mean Gaussian random numbers using Matlab® which are then rescaled to match strength of noise ($K = \sum_{i=1}^{N} \gamma(t)_i^2 \Delta t / N$) in simulations to the experiment and then used as input accelerations in the simulations. Here $\gamma(t)$ is the acceleration, Δt is the integration time step, N is the number of input accelerations used in the simulations. Since the hysteresis force $\sigma(V)\Delta$ always acts in the

direction opposite to the motion of the contact line, $\sigma(V)$ is set as $V/|V|$ in the simulations. When the net acceleration $|\bar{\gamma}+\gamma(t)|$ acting on the drop is less than the threshold acceleration $(\Delta = 4.8m/s^2)$ required to set the contact line into motion, the contact line gets stuck, hence the velocity is set to zero. The modified Langevin equation is integrated with an integration time step of Δt =0.0005s which is the resolution time of camera. The simulations are carried out for 50 tracks with a total integration time of 10sec for each track. The displacement data for a given time interval 'T' obtained from several tracks are combined to obtain a probability distribution for displacement as is done for the experimental analysis of the displacement data. We plot (Figure 3.13) the non-dimensional probability distributions of x_T from experiments as well as from numerical simulations. Similar to the drop moving on an inclined surface as discussed in previous section, here also the displacement distributions are non-Gaussian and asymmetric. We also carried out a simulation by switching off contact angle hysteresis. Here Δ is set as zero. As observed from Figure 3.13 (b) the displacement distribution is clearly Gaussian emphasizing the role of contact angle hysteresis in non-Gaussianity. In order to quantify the non-Gaussianity and asymmetry we plot the stretched exponential fits to the displacement distribution at various times. As observed from Figure 3.14, which shows stretched exponential fits to the experimental displacement distributions at various times, the exponents are not equal to 2. This observation quantitatively shows that displacements distributions are non-Gaussian.
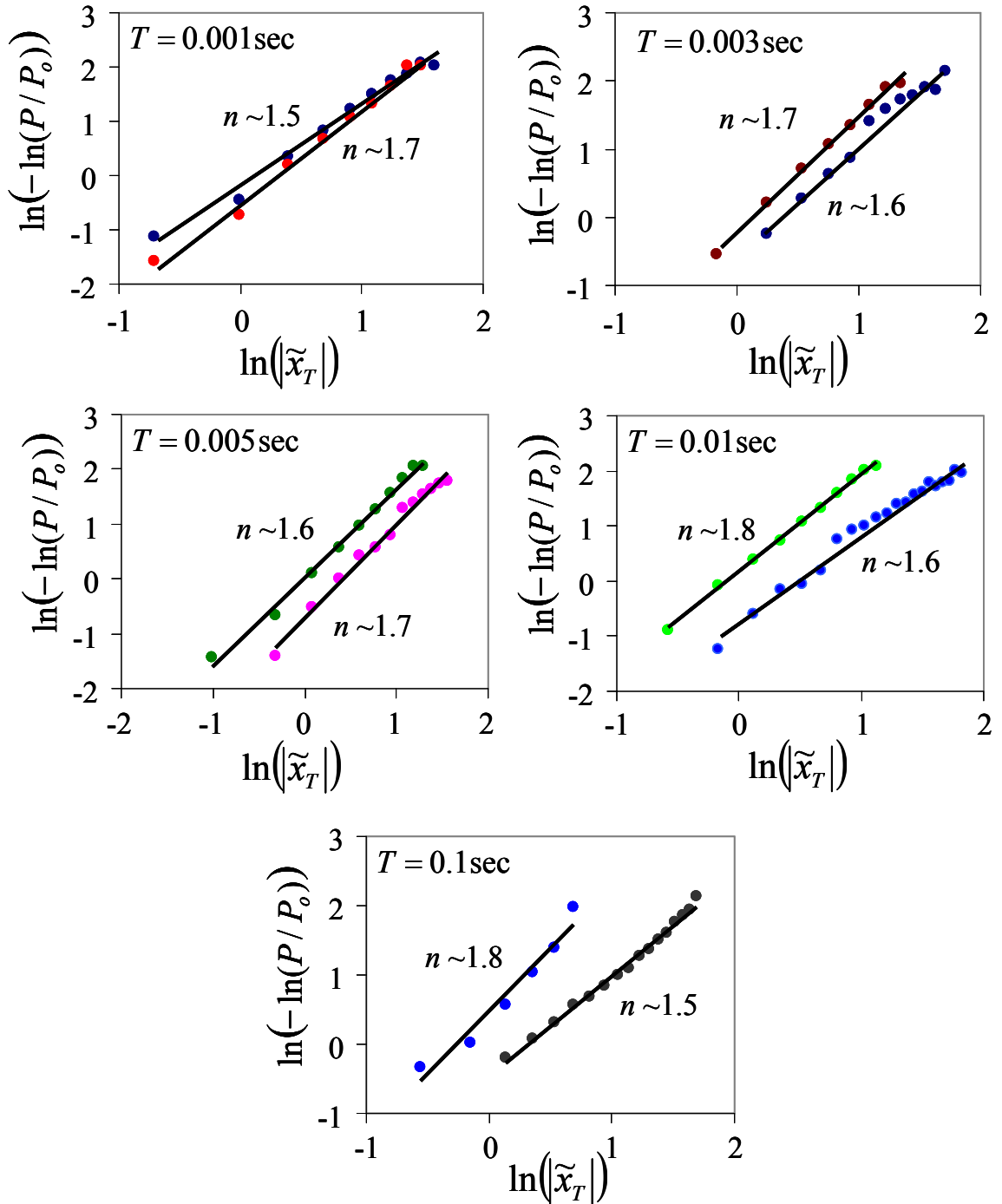
Figure 3.14. Stretched exponential fits to the right and left arms of experimental displacement distributions at various times for a water drop moving on energy gradient surface subjected to Gaussian noise of power 0.022 m^2/s^3.

3.13. Diffusivity Analysis

As mentioned earlier, for a colloidal particle undergoing Brownian motion, the velocity correlation is exponential; hence the diffusivity scales linearly $(D = K\tau_L^2 / 2)$ a function of power of external noise. However, in presence of threshold contact angle hysteresis the velocity correlation for a liquid drop undergoing Brownian like motion is not exponential. de Gennes[15] derived approximate scaling laws for diffusivity of either a solid block or a liquid drop moving on a substrate as a function of strength of noise as well as the threshold resistance (Δ) due to Coulombic friction or contact angle hysteresis. These scaling laws are derived ignoring kinematic friction altogether. We outline scaling laws for diffusivity below.

$$D \sim V_A^2 \tau_\Delta \sim \frac{K^2}{4\Delta^2} \tau_\Delta \qquad (3.17)$$

Here V_A is velocity amplitude and $\tau_\Delta \sim K / \Delta^2$ is correlation time for velocities in presence of hysteresis. Substituting $\tau_\Delta \sim K / \Delta^2$ into equation 3.17 results in the following scaling law for diffusivity.

$$D \sim \frac{K^3}{4\Delta^4} \qquad (3.18)$$

We wanted to check whether the diffusivity of liquid drop matches with this scaling law at the power of noise K = 0.022 m^2/s^3 used in the experiment. In order to calculate the diffusivity, we plot the variance of the displacement distribution of drop as a function of time as shown in Figure 3.15 for the case of drop moving on an inclined surface under the influence of white noise vibration. Here, the motion of liquid drop is diffusive as the

variance is linear with time. The diffusivity is half of the slope of variance versus time. The experimental diffusivity thus obtained is 1×10^{-8} m^2/s where as the scaling law predicts 1.8×10^{-8} m^2/s. Similarly, for liquid drop moving on an energy gradient surface experimental diffusivity is 8×10^{-9} m^2/s where as the scaling law predicts diffusivity as 4×10^{-9} m^2/s. These scaling laws are very crude for the liquid drop as the dissipation due to kinematic friction at the contact line is significant compared to the dissipation due to threshold contact angle hysteresis. However, it is surprising that the numerical simulations that include kinematic friction also predict diffusivity as 4×10^{-9} m^2/s. Nevertheless, these scaling laws give approximate theoretical values for diffusivity to compare the experimental data with. However, it is very interesting to check how the diffusivity scales with the strength of the noise. More experiments at various powers of noise are needed to verify this scaling law that is left for future work.
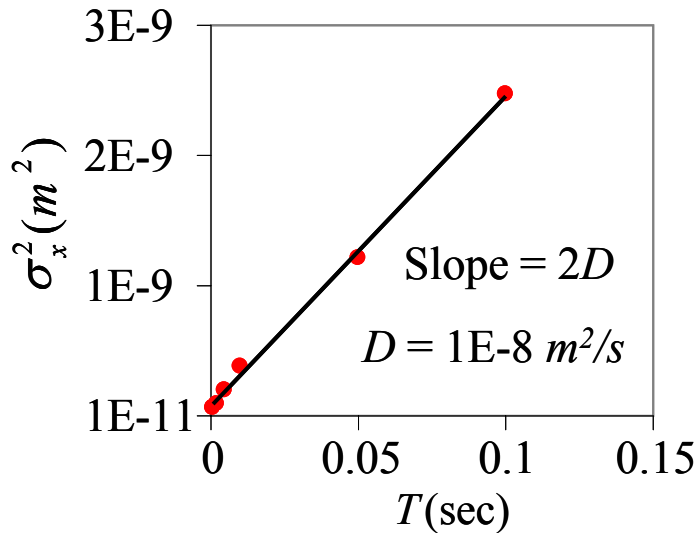
Figure 3.15. Plot of the variance (σ_x^2) of the displacement of the drop as function of time. The diffusivity is calculated from the slope of linear plot.

3.14. Work Fluctuation Relation

As described earlier, liquid drop shows drifted Brownian like motion when subjected to external white noise vibration on the inclined surface as well as on energy gradient surface that is kept horizontal. The contact line of the drop shows forward and backward motion on the surface due to random accelerations from white noise vibration, however showing a net drift on the surface. There are two types of external work being done on the drop; the first one is by vibration and second by gravity. The work done by external vibration on the drop over a time periods of T is given by

$$\int_{t}^{t+T} \gamma(t)V(t)dt \qquad (3.19)$$

Here $\gamma(t)$ random acceleration of drop due to white noise excitation and $V(t)$ is the velocity of contact line of drop. The work done by gravity on drop is given by

$$W_T^* = Mg\sin\alpha \sum_{t=t_i}^{t=t_i+T} \Delta x(t) \qquad (3.20)$$

Here M is the mass of the drop, g is acceleration due to gravity, α inclination of the surface, $\Delta x(t)$ displacement of drop over time period T. Here, due to the fluctuating nature of $\gamma(t)$, the velocity $(V(t))$ and displacement $(\Delta x(t))$ of contact line of drop can either have positive or negative values that result in the work done also to have positive and negative values. The drop is driven out of equilibrium by external vibration as well as by gravity. In the context of systems driven out of equilibrium by external driving, there have been few universal non-equilibrium relations proved recently[26-32] that are called "work fluctuation theorems". The steady state fluctuation theorem[32] states that at steady state as $T \rightarrow \infty$, the ratio of probability of finding positive work to the negative work is

exponential of the work. These work fluctuations have been verified by experimental studies as carried out by the dragging[33,34] of a fluctuating colloidal bead with an optical tweezers, vibrating granular particles[35], and the fluctuation of a torsional pendulum suspended in a liquid under external forcing[36]. In this study we focus on work done by gravity on the drop. The estimation of vibrational work involves measuring the accurate and simultaneous measurement of acceleration experienced by the drop due to external vibration as well as the velocity. Measuring these quantities at the same time is very cumbersome. Also, the estimation of velocity is not as accurate as of the estimation of displacement required for determining the work done by gravity. So we analyze the work fluctuation relations for the external work done by gravity on the drop.
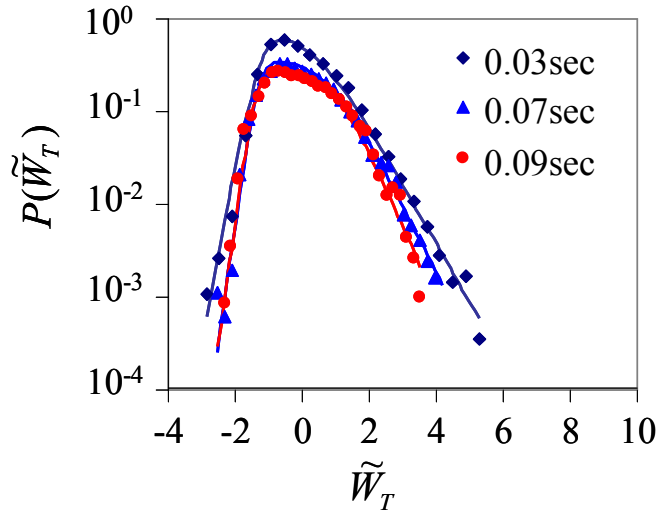
Figure 3.16. Probability distribution of normalized work $\left(\widetilde{W}_T = (W_T - \langle W_T \rangle)/\sigma_{W_T}\right)$ of a water drop moving on an inclined surface. The drop is subjected to Gaussian noise of power 0.022 m^2/s^3. The solid symbols are experimental data. Solid lines are asymmetric double sigmoid fits to the data. The work distribution at all the time steps shown in the figure is asymmetric and non-Gaussian.

Here, we examine the steady state work fluctuation of contact line fluctuations of drop by studying the stochastic movements of several small (10^{-5} kg) drops

relative to a plate when subjected to a low power (0.022 m^2/s^3) vibration. A total of five

tracks, each lasting about 1.8 seconds, were used for this analysis. An example of such a

track is shown in figure 3.10. According to the steady state fluctuation theorem[31],

$$\frac{P_S(W_T)}{P_S(-W_T)} = e^{W_T} \text{ as } T \to \infty \tag{3.21}$$

Here $W_T = W_T^*/(MK\tau_L/2)$ is the amount of non-dimensional work performed on the drop

by external bias for a duration T. We plot the normalized work distribution at various T

values in Figure 3.16. Similar to the displacement distribution as shown Figure 3.11, the

work distribution is also asymmetric and non-Gaussian. We could fit this data using an

asymmetric double sigmoid function which has exponential tails. In order to check

whether the work done by gravity follows conventional steady state fluctuation theorem

we plot the logarithm of ratio of probabilities of finding positive work to the probability

of finding the negative work of the same quantity as function of work. As there is an

extra dissipation due to contact angle hysteresis we expect that conventional work

fluctuation theorem is not valid in this case. This is due to the fact that the velocity

correlation is not exponential due to presence of hysteresis. In fact, we observed that the

data at various times did not collapse and did not follow steady state fluctuation theorem

when plotted in conventional way of plotting equation 3.6. However, when work values

are rescaled as $W_T = W_T^*/(0.6*MK\tau_L/2)$ and plotted as below we observe the collapse of

data as observed in Figure 3.17

$$\frac{\sigma_{W_T}^2}{2\langle W_T \rangle^2} \ln\left(\frac{P_S(+W_T)}{P_S(-W_T)}\right) = W_T \tag{3.22}$$

Such an unconventional work fluctuation theorem emphasizes the importance of role

91

played by hysteresis on drop motion.
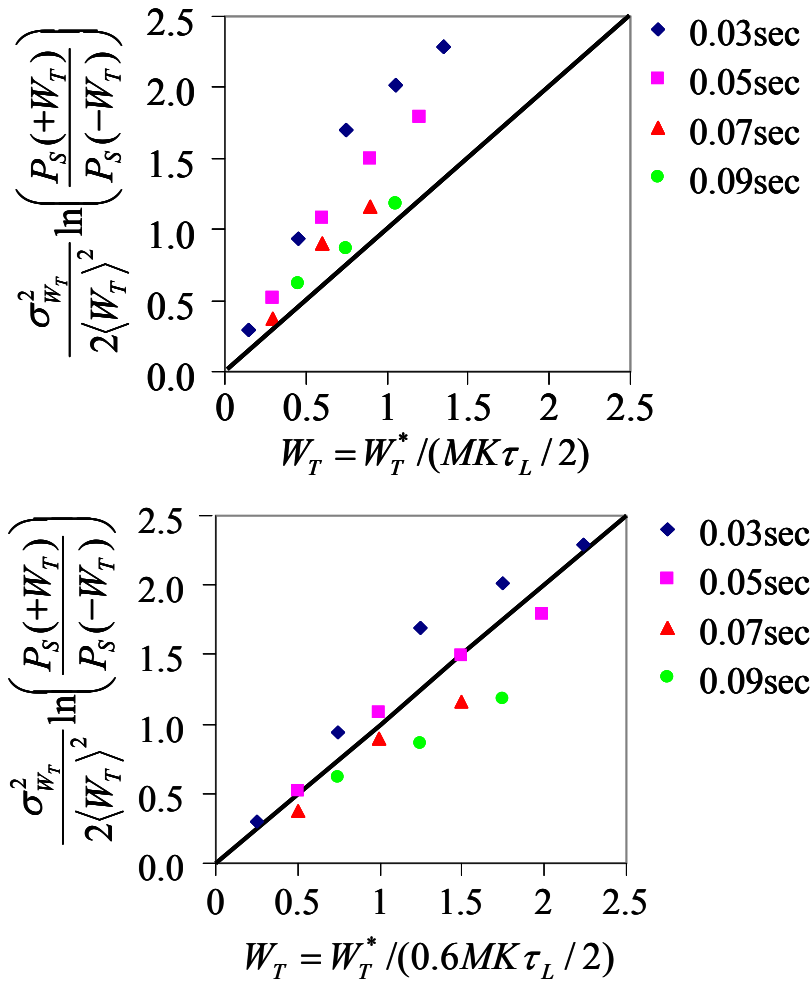
Figure 3.17. (top) Work fluctuation plot of non-dimensional work $\left(W_T = W_T^* /(MK\tau_L /2)\right)$ of a water drop moving on an inclined surface. Here the data collapses but does not follow fluctuation theorem **(bottom)** Work fluctuation plot of rescaled non-dimensional work $\left(W_T = W_T^* /(0.6 * MK\tau_L /2)\right)$ follows fluctuation theorem. The drop is subjected to Gaussian noise of power 0.022 m^2/s^3. The solid symbols are experimental data.

3.15. Conclusions

We studied the drifted Brownian like motion of a liquid drop on an inclined and on an energy gradient surface when subjected to external white noise vibration. Unlike the drift velocity of colloidal particle which is independent of strength of the noise, the drift velocity of drop is a non-linear function of strength of noise. The non-linearity results from threshold contact angle hysteresis force. The drift velocity of drop does not saturate to Stokes-Einstein limit indicating that the contact angle hysteresis plays crucial role in the contact line motion of drop. This provides solid evidence to our hypothesis that in usual laboratory conditions where low powers of noise are used, the contact angle hysteresis is not eliminated. The displacement distribution of drop is found to be non-Gaussian and asymmetric with exponential tails. The observed non-Gaussianity is due to the non-linearity resulting from contact angle hysteresis. We quantified the non-Gaussianity and asymmetry in the displacement distribution by fitting the tails to a stretched exponential function. We also studied the detailed contact lime fluctuations of drop in order to check whether the work done by gravity on the drop follows conventional work fluctuation theorem. We showed that the work distribution does not follow conventional fluctuation theorem due to the presence of contact angle hysteresis. Unlike the case of a colloidal particle the correlation in the case of drop does not follow exponential correlation. Here, the contact line fluctuations of drop follow a different work fluctuation relation that is obtained by rescaling the work.

3.16. References

1. Brown, R. *Phil. Mag.* **1828**, *4*, 161.

2. Sutherland, W. *Phil. Mag.* **1902**, *3*, 161

3. Einstein, A. *Ann. Phys.* **1905**, 17, 549, Edited by R. Furth, translated by A.D. Cowper, Dover Publications Inc., **1956,** pp. 1-18.

4. Smoluchowski, M. V. *Ann. Phys. (Leipzig).* **1906**, *21*, 756.

5. Langevin, P. *C. R. Acad. Sci. (Paris).* **1908**, *146*, 530. Translated by Lemons, D. S. and Gythiel, A. *Am. J. Phys.* **1997**, 65, 1079.

6. Chandrasekhar, S. *Rev. Mod. Phys.* **1943**, *15*, 1.

7. Chandrasekhar, S. Rev. *Mod. Phys.* **1949**, *21*, 383.

8. Kubo, R. *Rep. Prog. Phys.* **1966**, *29*, 255.

9. Daniel, S.; Chaudhury, M. K.; Chen, J. C. *Science*. **2001**, *291*, 633.

10. Caughey T.K; Dienes J. K. *J. Appl Phys*, **1961**, *32*, 2476.

11. Caughey T. K. *J. Acoust. Soc. Am.* **1963**, *35*, 1706

12. Johnsen J. M.; Naess A. *Structural Dynamics*, EURODYN'93, Moan et al (eds), 1993 Balkerna, Rotterdam, ISBN 90 5410336 1.

13. Ahmadi, G. *Int. J. Eng Sci*. **1983**, *21*, 93.

14. Crandall, S. H.; Lee, S. S; Williams Jr., J. H. *J. Appl. Mech*. **1974**, *42*. 1094.

15. De Gennes, P. -G. *J. Stat. Phy*s. **2005,** *119*, 953.

16. Chaudhury, M. K.; Mettu, S. Langmuir 2008,

17. Kawarada, A.; Hayakawa, H.; *J. Phys. Soc. Jpn.* **2004**, *73*, 2037.

18. Hayakawa, H. *Physica D* **2005**, *205*, 48.

19. Mauger, A. *Physica A* **2006**, *367*, 129.

20. Brunet, P.; Eggers, J.; Deegan, R. D. *Phys. Rev. Lett.* **2007**, *99*, 144501.

21. John, K.; Hanggi, P.; Thiele, U. *Soft Matter* **2009**, *4*, 1183.

22. Thiele, U.; John, K. *Chem. Phys* **2010**, *375*, 578.

23. Daniel, S.; Chaudhury, M. K. *Langmuir* **2002**, *18*, 3404.

24. Risken, H., *The Fokker–Planck Equation, Methods of Solution and Applications*, 2nd ed.; Springer-Verlag: Berlin, Heidelberg and New York. 1989.

25. Gillespie, D. T. *Am. J. Phys.* **1996**, *64*, 225.

26. Gallavotti, G.; Cohen, E.G.D. Phys. Rev. Lett. 1995, 74, 2694.

27. Gallavotti, G.; Cohen, E. G. D. J. Stat. Phys. 1995, 80, 931.

28. Evans, D. J.; Cohen, E.G.D.; Morriss, G.P. Phys. Rev. Lett. 1993, 71, 2401.

29. Evans, D. J.; Searles, D. J. Phys. Rev. E 1994, 50, 1645.

30. Evans, D. J.; Searles D. J. Adv. Phys. 2002, 51, 1529.

31. van Zon, R.; Cohen, E.G.D. Phys. Rev. E 2003, 67, 046102.

32. van Zon, R.; Cohen, E.G.D. Phys. Rev. Lett. 2003, 91, 110601.

33. Wang, G.M.; Sevick, E. M.; Mittag, E.; Searles D. J.; Evans, D. J. Phys. Rev. Lett. 2002, 89, 050601.

34. Imparato, A.; Peliti, L.; Pesce, G.; Rusciano, G.; and Sasso, A.; Phys. Rev. E 21, 2007, 76, 050101.

35. Douarche, F.; Joubaud, S. ; Garnier, N. ; Petrosyan, A.; Ciliberto, S. *Phys. Rev. Lett.* **2006,** *97*,140603.

36. Feitosa, K.; Menon, N. *Phys. Rev. Lett.* **2004**, *92*, 164301.

Chapter 4: Relaxation Behavior of Contact Line of a Liquid Drop on a Solid Substrate Subjected to White Noise Vibration

4.1. Introduction:

Wetting of a solid substrate by liquids is encountered in many technological processes such as surface coating, printing, waterproofing, cleaning and lubrication[1,2,3]. Wetting also plays a fundamental role in designing and improving the efficiency of micro and nanofluidic applications[3]. It has also been found that wetting acts as a useful mechanism in many natural systems such as lotus leaves and all of the plants[3]. Hence, studying wetting and spreading behavior of liquids on solid substrate is of fundamental importance[1]. As described earlier, when a liquid drop contacts an ideally smooth and chemically homogenous solid substrate, three phase contact line of drop makes an equilibrium angle with solid substrate given by Young's law[4]

$$\gamma_{lv} \cos\theta_e = \gamma_{sv} - \gamma_{sl} \tag{4.1}$$

Where θ_e is equilibrium contact angle and $\gamma_{sv}, \gamma_{sl}, \gamma_{lv}$ are interfacial tensions of solid-vapor, solid-liquid, and liquid-vapor respectively. However, when a liquid drop contacts a solid substrate which is neither ideally smooth nor chemically homogenous, the contact angle formed by the drop is not always the equilibrium contact angle predicted by Young's equation. As described earlier in earlier chapters, a sessile liquid drop on solid substrate can subtend a range of contact angles from receding angle to advancing angle. The difference between advancing and receding angles is called contact angle hysteresis $(\theta_R - \theta_A)$.

Contact angle hysteresis is interpreted as a phenomenon resulting from

chemical heterogeneity and physical roughness of solid substrate. It has been pointed out by Good[5-7] that roughness and heterogeneity of solid substrate modify the parabolic free energy profile of drop to a corrugated energy profile with metastable equilibrium states. In case of a solid substrate that is contact angle hysteresis free, if the contact angle of the drop on such as surface is increased or decreased beyond its equilibrium value (θ_e), the contact angle of the drop is readily restored to its equilibrium like a spring. Here spring constant proportional to the surface tension of liquid (γ_{lv}). However, in presence of contact angle hysteresis, drop shows multiplicity of contact angles ranging from receding angle (θ_R) to advancing angle (θ_A). The drop can get stuck to any of metastable states due to the corrugated nature of free energy profile that prevents the drop from relaxing to global equilibrium state[5-10]. These contact angles correspond to the local minima of these metastable equilibrium states. Johnson and Dettre[8-10] developed a detailed model for contact angle hysteresis on a heterogeneous solid substrate and shown that the contact angle hysteresis is controlled by vibrational energy available to drop as well as free energy barriers between each of the metastable equilibrium states. They suggested that the energy required in overcoming metastable equilibrium states can be supplied to the drop in the form of vibrational energy. Given sufficient vibrational energy the drop would relax to global equilibrium state. Subsequent simulation studies as carried out by Marmur[11-13] showed that the advancing contact angle would decrease and receding angle would increase relaxing to equilibrium contact angle if energy is available to overcome the metastable equilibrium states.

The concept of metastable equilibrium states in free energy of drop has also been investigated in many experimental studies[14-18]. Smith and Lindberg[14] carried out

first such an experimental study on the effect of acoustic vibrational energy on contact angle measurements showing that the contact angle relaxes towards equilibrium when supplied with acoustic vibrational energy. Andrieu et al[15] studied the effect of vibrational energy on the advancing and receding contact angles. They subjected a liquid drop on a solid substrate to harmonic vibration of varying amplitudes and found that, at high enough amplitudes of vibration, both the advancing and receding angles relaxed to the same equilibrium angle. Cosine of final equilibrium angle was found to be the average of cosine of advancing and receding angles. In a similar experimental study with a solid plate immersed and removed from a pool of liquid, Decker and Garoff[17] studied the effect of vibrational noise on the advancing, receding contact angles and capillary rise heights. They used pulsed vibrational noise to study the effect of individual noise pulses and also the accumulated effect of multiple noise pulses on metastable equilibrium states of contact angles and capillary rise heights. It was shown that contact angles and capillary rise height reached equilibrium values only after the application of many vibrational pulses. They found that contact angle and capillary heights relax to the same equilibrium state both from advancing and receding modes. In a recent experimental study, Meiron et al[18] established optimal conditions for measuring equilibrium contact angle corresponding to global energy minimum. They placed liquid drop on rough solid substrate and applied vertical sinusoidal vibrations to allow the drop to reach global energy minimum state. They concluded that contact angle hysteresis disappears when drop reaches global energy minimum state. Similar experiments studies carried out by Bormashenko et al[19-21] deal with Cassie-Wenzel wetting transition of a drop on a solid substrate subjected to vibrations. Liquid drops sitting on rough surface when

subjected to vibration penetrate the cavities and show transition from Cassie to Wenzel state. Noblin et al[22,23] studied the transition of contact line of drop from pinned state to moving state when subjected to vertical harmonic vibrations of high enough amplitudes. They showed that the contact line is in pinned state at low amplitudes, shows stick-slip regime at intermediate amplitudes, showing a freely moving state at very high amplitudes of vibration.

The experimental studies available in the literature about drops subjected external vibration consist of studying the final contact angle of drop as a function of amplitude of vibration to establish the optimal conditions for measuring true equilibrium contact angle on a solid substrate. Another aim of these studies was to show that the contact angle reached from both advancing and receding modes is equal to the equilibrium contact angle. However, there are no experimental or theoretical studies in the literature which looked at time dependent kinetic behavior of a drop at non-equilibrium state relaxing to equilibrium state under the influence of external vibration. In all of the experimental studies described above, striking conclusion is that contact angle hysteresis totally disappears when contact angle reaches equilibrium angle. In recent experimental studies carried out by Brunet[24], Thiele and John et al[25,26] , the authors claim that contact angle hysteresis is completely eliminated when a liquid drop is moving under the influence of external vibration. However, it is not clear from these experimental studies whether contact angle hysteresis is eliminated completely or there is a relaxation time associated with the process. If there is any relaxation time associated with the process, its dependency on the strength of vibration used is unknown. Also, the nature of relaxation from non-equilibrium state to equilibrium   is not studied in the previous experiments. In

order to elucidate the nature of relaxation, we studied detailed kinetics of drop relaxing to equilibrium under the influence of external white noise vibration.

In most of the previous experimental studies harmonic vibration has been used[14,15,18-23]. However, we subjected drop in non-equilibrium state to white noise vibration in our experiments. The rational for using white noise vibration instead of harmonic vibration is as follows. The first reason being, power spectrum of white vibration is flat in which all frequencies have equal power. This ensures that all possible vibration modes of drops are excited resulting in the effective relaxation of drop from non-equilibrium to equilibrium. The second reason being, when the drop is in non-equilibrium state, the noises that the drop experiences from disturbances in environment are random in nature which can be approximated as a Gaussian white noise. Also, the fluctuations in thermal environment in the vicinity of contact line are also approximated as a Gaussian white noise that results in the fluctuations of the contact line of drop about the mean position. Many natural systems (Chemical reactions, radio active decay and colloidal particle in a potential well) that are in non-equilibrium state relaxing towards equilibrium state are driven by thermal Gaussian white noise. In order to mimic the natural noise that the drop experiences as well as for the effective relaxation of drop, Gaussian white noise is an appropriate choice in driving the drop from non-equilibrium state to equilibrium state rather than using harmonic vibrations.

We carry out our experimental analysis in terms of radius of drop (a) rather than the traditional way of analyzing in terms of contact angles (θ) due to the ease of analysis of experimental data. Another advantage of working in terms of radius of drop is that the errors associated with measuring contact angles from experiments are completely

eliminated.

When a sessile drop on a solid substrate makes an angle θ other than the equilibrium contact angle θ_e there is always constant driving force acting on the contact line of drop that tries to relax the drop to equilibrium state (Figure 4.1). The driving force[22,23] is equal to $-2\pi\gamma_{lv}(a-a_o)$ where a is radius of drop corresponding to contact angle θ other than equilibrium contact angle and a_o is radius of drop corresponding to equilibrium contact angle (θ_e). When there is no contact angle hysteresis, if the radius (or contact angle) of the drop is increased or decreased beyond its equilibrium value a_o (or θ_e), drop is readily restored to its original position. However, in presence of hysteresis, drop can get stuck at any radius ranging from a_A (or θ_A) to a_R (or θ_R) which correspond to drop radius at advancing and receding angles (Figure 4.1). The contact line of drop has to overcome the resistance due to contact angle hysteresis before retracting or advancing. However, when external energy is supplied to the drop by white noise vibration, drop relaxes to equilibrium state. Before discussing the experimental results, we described the procedure used to prepare the flat PDMS (Polydimethylsiloxane) substrate used in the experiments. The reason for using flat PDMS substrate in the experiments is the high contact angle hysteresis of the surface which facilitates in observing the contact line relaxation behavior over a long period of time.
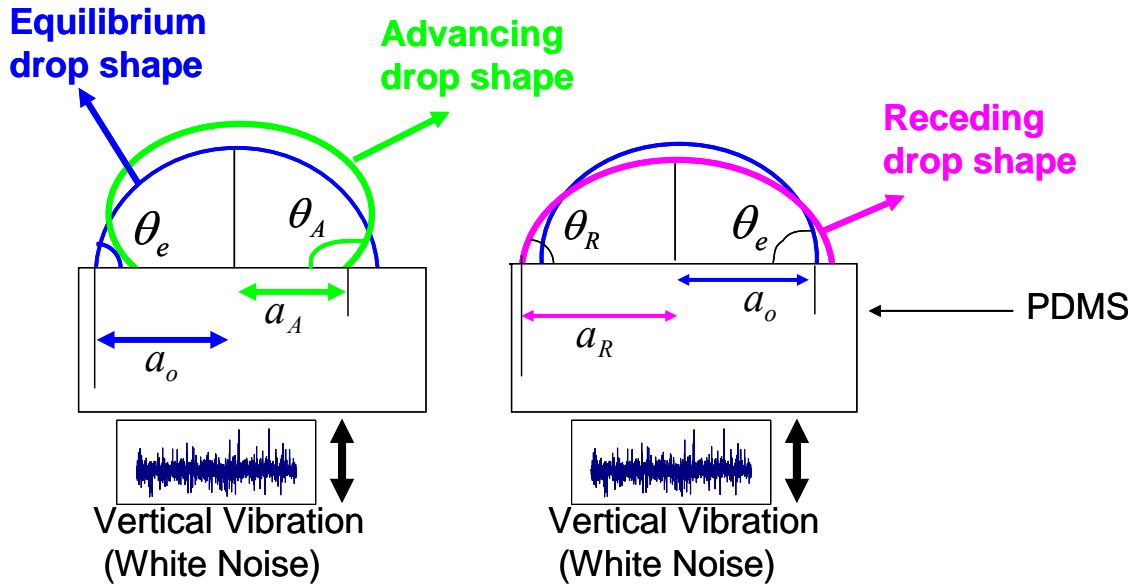
Figure 4.1. Schematic of a drop on a solid substrate subjected to white noise vibration in vertical direction. Left) drop on a solid substrate in advancing mode. The radius of drop in this case a_A is less than equilibrium radius of drop a_o. Right) drop on a solid substrate in receding mode. The radius of drop in this case $a_R > a_o$.

4.2. Preparation of Flat PDMS (Polydimethylsiloxane) Substrate

In this section we describe the procedure used to prepare the PDMS substrate used in the experiments of drop relaxation. After thoroughly mixing the oligomeric component of the Sylgard 184 (Dow Corning) with the crosslinker in a 10:1 ratio by weight, it was degassed by applying in house vacuum for 2hrs. The degassed mixture was then cast between two silanized microscopic glass slides spaced 0.64 mm apart using spacers. These microscopic glass slides are silanized with monolayer of decyltrichlorosilane for the easy removal of PDMS substrate after crosslinking. The crosslinking of the elastomer is carried out overnight at 75°C. After crosslinking, the substrate is removed manually from the glass slides and Soxhlet extracted in toluene for 24 hrs in order to remove any uncured   monomer. The sample is then dried in

vacuum for 48hrs before using in the experiments. This PDMS substrate (elastic modulus ~3MPa) is used in all the experiments except one experiment that was carried out on a self-assembled monolayer of per-fluoroalkylsiloxane on glass slide. The advancing and receding contact angles on the PDMS substrate measured using drop inflation and deflation method were 115° and 70° respectively. The roughness of PDMS substrate measured using atomic force microscopy is found to be ~2 nm.

4. 3. Experiment

The substrate (PDMS) (Figure 4. 1) was firmly attached to an aluminum platform (not shown here) which was connected to a mechanical oscillator (Pasco Scientific, Model No: SF-9324). White noise generated by signal generator (Agilent, Model 33120A) was sent to the oscillator after it is being amplified by a power amplifier (Sherwood, Model No: RX-4105). A calibrated accelerometer (PCB Peizotronics, Model No: 353B17) driven by Signal Conditioner (PCB Peizotronics, Model No: 482) connected to an oscilloscope (Tektronix, Model No. TDS 3012B) was used to measure the acceleration of the supporting aluminum plate. The acceleration of the plate is found to follow Gaussian distribution. The whole set-up was placed on a vibration isolation table (Micro-g, TMC) to eliminate the effect of ground vibration. We used a constant volume (V=10μL, M=10^{-5} Kg) of drop in all the experiments. The test liquid used in the experiments is water that is de-ionized using Barnstead NanopureII water purifying system. The purified water used in the experiments had a resistivity of 18 Ω Ohm-cm and a surface tension of 72.8 mN/m. We studied the relaxation of contact line of drop in advancing and receding modes. In advancing mode, a 10μL water drop is placed on PDMS substrate using a micro syringe by   inflating a small drop until the drop volume

is reached 10μL. We observed that the contact angle of drop was greater than the equilibrium contact angle of 90° and radius of drop was less than equilibrium radius of drop (a_o) when drop is in advancing mode (Figure 4.2(a)). When the substrate is vibrated vertically using white noise, radius of drop increases and contact angle decreases (Figure 4.2 (a), (b)). Here it is to be noted that the vibration applied to the drop is in vertical direction unlike in the Chapter 3 where lateral vibration was applied. In receding mode, a 20μL water drop is placed on PDMS substrate using a micro syringe, then the drop is deflated by removing 10μL using a micro needle. We observed that the contact angle of water drop was less than the equilibrium contact angle of 90° and radius of drop was greater than equilibrium radius of drop (a_o) when drop was deflated (Figure 4.2(c)). When the substrate is vibrated vertically using white noise, radius of drop decreases and contact angle increases (Figure 4.2(c), (d)). We carried out the experiments at different powers of noise (K) to study the effect on the final radius attained by drop at steady state. The stochastic motion of the contact line of drop is recorded with a high speed (1000 frames/sec) Redlake Motion-Pro video camera. These videos are stored in computer for analysis in leisure. The fluctuating motions of contact line on both the ends of the drop are tracked as a function of time using motion analysis software MiDAS.
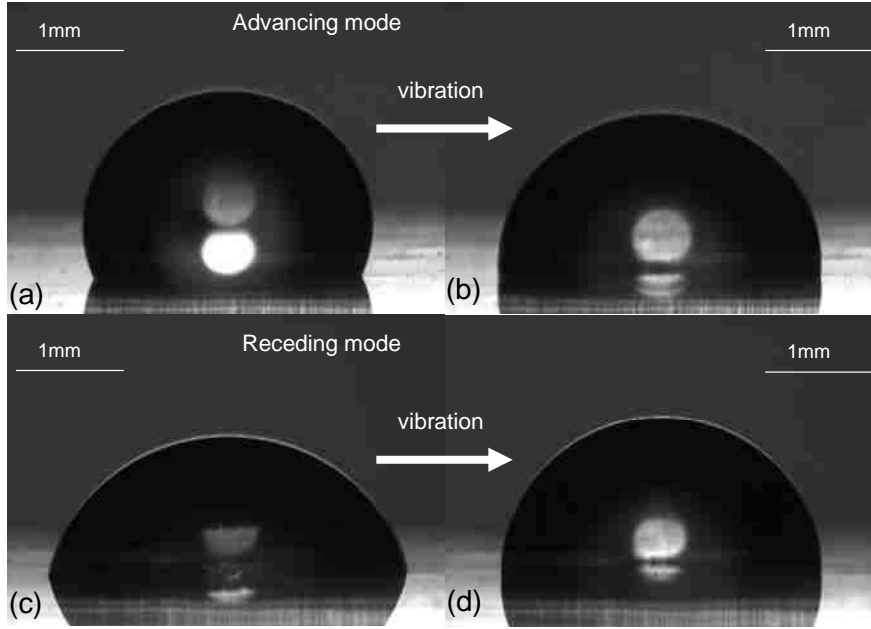
Figure 4.2. Initial and final configurations of a drop (V=10μL) on a solid substrate subjected to white noise vibration in advancing and receding modes.

4.4. Experimental Results

The drop resting on a solid either in advancing or receding mode has contact radius that is not its equilibrium radius. When contact radius of water drop (a) is not equal to equilibrium radius (a_o), the drop is in non-equilibrium state and there is always a constant driving force ($-k_s(a-a_o)$) arising from surface tension of liquid acting on the contact line of drop that tries to relax the drop to equilibrium. Here $k_s = 2\pi\gamma_{lv}$ is the spring constant of the drop due to the surface tension of liquid. If there is no contact angle hysteresis on the surface, when the drop is deformed from its equilibrium radius by applying some external force, drop readily relaxes to its equilibrium radius once the external force is removed. However, when the solid substrate possesses some amount of contact angle hysteresis, there is a resistive force proportional to $\gamma_{lv}a(\cos\theta_R - \cos\theta_A)$ that always opposes the motion of contact line of drop. The contact line of

drop gets pinned to the solid surface in non equilibrium state when the resistive force due to contact angle hysteresis $(\gamma_{lv} a(\cos\theta_R - \cos\theta_A))$ is greater than the driving force due to spring constant of liquid $(k_s(a - a_o))$. In order to relax the contact line of drop from non equilibrium state to equilibrium state, some amount of external vibration is required. When white noise vibration of sufficient power is applied to drop, contact line starts relaxing towards its equilibrium position. The final equilibrium radius value to which the drop relaxes depends on the strength of noise. We carried out the experiments at various strengths of white noise vibration in order to elucidate the effect of power of noise (K) on the final radius reached by drop. Here, we present the results for drop relaxing from advancing mode. We observed that the drop reaches its equilibrium radius value a_o only when power of noise is above a threshold power. The final radius of drop is plotted against power of noise in Figure 4.3. The drop reaches equilibrium radius only when power of noise is above $0.15 m^2/s^3$. This experimental observation is in accordance with the experiments of Andrieu et al[15], Decker and Garoff[17]. The dependence of final radius of drop on power of noise is the consequence of metastable equilibrium states in free energy profile of drop. At low powers of noise, the maximum energy supplied by white noise vibration is limited by the maximum acceleration pulse at a given power of noise. This highest acceleration may not be sufficient enough to drive the drop out of the metastable equilibrium state. Hence, at low powers of vibration, the drop is stuck in a metastable equilibrium state that is far from the global equilibrium state. At high powers of white noise vibration, acceleration pulses of high energy facilitate in driving the drop out of all of metastable equilibrium states resulting in the drop relaxing to global

equilibrium state. Hence, as the power of noise increases, the drop relaxes more towards equilibrium state.

If the noise used in the experiments is ideal white noise, there is always a finite probability of encountering an acceleration pulse of infinite energy at any power of noise that would drive the drop out of all the metastable equilibrium states resulting in relaxation of the drop to global equilibrium state. However, in any practical systems, there is always a cut off energy that can be supplied to the system. The white noise vibration that we have used in our experiments is a truncated white noise. The maximum acceleration pulse is a function of power of noise as well as the cut off value used in generating the white noise. Hence, the final radius reached by drop depends strongly on power of white noise vibration.

In order to test whether the drop radius would reach global equilibrium radius even at low powers when the vibration is applied to the drop for a long time, we carried out the experiments by subjecting the drop to white noise vibration for about 1min. We observed that the final radius values for both short and long time vibrations were equal indicating that the final radius reached is only function of power of noise.
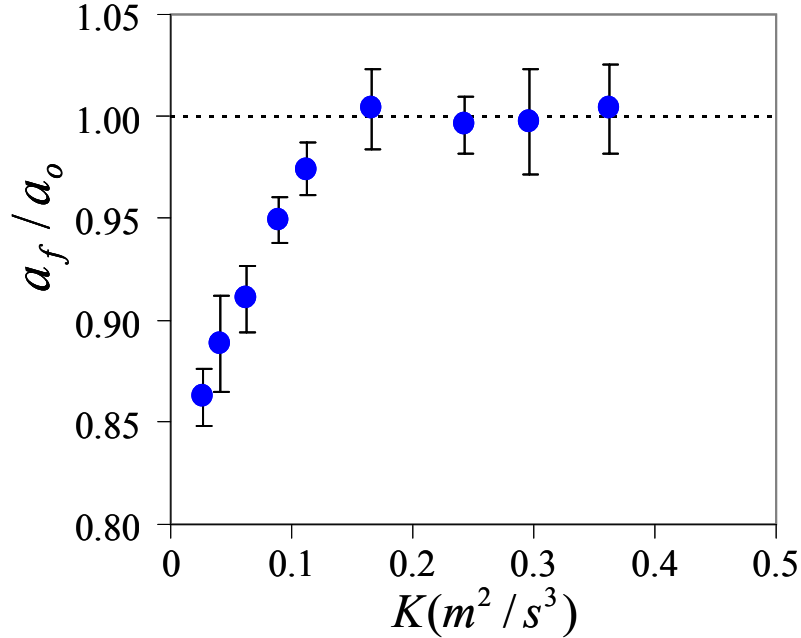
Figure 4.3. Final non-dimensional radius (a_f / a_o) of a $10 \mu L$ water drop on a PDMS substrate subjected to white noise vibration as a function of power of noise (K). Here a_0 is the final equilibrium radius of the drop corresponding to global equilibrium, which is achieved only with a high power noise. However, the drop does not always reach a_0. With a low power noise, it reaches a final value of a_f, which is less than a_0.

4.5. Stepwise Relaxation of Liquid Drop

We plot the stochastic relaxation behavior of contact line of drop as a function of time in Figure 4.4. The drops are relaxing from advancing mode when they are subjected white noise vibration of $K = 0.3 m^2 / s^3$. The relaxation is stepwise as well as stochastic in all of the tracks. As observed from Figure 4.4, the relaxation behavior is not smooth showing stick slip relaxation. This stick-slip like behavior is also present when the contact line of drop is relaxing at other powers of noise as well as it is relaxing from receding mode as shown in Figure 4.5. Such a step wise relaxation provides the evidence for the existence of metastable equilibrium states in the energy profile of drop as shown

schematically in Figure 4.6. Here, point 'B' is the global minimum in the free energy of the drop. A liquid drop in receding state relaxing from point 'A', would relax to 'B' if sufficient energy is supplied to the drop. However, at low powers the drop gets stuck to local equilibrium state far from global equilibrium as the maximum acceleration is not sufficient to drive the drop out of local equilibrium. The contact line of drop escapes from a metastable equilibrium state when a vibration pulse of sufficient power dislodges it from metastable state otherwise it dwells in that particular metastable state for long time. At low powers of noise, dwell time in a metastable state is longer as seen from a track at a power of $K = 0.026 m^2 / s^3$ in Figure 4.5. Other reason for long dwell time is that energy barriers of the metastable states increase towards B. Such a behavior is observed at $K = 0.09 \ m^2/s^3$ and $0.04 m^2/s^3$. It is also very interesting to note that at $K = 0.026 m^2/s^3$, the drop gets stuck in metastable state for long time before a large acceleration pulse drives the drop of out that state. Also, the relaxation behavior from advancing and receding mode are very different as observed for the case of $K = 0.3 m^2/s^3$. Such an asymmetric relaxation can be explained only when the resistance to contact line motion in advancing and receding modes are very different. When the contact line is pinned to a defect, the local distortion of contact line, dependent on whether contact line is advancing or receding and non-linear resisting force from defect may cause the asymmetry in resistance in advancing and receding modes.
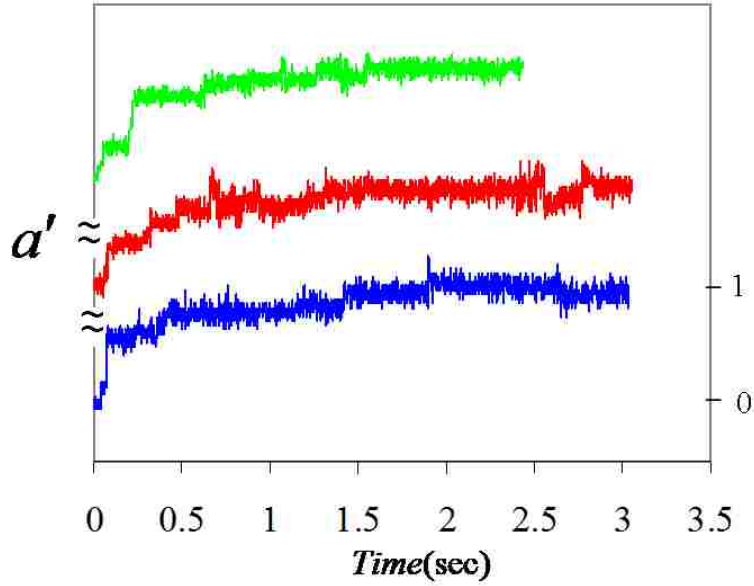
Figure 4.4. Three tracks of the contact line fluctuations are shown for a 10μL water drop on a PDMS substrate subjected to white noise vibration at $K = 0.3m^2/s^3$. The data illustrates the stochastic and stepwise relaxation behavior of the contact line kinetics. Here $a' = (a(t) - a(0))/(a_o - a(0))$ which varies from 0 to 1 as drop relaxes from advanced to the equilibrium state. All the three tracks have same range, but are shifted upwards for clarity.

4.6. Kinetics of Relaxation of Liquid Drop

There have been many experimental and theoretical studies[27-33] in the literature that looked at spontaneous relaxation of drops placed on a solid substrate from non equilibrium contact angle to equilibrium contact angle. These studies deal with the spontaneous relaxation (without any external force or vibration acting on the drop) of highly viscous liquid drops within first few seconds of depositing the drop on a solid substrate. Due to high viscosities of liquids used in these experimental studies spontaneous relaxation time is higher. The liquid that we have used in our experiments is water which has low viscosity, hence shows spontaneous relaxation within few milliseconds of depositing on solid. Also, we have applied white noise vibration to the

110

water drop after about 5 seconds of depositing the drop on the solid substrate. Therefore, relaxation dynamics that we observed here are only due to the applied external white noise vibration and there is no effect of spontaneous relaxation dynamics on the forced relaxation process. As described earlier, when a drop is in advancing mode, the contact angle of drop is greater than the equilibrium contact angle and radius of drop is less than equilibrium radius of drop (a_o) (Figure 4.1, Figure 4.2 (a) and Figure 4.5). When the substrate is vibrated using white noise, radius of drop increases resulting in relaxing of contact line of drop to equilibrium radius. If the drop is in receding mode, the contact angle of drop is less than the equilibrium contact angle and radius of drop is greater than equilibrium radius (a_o) and when the substrate is vibrated using white noise, radius of drop decreases and contact angle increases (Figure 4.1, Figure 4.2 (c) and Figure 4.5). We plotted the radius of drop relaxing to equilibrium as a function of time at different powers of noise in advancing and receding modes in Figure 4.5. The radius of drop relaxes to different equilibrium radius values depending on the power of white noise vibration. The drop relaxes to global equilibrium radius only when the power of noise is above $0.15 m^2/s^3$. At high powers of noise the radius of drop in receding mode also relaxes to same global equilibrium radius reached in advancing mode. As observed from the relaxation behavior at different powers of noise, the overall relaxation is exponential. However, the detailed relaxation behavior is step wise showing exponential relaxation in each step.
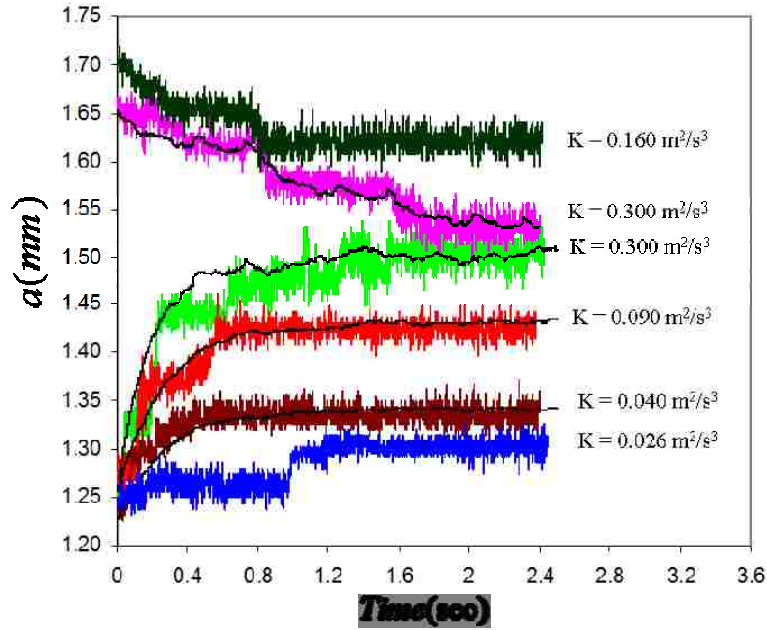
Figure 4.5. Relaxation behavior of contact line of a drop on a solid substrate subjected to white noise vibration at various powers of noise. The solid lines are the numerical solutions of equation 4.2 with $\tau_L = 0.01s$ and $\Delta = 47.8 m/s^2$.
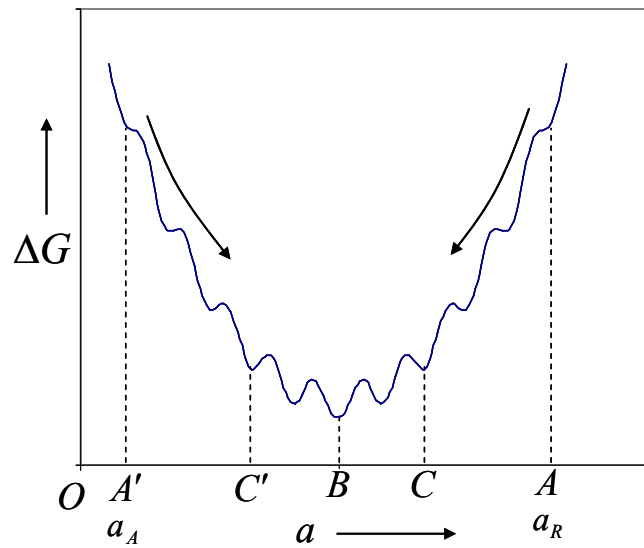
Figure 4.6: Schematic of a corrugated free energy (ΔG) profile of drop showing metastable equilibrium states. Here O indicates the center of the drop; OB is the radius of the drop corresponding to global equilibrium. A and A' are the inflection points that correspond closely to receding and advancing contact angles of the drop The figure is not drawn to scale. E.g., OA', in reality, is much larger than what is shown here.

4.7. Theory

In order to theoretically understand the experimental observations described above, we have drawn analogy between a drop subjected to external white noise vibration and a harmonically bound particle undergoing Brownian motion due to thermal fluctuations. The retracting force due to surface tension of liquid $(-k_s(a-a_o))$ induces harmonic potential where as external white noise vibration mimics the thermal fluctuations. Brownian motion of a harmonically bound particle is described by Langevin equation that has an inertial term, a dissipation term due to kinematic friction as well as retracting spring force term due to the presence of harmonic potential which are balanced by acceleration due to thermal fluctuations[34,35]. However, in the case of liquid drop subjected to white noise vibration, apart from inertial term, dissipation term due to kinematic friction, retracting spring force term due to the surface tension of liquid, there is also an extra dissipation term is present that is due to contact angle hysteresis on the surface. Taking into account of all the forces acting on drop, equation of motion for contact line (or radius) of drop on a solid substrate subjected to an external white noise vibration ($\gamma(t)$) can be written as the following modified Langevin equation[36-39]

$$\frac{d^2 a}{dt^2} + \frac{1}{\tau_L}\frac{da}{dt} + \omega_0^2(a - a_o) + \sigma(V)\Delta = \gamma(t) \qquad (4.2)$$

Here, a is the non-equilibrium radius of drop, a_o is the equilibrium radius of drop, τ_L is the Langevin relaxation time (ratio of the mass M of the drop and its kinematic friction coefficient ζ), $\omega_0 = \sqrt{k_s/M}$ is frequency term where $k_s = 2\pi\gamma_{lv}$ is spring constant of liquid drop due to surface tension of liquid. The term $\Delta\sigma(V)$ accounts for the dissipation

due to contact angle hysteresis. Δ is a measure of the contact angle hysteresis (force/mass) which is proportional to $a\gamma_{lv}(\cos\theta_R - \cos\theta_A)/M$. Here, $\sigma(V) = V/|V|$ is signum function of velocity of contact line $(V = da/dt)$ with $\sigma(0) = 0$ when drop is stationary $(V = 0)$. $\sigma(V) = -1$ when $V < 0$ and $\sigma(V) = +1$ when $V > 0$. Therefore, $\sigma(V)$ ensures that the resistive force due to contact angle hysteresis always acts against the motion of contact line of drop. $\gamma(t)$ is the time dependent acceleration that the drop experiences from the white noise source. The acceleration $\gamma(t)$ of white noise is ideally delta correlated with zero mean value. However, due to finite width and heights of the acceleration pulses in the experiments, the following approximation introduced by de Gennes[36] is used:

$$\langle \gamma(t_1)\gamma(t_2)\rangle = \Gamma^2 \qquad \text{for } |t_1 - t_2| < \tau_c$$

$$\langle \gamma(t_1)\gamma(t_2)\rangle = 0 \qquad \text{for } |t_1 - t_2| > \tau_c \qquad (4.3)$$

where, Γ is the root mean square acceleration and τ_c is the correlation time of the noise. The contact line of drop moves when the magnitude of applied acceleration $\left| -\omega_0^2(a - a_0) + \gamma(t)\right|$ is larger hysteresis (Δ) otherwise it remains stuck to the surface until a large acceleration pulse dislodges it from pinned state. Recently Noblin et al[22] have derived an equation similar to equation 4.2 for the contact line motion of a drop on solid substrate subjected to sinusoidal vibrations using energy balance method. In our case, the contact line motion is stochastic as it is driven by white noise vibration where as equation derived by Noblin et al[22] is for contact line motion driven by deterministic vibration.

114

The unknown parameters in equation 4.2 are the Langevin relaxation time (τ_L) and threshold acceleration required to overcome hysteresis force (Δ). Below we describe in detail the methods used to estimate the approximate values.

4.8. Estimation of Approximate Langevin Relaxation Time of Drop

As already described in Chapter 3, we have determined the Langevin relaxation time for a 10μL drop in our previous publications[38, 39] by fitting drift velocities of drops on an inclined silanized substrate that are subjected to white noise vibration at various powers of noise. The Langevin relaxation time of a 10μL drop on decyltrichlorosilane monolayer coated silicon wafer thus determined is 0.01s. Apart from fitting the drift velocities, we also used another simple experiment to estimate the approximate Langevin relaxation time for a 10μL drop on the same surface. In this experiment, noise free drift velocity of a 10μL drop sliding on silanized silicon wafer is measured at various inclination angles of the substrate to the horizontal. The limiting velocity of drop in noise free sliding is given by $V_s = \bar{\gamma}\tau_L$ where $\bar{\gamma} = g\sin\alpha$. Here g is acceleration due to gravity and α is angle of inclination the substrate to the horizontal. The slope of drift velocity versus $g\sin\alpha$ gives an approximate value of Langevin relaxation time to be 0.005s which is in the same order of 0.01s estimated from drift velocity fitting.

We also used two other well known theoretical methods to estimate the approximate Langevin relaxation time. The first method is hydrodynamic and the second method is based on a molecular kinetic theory. Based on Subramanian et al's[40] approximate solution of the hydrodynamic equation of Cox[41], the ratio of the mass of the drop and the contact line resistance (i.e. M/ζ) using wedge approximation gives M/ζ

value as 0.04 s whereas the lubrication approximation yields a value of 0.13 s. The value of M/ζ =0.01 s as used in our calculations are smaller than that estimated using the hydrodynamic method.

We also estimated ζ from the molecular kinetic theory of Blake and Haynes[42], which is based on the following relationship between the contact line velocity V and the molecular kinetic parameters:

$$V = V_o \sinh(F/2nK_BT) \tag{4.4}$$

where, V_o is a molecular velocity, F is the driving force, n is the number density of adsorption sites on surface, k_B is the Boltzmann constant and T is the temperature. Using the values provided for the various parameters of the above equation by Blake et al[43], i.e. $V_o \sim 108\,m/s$, and $\gamma_{lv}/(2nk_BT) \sim 0.2$, we can estimate $\zeta = F/V = 2nk_BT/V_o$ from a linear approximation of equation 4.4. The ratio M/ζ is thus estimated to be about 0.003s for our system. Thus, all of the above mentioned theoretical as well as experimental estimation methods yield the relaxation time of 10μL drop on a silanized silicon wafer in the same order of magnitude. However, we used a PDMS substrate in our experiments to study contact line relaxation of a 10μL drop. We expect that the Langevin relaxation time for a 10μL drop on PDMS substrate would be of the same order to that on decyltrichlorosilane monolayer coated silicon wafer since the surface energy of PDMS ($\sim$ 24 mJ/m^2)[44] is close to that of a SAM-coated surface ($\sim$21-22 mJ/m^2)[1] even though the packing density of the methyl groups should be somewhat different on these two surfaces.

4.9. Estimation of Contact Angle Hysteresis Term

According to Noblin et al[22], threshold acceleration required to overcome hysteresis force (Δ) can be approximately calculated as

$$\Delta = \frac{4\pi a \gamma (\cos\theta_r - \cos\theta_e)}{M} \tag{4.5}$$

Where θ_r is receding contact angle and θ_e is equilibrium contact angle which we have measured on the PDMS substrate that we used in the experiments as 70° and 90° respectively. Experimentally determined value of Δ using equation 4.5 is 47.8 m/s^2 which we have used in the simulations.

4. 10. Estimation of Approximate Spring Constant of Liquid Drop

The total surface energy of a spherical cap on a solid surface is contributed by the liquid-vapor, solid-vapor and solid-liquid interfaces as follows:

$$U = \frac{2\pi\gamma_{\ell v} a^2}{1 + \cos\theta} + \pi(\gamma_{sl} - \gamma_{sv})a^2 \tag{4.6}$$

By expanding U in Taylor series up to two terms with respect to a, one obtains equation 4.7.

$$U = U_0 + \frac{\partial U}{\partial a}\bigg|_\upsilon (a - a_o) + \frac{1}{2}\frac{\partial^2 U}{\partial a^2}\bigg|_\upsilon (a - a_o)^2 + \dots \tag{4.7}$$

Here, the volume (υ) of the liquid drop is used as a constraint. In order to evaluate the first and second derivatives of U, a relationship between a and θ is needed, which can be obtained from the volume of a spherical cap and setting its derivative with respect to a as zero. One thus obtains:

$$a\frac{d\theta}{da} = -(2 + \cos\theta)\sin\theta \qquad (4.8)$$

Equation 4.7, in conjunction with equations 4.6 and 4.8 now becomes equation 4.9.

$$U = U_0 + 2\pi a\left(\gamma_{\ell v}\cos\theta + \gamma_{sl} - \gamma_{sv}\right)\left(a - a_o\right)$$

$$+ 2\pi\gamma_{\ell v}\left(\sin^2\theta(2 + \cos\theta)\right)\left(a - a_o\right)^2/2 \qquad (4.9)$$

At equilibrium ($\partial U/\partial a = 0$), the term $\left(\gamma_{\ell v}\cos\theta + \gamma_{sl} - \gamma_{sv}\right)$ vanishes, which leads to the Young's equation. The spring constant is given by equation 4.10:

$$k_s = 2\pi\gamma_{\ell v}\sin^2\theta\left(2 + \cos\theta\right) \qquad (4.10)$$

Since the equilibrium contact angle of water on PDMS is ~90°, k_s is estimated to be $4\pi\gamma_{lv}$, which is twice the value of the spring constant ($2\pi\gamma_{lv}$) used in the simulations. The derivation used in this appendix is however very approximate as we assume a minor perturbation of the drop from the equilibrium value. The drop shape is also assumed to be perfectly that of a spherical cap, which may not be the case due to vibration and gravity. Furthermore, the free surface of the water drop may have small scale corrugations during vibration that will involve additional surface energy. In reality many of these assumptions underlying the derivation of equation 4.10 may be violated.

4.11. Numerical Simulations of Modified Langevin Equation

We carried out numerical simulations of modified Langevin equation (equation 4.2), in order to theoretically predict the relaxation behavior of drop observed in the experiments. Numerical integration of the modified Langevin equation is carried out using a generalized integration method for stochastic differential equations as outlined by Gillepsie[45]. The update formula for the stochastic output variable (velocity or

displacement) consists of rescaling stochastic input (acceleration, $\gamma(t)$) to simulations in order to match strength of noise (K) in simulations to strength of noise in experiments. We measured stochastic accelerations of oscillating plate using accelerometer as described in the experimental section. These measured accelerations are rescaled to match various strengths of noise in experiments and then used as input accelerations in the simulations. Since the hysteresis force $\sigma(V)\Delta$ always acts in the direction opposite to the motion of the contact line, $\sigma(V)$ is set as $V/|V|$ in the simulations. When the net acceleration $\left|-\omega_0^2(a-a_0)+\gamma(t)\right|$ acting on the drop is less than the threshold acceleration (Δ) required to set the contact line into motion, the contact line gets stuck, hence the velocity is set to zero. The modified Langevin equation is integrated with an integration time step of $\Delta t = 0.00025s$ which is smaller than all of the relaxation times in the system. The simulations are carried out for 50 tracks with a total integration time of 2.5sec for each track at each power of noise. The solid black color lines shown in Figure 4.5 are average of such 50 stochastic realizations of drop relaxing to equilibrium. Further increase in the number of tracks did not affect the average. As observed from the relaxation behavior of drop in advancing mode at powers 0.3, 0.09 and $0.04m^2/s^3$, numerical solution of modified Langevin equation agrees very well with the experimental results predicting the overall exponential relaxation of drop from non-equilibrium state to equilibrium state.

119
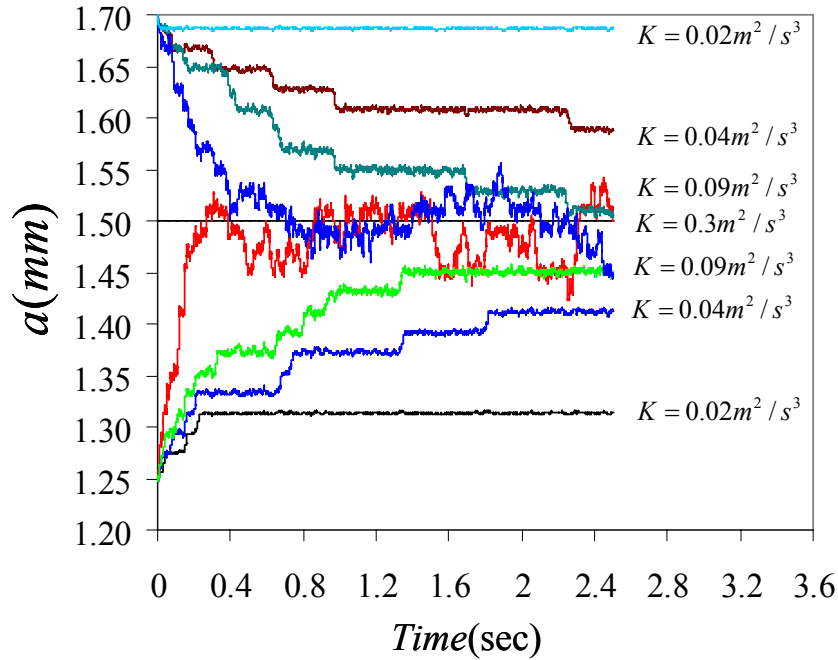
Figure 4.7. Simulated relaxation of a drop on a surface starting from either an advanced ($a > 1.5$ mm) or a receded ($a < 1.5$ mm) state to global equilibrium ($a_o = 1.5$ mm) by incorporating a sinusoidal perturbation term $[B\sin(2\pi a / \lambda)]$ to hysteresis in equation 4.2. The arbitrary values of B and λ used here are 10 m/s^2 and 20 μm respectively. Short and long time pinning of the contact line are evident here. Note that when a low power noise is used, the drop gets stuck at a radius that is lower than the equilibrium radius. Many of the features of the drop relaxation seen in this simulation are observed experimentally (Figures 4.4 and 4.5).

4.12. Numerical Simulation of Step Wise Relaxation

In the numerical simulations, we specified intermediate (a) values as final equilibrium (a_o) radius in order to simulate stepwise relaxation. Even though these simulations agree well with experimental relaxation behavior observed at $K=0.3$ m^2/s^3 in receding mode, it is not a generalized method to predict such behavior. In order to predict such behavior we followed the method used by Sakaguchi[46]. In these simulations, we have added an extra sinusoidal perturbation term $B\sin(2\pi a / \lambda)$ on the right side of equation 4.2. Therefore, the hysteresis has an average value coming from a

120

constant Δ along with spatially varying hysteresis resulting from sinusoidal term. We plot trajectories of contact line relaxation behavior at various powers of noise from advancing as well as receding modes obtained using Sakaguchi's[46] method in Figure 4.7.

As observed from Figure 4.7, many experimental features are reproduced well in the simulations. At low powers of noise the drop gets stuck to metastable states far from equilibrium. At intermediate powers, the drop gets stuck at a metastable state for long time before a huge acceleration pulse dislodges it from one metastable state to the other. Such jumps clearly represent the stick slip motion observed in the experiments. However, at very high powers of noise the drop smoothly relaxes to global equilibrium without getting stuck at the intermediate metastable states. The motion of the contact line, as simulated with this modification to equation 4.2, is presented in Figure 4.7. We used arbitrarily chosen values of B and λ in the simulations. However, we note that, though the value of amplitude (B) of sinusoidal perturbation term is arbitrary, choosing wavelength (λ) was based on the fact that the length of jumps of contact line as observed from Figure 4.5 at a power of $0.026 m^2/s^3$ at $t\sim$1sec is approximately 30μm which is close to 20μm that we have used in the simulation. Further research is required in order to accurately estimate these values.

We note that in theoretical studies of contact angle hysteresis[6-13], the authors have used periodic spatial variation of contact angles in order to show that there exist metastable equilibrium states in the free energy of drop on a heterogeneous solid substrate. However, in reality there is no concrete evidence to prove that the variation of contact angles due to surface heterogeneity follows well defined periodicity. Instead, the variation of contact angles might be random following a Gaussian distribution

121

due to the randomness of heterogeneity on the substrate. It is very interesting to study how the metastable states are distributed around the global equilibrium state in case of random variation of contact angles on heterogeneous solid substrate.
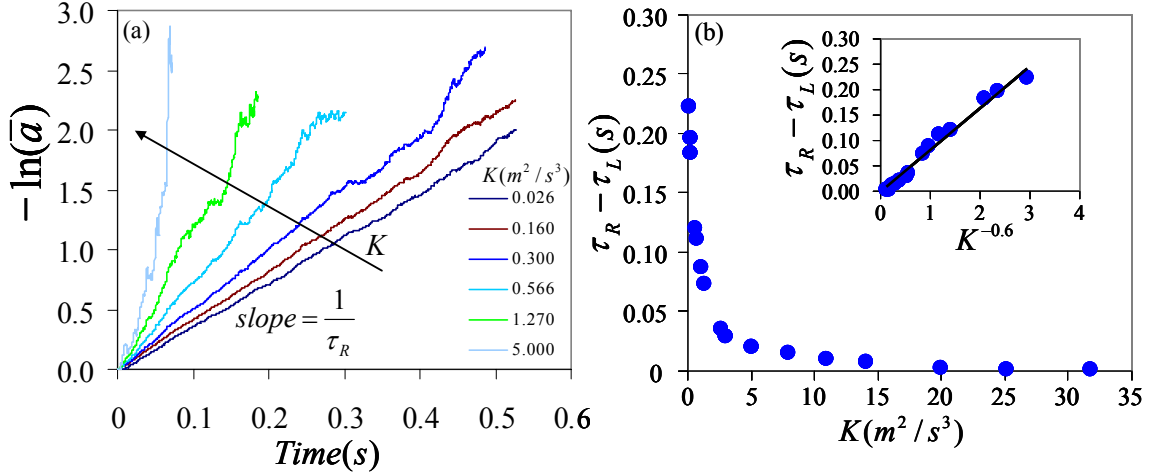
Figure 4.8. Relaxation time is calculated from the slope of $-\ln(\bar{a})$ versus time of vibration where $\bar{a} = \dfrac{a(t) - a_o}{a(0) - a_o}$. **(b)**. Relaxation time (τ_R) of the contact line of a drop obtained from numerical simulations at various powers of noise. Inset of figure shows the plot of $\tau_R - \tau_L$ as a function of $K^{-0.6}$.

4.13. Effect of Power of Noise on Relaxation Time

We also looked at the effect of power of white noise vibration on relaxation time. As shown in Figure 4.8(b), the relaxation time is on the order of 0.2 sec when the contact line relaxes towards equilibrium at a power of $0.3 m^2/s^3$. For lower strength noise this time is larger than 0.2 sec. This is contrary to the expectation that the contact angle hysteresis is eliminated instantly when external vibration is applied to a drop. In order to estimate the power of noise needed to completely eliminate contact angle hysteresis, the experiments have to be carried out at very high powers of noise. We could not carry out the experiments at very high power of noise due to experimental constraints. Hence, we

carried out numerical simulations over a wide range of powers of noise to determine the dependence of relaxation time on power of noise. As the relaxation behavior is approximately exponential, we used the following equation to determine the relaxation time

$$\frac{a(t) - a_o}{a(0) - a_o} = \exp\left(-\frac{t}{\tau_R}\right) \tag{4.11}$$

The relaxation time is determined from the slope of $-\ln\left(\frac{a(t) - a_o}{a(0) - a_o}\right)$ versus time of

vibration plot (Figure 4.8 (a)). As expected, relaxation time decreases with increase of power of white noise vibration (Figure 4.8 (b)). Ideally, when the power of noise approaches zero i.e. when there is no vibration, the drop would never relax, hence the relaxation time tends to infinity. We could not predict this behavior from our numerical simulations as the numerical methodology that we used would not give accurate results at very low powers of noise. We attempted to plot Arrhenius type plot of relaxation time versus power of noise as the relaxation process is exponential. However, the relaxation time follows power law $\left(\tau_R - \tau_L \sim K^{-0.6}\right)$ with a scaling exponent of 0.6 with power of white noise vibration. As power of noises increases, the relaxation time decreases reaching the Langevin relaxation time at very high powers of noise. Saturation of relaxation time to Langevin relaxation time indicates that at high powers of noise, the dynamics of relaxation of drop are controlled only by kinematic friction rather than hysteresis. We wanted to check what is the power required to completely eliminate contact angle hysteresis. When contact angle hysteresis is completely eliminated, the relaxation time would in the order of Langevin relaxation time. As observed from the

numerical simulations, the relaxation time of drop reaches Langevin relaxation time only when the power of noise ($K = \Gamma^2 \tau_c$) is ~30 m^2/s^3. The corresponding root mean square acceleration $\Gamma = (K/\tau_c)^{1/2}$ for $\tau_c = 40\mu s$ is ~860m/s^2. If the contact angle hysteresis were to disappear, such a high power noise has to be applied to the drop. However, supplying such high energy vibrations to drop is not feasible experimentally. Hence, drop reaching the equilibrium radius does not imply that the hysteresis is completely eliminated.

4.14. Fokker Planck Equation

So far, we looked at the relaxation behavior of contact line as a function of strength of noise using experiments as well as numerical simulation of Langevin equation. However, as the relaxation of contact line of drop is stochastic showing fluctuations, there is a need to look at these fluctuations in detail. The fluctuations of contact line of relaxing drop contain rich information about the non-equilibrium behavior. As the noise input to the drop is stochastic, the displacement of contact line drop over a certain interval of time is also stochastic following a probability distribution unlike when the contact line relaxing under the influence of deterministic vibration. Hence, it is worthwhile to look the probability distribution of contact line of drop as a function time in order to draw conclusions about the effect of contact angle hysteresis while the contact line is in motion. In order to proceed in this direction, we look at the Klein-Kramers form of the Fokker-Planck equation[34-37,38,39,47,48] corresponding to equation 4.2 for the transition probability density $P(V,a,t)$ as follows:

$$\frac{\partial P(V,a,t)}{\partial t} = \left[-\frac{\partial(VP)}{\partial a} + \omega_o^2 \frac{\partial(a-a_0)P}{\partial V} + \frac{1}{\tau_L}\frac{\partial(VP)}{\partial V} + \Delta\frac{\partial P(V/|V|)}{\partial V} + \frac{K}{2}\frac{\partial^2 P}{\partial V^2} \right] \quad (4.12)$$

The derivation of equation 4.12 can be obtained using a method followed by Chandrasekhar[32]. The transition probability density for the radius of drop $P(a,t)$ can be obtained by solving equation 4.12 for $P(V,a,t)$ with initial condition that at $t=0$, $a=a_A$ or a_R, $V=0$ and then integrating over velocity (V) as follows

$$P(a,t) = \int_{-\infty}^{+\infty} P(V,a,t) dV \tag{4.13}$$

The mean of transition probability density for radius of drop $P(a,t)$ at $t=0$ is either a_A or a_R depending whether drop is relaxing from advancing or receding mode. Then mean varies as a function of time reaching equilibrium radius of drop a_o after a certain period of time. However, obtaining an analytical solution of equation 4.12 is rather difficult as it involves $\sigma(V) = V/|V|$ which results in the discontinuity at $V=0$ in force versus velocity relationship. There have been recent attempts to obtain transition probability from the solution of an equation similar to equation 4.12 involving Coulombic dry friction between two solid surfaces using parabolic cylinder functions[49] and also using path integral formalism[50]. However, in our study we look at the steady state solution of equation 4.12 to gain some insights into the effect of contact angle hysteresis on relaxation dynamics.

4.15. Displacement Fluctuation of the Contact Line of Water on PDMS

In order to study the effect of contact angle hysteresis on the non-Gaussian probability distribution of the displacement fluctuations of contact line of drop, we looked at the spatially homogeneous and steady state solution[44,45] of equation 4.12, which reduces to a simple balance of the diffusive and convective fluxes in the velocity space as

125

follows:

$$\frac{K}{2}\frac{\partial P}{\partial V} + \Delta\frac{|V|}{V}P + \frac{VP}{\tau_L} = 0 \tag{4.14}$$

here, $P(V)$ is the steady state probability density function of the velocity which is obtained by integrating equation 4.14.

$$P(V) = P_o \exp\left(-\frac{V^2}{K\tau_L} - \frac{2|V|\Delta}{K}\right) \tag{4.15}$$

where, P_o is a normalization constant. According to equation 4.15, when $\Delta = 0$, the velocity distribution is Gaussian with zero mean. However, when $\Delta \neq 0$, the probability distribution of velocity has also an exponential component $\left(\exp\left(-2|V|\Delta / K\right)\right)$ that results in the tails of the distribution to be exponential while at the center of the distribution, i.e. at $V \sim 0$, it is dominated by Gaussian term $\left(\exp\left(-V^2 / K\tau_L\right)\right)$. In our experiment, we measured the displacement of the contact line of the drop with a high speed camera with a time scale $\tau* = 0.001$ sec, with $V = \bar{x}/\tau*$, it gives us an approximate probability distribution of the jump length ($\bar{x}$) distribution as:

$$P(\bar{x}) = P_o' \exp\left(-\frac{\bar{x}^2}{K\tau_L\tau*^2} - \frac{2|\bar{x}|\Delta}{K\tau*}\right) \tag{4.16}$$

Equation 4.16, shows that the distribution of $\bar{x}$ is Gaussian in the absence of hysteresis, but has an extra exponential term in the presence of hysteresis. In order to estimate the displacement over a certain time $\tau > \tau*$, we generated a large matrix of the jump vectors ($\bar{x}$) using equation 16 and randomly selected them to construct a stochastic path over a much longer time scale. The probability distribution of these randomly selected jump vectors is shown in the   inset of Figure 4. 9 b along with the

126

experimentally obtained jump length distribution at τ =0.001sec. Although the match is not exact, the discrepancy between experimental and simulation results is small. The simulations could reproduce the exponential nature of the distribution. From the stochastic path created over a large time scale, displacement distributions for various values of τ can be constructed. Such a displacement distribution obtained for τ = 0.01 sec (Figure 4. 9b) is found to be exponential thus indicating the effect of hysteresis. In Chapter 3 we studied the motion of a drop on a surface subjected to white noise and a bias. The bias was generated by tilting the plate or by creating a gradient of wettability. In these experiments the entire drop slides on a surface unlike here where only contact line of drop relaxes but there is no net translation of the drop. Here, the displacement distribution of the drop was found to be exponential and asymmetric. We also showed using numerical simulation of Langevin equation that both asymmetry and exponential displacement distribution are result of non-linear hysteresis force. The simplified equation 4.14 only leads to a non-Gaussian nature of the distribution, but does not predict any other features that are associated with a non-linear friction. Indeed the experimental data presented in Figure 4.9(a) reveal several higher order features, such as the distribution becomes asymmetric as time progresses and that a secondary peak appears at a higher value of the displacement that grows with time as well.
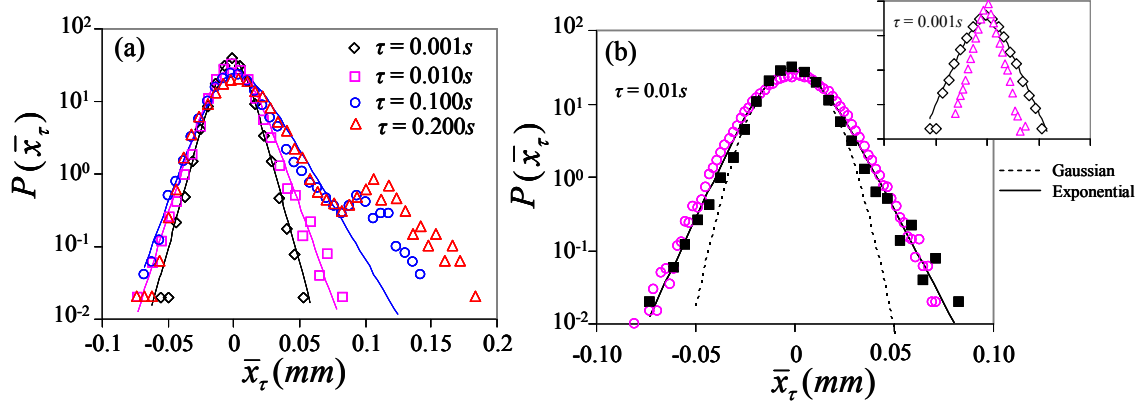
Figure 4.9: (a). Experimentally obtained distribution of displacement fluctuation of contact line of a $10\mu L$ drop subjected to white noise vibration of power $K = 0.3 m^2/s^3$. Here $\bar{x}_\tau = \Delta a(\tau)$ is the net displacement fluctuation of the contact line in time 'τ' sec. The distribution of displacement fluctuations of drop is exponential and asymmetric. At longer times, a secondary peak appears as well. The data can be fitted with an asymmetric double sigmoidal function (solid line), the tails of which are exponential **(b).** The displacement distribution (pink circles) for $\tau = 0.01$sec as obtained from the paths constructed by joining the jump vectors randomly are compared with that obtained experimentally. A Gaussian function (dotted line) fails to fit the experimental data. Inset (axis and units are same as (b)) compares the experimentally obtained jump length distribution (open diamonds) with that obtained from equation 4.16. Both the distributions have pronounced exponential tails.

4.16. Displacement Fluctuation to Study Surface Chemical Properties

So far, we looked at the relaxation behavior of contact line of drop on a flat PDMS substrate that had high contact angle hysteresis (45°). We also looked at the effect of magnitude of contact angle hysteresis on the relaxation time of contact line as well as the displacement distribution by carrying the experiment on a fluorocarbon monolayer coated glass slide that had lower hysteresis (24°) than flat PDMS substrate. The main interest in doing this experiment is to see whether it is possible to distinguish two surfaces of different chemical properties. Before discussing the experimental results, we describe the procedure used to prepare fluorocarbon monolayer coated glass slide.

4.17. Preparation of Fluorocarbon Monolayer Coated Glass Slide

Self assembled monolayer of 1H, 1H, 2H, 2H-Perfluorodecyltricholorsilane was prepared on microscopic glass slides using vapor deposition method[41]. The microscopic glass slides (Fisher Scientific) of dimensions of 75×25×1mm were placed in Piranha solution (30% Hydrogen Peroxide and 70% Sulfuric Acid by volume) for 30 min followed by rinsing with copious amount of distilled deionized (DI) water. After drying with ultra purified nitrogen gas, the glass slides were treated with oxygen plasma (model PDC-32G; Harrick Plasma) at 0.2Torr for 45s. The plasma treated glass slides were immediately transferred to a vapor deposition chamber. The vapor deposition of silane onto glass slide was carried for 2h in vacuum. After deposition, the glass slides were baked in oven for 15 min at 75°C. After cooling the samples to room temperature they are rinsed with DI water followed by drying with nitrogen. The advancing and receding contact angles of water on this fluorocarbon surface measure using drop inflation and deflation method are 116° and 92° respectively.

4.18. Comparison of Displacement Fluctuations on PDMS and Fluorocarbon Monolayer Coated Glass Slide

The relaxation behavior of contact line of a $10\mu L$ water drop on a flat PDMS substrate and on fluorocarbon monolayer coated glass slide subjected to white noise vibration of power $K = 0.3 m^2/s^3$ is shown in Figure 4.10 (a). The relaxation observed in the experiments is in accordance with the magnitude of hysteresis on the surfaces, i.e. the relaxation time of drop on high hysteresis (45°) PDMS substrate is ~1.5sec where as it is ~0.25sec on low hysteresis (14°). The larger relaxation time signifies larger contact angle

hysteresis on the surface. It is also observed from Figure 4.10 (a) that the magnitude of fluctuations of contact line on fluorocarbon coated glass slide (blue) are much higher than the fluctuations on PDMS substrate due to higher contact angle hysteresis on PDMS. In order to compare the magnitudes of fluctuations we plotted the probability distribution of fluctuations of contact line of drop in Figure 4.10(b) at τ = 0.01s. The variance of displacement distribution in case of fluorocarbon coated glass slide is higher than that of PDMS. We calculated the kurtosis of displacement distributions on both the surfaces. Kurtosis of a distribution is defined as the ratio of fourth moment to the fourth power of standard deviation of distribution ($\beta_2 = \mu_4 / \sigma^4$) which gives the sharpness of a distribution. A Kurtosis value of close to 3 indicates the distribution is Gaussian, while higher values indicate that the distribution is highly sharp and non-Gaussian. The kurtosis of displacement distribution thus calculated for contact line fluctuations on PDMS is found to be 4.5 where as it is 3.6 for fluorocarbon surface. The kurtosis values in both cases are higher than 3 indicating that the displacement distribution of contact line on both the surfaces is highly non-Gaussian. This tells us that relaxation of contact line is controlled by contact angle hysteresis. Higher kurtosis value on PDMS surface than on fluorocarbon coated glass slide clearly reflects that effect of contact angle hysteresis on the sharpness of distribution. As shown in Figure 4.10(b), we could fit the data on both surfaces with an asymmetric double sigmoid function that has exponential tails.
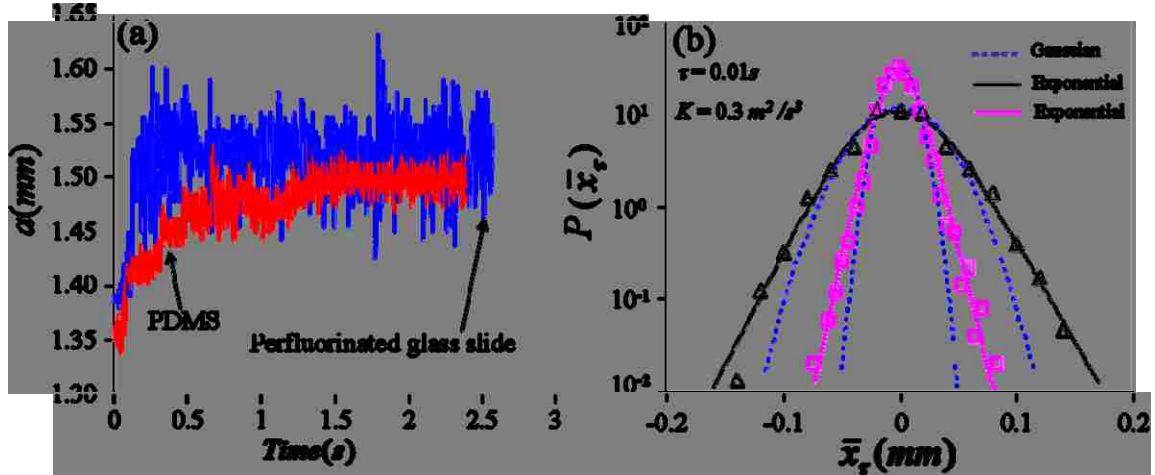
Figure 4.10: **(a).** The relaxation kinetics of the contact line of a $10\mu L$ water drop on PDMS (red) and a perfluorinated glass slide (blue). **(b).** The probability distribution functions of the displacement fluctuations $(\bar{x}_\tau = \Delta a(\tau))$ of the contact line on both the surfaces: PDMS (square) and per-fluorinated glass slide (triangle). These probability distribution functions have distinctive exponential features. The dotted lines indicate fits attempted by Gaussian functions and solid lines are exponential fits.

4.19. Conclusions

Liquid drop that is in non equilibrium state on a solid substrate, when subjected to external white noise vibration shows relaxation towards equilibrium. The final radius reached by drop strongly depends on power of white noise vibration applied to the drop. The drop reaches equilibrium radius only when the power of white noise vibration is above a threshold power. The radius of drop reaches same final equilibrium value both from advancing and receding modes at high powers of noise. The over all relaxation behavior of contact line from non-equilibrium state to equilibrium state is exponential. However, the detailed relaxation shows step wise relaxation with stick slip motion of contact line. Theory based on modified Langevin equation predicts the relaxation behavior of contact line accurately. The relaxation time of contact line decreases with increase in power of white

noise vibration following a power law relation with an exponent of 0.6. The relaxation time approaches Langevin relaxation time at very high powers of white noise vibration. According to numerical simulations, the contact angle hysteresis disappears at very high powers of noise that are experimentally infeasible to generate, indicating that reaching global energy minimum state does not imply that the contact angle hysteresis totally disappears.

4.20. References

1. De Gennes, P. -G. *Rev. Mod. Phys* **1985,** *57*, 827.

2. Leger, L.; Joanny, J. F. *Rep. Prog. Phys* **1992**, *55*, 431

3. Bonn, D.; Eggers, J.; Indekeu, J.; Meunier, J.; Rolley, E. *Rev. Mod. Phys*. **2009,** *81*, 739.

4. Young,T. *Trans. Roy. Soc* **1803**, *95*, 65.

5. Good, R. J. *J . Am. Chem. Soc* **1952**, *74*, 5041.

6. Neumann, A. W.; Good, R. J. J. *Colloid Interface Sci.* **1972**, *38*, 341.

7. Eick, J. D.; Good, R. J.; Neumann, A. W. *J. Colloid Interface Sci.* **1975**, *53*, 235.

8. Johnson, R. E.; Dettre, R. H. *Contact Angle, Wettability and Adhesion, Adv. Chem.* Ser. No 43, 112, American Chemical Society, Washington, DC (1964).

9. Johnson, R. E.; Dettre, R. H. *J. Phys. Chem.* **1964**, *68*, 1744.

10. Dettre, R. H.; Johnson, R. E. *J. Phys. Chem.* **1965**, *69*, 1507.

11. Marmur, A. *Adv. Colloid Interface Sci.* **1994**, *50*, 121.

12. Marmur, A. *J. Colloid Interface Sci.* **1994**, *168*, 40.

13. Marmur, A. *J. Colloid Interface Sci.* **1996**, *183*, 351.

14. Smith, T.; Lindberg, G.; *J. Colloid   Interface Sci.* **1978**, *66*, 363.

15. Andrieu, C.; Sykes, C.; Brochard, F. *Langmuir* **1994**, *10*, 2077.

16. Nadkarni, G. D.; Garoff, S. *Langmuir* **1994**, *10*, 1618.

17. Decker, E. L.; Garoff, S. *Langmuir* **1996**, *12*, 2100.

18. Meiron, T.S.; Marmur, A.; Saguy, I.S. *J. Colloid Interface Sci.* **2004**, *274*, 637.

19. Bormashenko, E.; Pogreb, R.; Whyman, G.; Erlich, M. *Langmui* **2007**, *23*, 6501.

20. Bormashenko, E.; Pogreb, R.; Whyman, G.; Erlich, M. *Langmuir* **2007**, *23*, 12217.

21. Bormashenko, E.; Pogreb, R.; Whyman, G.; Bormashenko, E.; Erlich, M. *Appl. Phys. Lett.* **2007**, *90*, 201917.

22. Noblin, X.; Buguin, A.; Brochard, F. *Eur. Phys. J. E* **2004**, *14*, 395.

23. Noblin, X.; Buguin, A.; Brochard, F. *Eur. Phys. J. Special Topics* **2009**, *166*, 7.

24. Brunet, P.; Eggers, J.; Deegan, R. D. *Phys. Rev. Lett.* **2007**, *99*, 144501.

25. John, K.; Thiele, U. *Phys. Rev. Lett.* **2010**, *104*, 107801.

26. Thiele, U.; John, K. *Chem. Phys.* **2010**, *375*, 578.

27. Cherry, B. W.; Holmes, C. M. *J. Colloid Interface Sci.* **1969**, *29*,174.

28. Blake, T. D.; Haynes, J. M. *J. Colloid Interface Sci.* **1969**, *30*, 421.

29. de Ruijter, M. J.; De Coninck, J. ; Blake, T. D. ; Clarke, A. ; Rankin, A. *Langmuir* **1997**, *13*, 7293.

30. Blake, T. D. ; Clarke, A. ; De Coninck, J. ; de Ruijter, M. J. *Langmuir* **1997**, *13*, 2164.

31. de Ruijter, M. J.; Charlot, M. ; Voue, M. ; De Coninck, J. *Langmuir* **2000**, *16*, 2363.

32. Iliev, S.; Pesheva, N.; Nikolayev, V. S.; *Phys. Rev. E* **2005**, *72*, 011606.

33. Nikolayev, V. S.; Beysens, D. A. *Phys. Rev. E* **2002**, *65*, 046135.

34. Risken, H., *The Fokker–Planck Equation, Methods of Solution and Applications*, 2nd ed.; Springer-Verlag: Berlin, Heidelberg and New York. 1989.

35. Chandrasekhar, S. *Rev. Mod. Phys* **1943**, *15*, 1.

36. De Gennes, P. -G. *J. Stat. Phy*s. **2005,** *119*, 953.

37. Buguin, A.; Brochard, F.; De Gennes, P.-G. *Eur. Phys. J.E* **2006**, *19*, 31.

38. Chaudhury, M. K. ; Mettu, S. *Langmuir* **2008**, *24*, 6128.

39. Goohpattadar, P. S. ; Mettu, S. ; Chaudhury, M. K. *Langmuir* **2009**, *25*, 9969.

40. Subramanian, R. S.; Moumen, N.; McLaughlin J. B. *Langmuir* **2005**, *21*, 11844.

41. Cox, R. G., *J. Fluid Mech.* **1986**, *168*, 169.

42. Blake, T. D.; Haynes, J. *M .J. Colloid Interface Sci.* **1969**, *30*, 421.

43. Blake, T. D.; Clarke, A.; De Coninck, J.; de Ruijter M. J. *Langmuir* **1997**, *13*, 2165.

44. Chaudhury, M. K.; Whitesides, G. M. *Langmuir* **1991**, *7*, 1013.

45. Gillespie, D. T. *Am. J. Phys.* **1996**, *64*, 225.

46. Sakaguchi, H. *J. Phys. Soc. Japan.* **2006**, *75*, 124006.

47. Kawarada, A.; Hayakawa, H. *J. Phys. Soc. Jpn.* **2004**, *73*, 2037.

48. Hayakawa, H. *Physica D* **2005**, *205*, 48.

49. Touchette, H.; Van der Straeten, E.; Just, W. *J. Phys. A: Math. Theor.* **2010**, *43*,445002 (P 1).

50. Baule, A.; Touchette, H.; Cohen, E. G. D. *Nonlinearity* **2011**, *24*, 351.

Chapter 5: Motion of Liquid Drops on Surfaces induced by Asymmetric Vibration: Role of Contact Angle Hysteresis

5.1. Introduction:

Motion of liquid drops on a solid surface is of fundamental importance in understanding the phenomena of wetting and contact angle hysteresis. It is also of technological importance in applications such as microfluidic[1-6], heat transfer devices[7-10], surface coatings, printing, water proofing and lubrication[11-13]. The actuation of liquid drops in micro fluidic and heat transfer devices is generally achieved by utilizing physical forces that arise due to surface energy gradient[2,10] or thermal energy gradient[7-9]. However the liquid drops get pinned to solid surface due to resistive force arising from contact angle hysteresis on the surface which is proportional to $a\gamma_{lv}(\cos\theta_R - \cos\theta_A)$. Here a is the contact radius of liquid drop, γ_{lv} is the surface tension of liquid and θ_A, θ_R are advancing and receding contact angles of liquid on the surface. In order for liquid drop to move on a surface, external forces acting on drop have to be higher than the threshold resistive force due to contact angle hysteresis. Apart from the technological applications mentioned above, water drops sticking to an inclined solid surface is observed frequently in natural settings such as drops on glass windows, windshield of car and shower curtains. These drops run down on the surface with a slight tapping or mild shaking of the surface. However, if the drops are sitting on a horizontal solid surface instead of an inclined surface, tapping or shaking would cause the drops to oscillate back and forth with no net motion. A common feature in the above mentioned techniques used in microfluidic and heat transfer devices to induce liquid drop motion on a solid surface is that there is an externally applied bias that is responsible for the motion of drops.

A pertinent question that arises here is how drops pinned to a horizontal solid surface can be set into motion where external bias force such as gravity is not acting on the drop. It has been shown that liquid drops can be moved by exciting them with symmetric periodic vibrations on an asymmetrically structured solid surface[14,15]. The oscillations of drop get rectified resulting in drop moving in one direction due to asymmetric structure on the solid surface. Here asymmetric structure amounts to having triangular groves on the surface with unequal slopes. Recent theoretical study of Cebiroglu et al[21] suggested that rectified motion can also be achieved in nonlinear media subjected to asymmetric random driving. A recent review by Hanggi and Marchesoni[22] discusses the mechanism of rectified transport at various scales in the presence of a stochastic or a deterministic driving. This kind of ratcheting mechanism resulting from asymmetric structure on the surface is discussed extensively in the literature and it is well understood[14-20]. A simple example of such a ratchet is a microscopic particle that is undergoing Brownian motion in an asymmetric potential instead of classical parabolic potential. In case of particle in parabolic potential, position of the particle fluctuates around the minimum of potential where as in asymmetric potential the particle moves in one preferred direction. Another way of inducing motion of drops is by exciting the drop on a uniformly symmetric and smooth solid surface with asymmetric periodic vibrations of zero mean force[1]. Such a directed motion of liquid drops in the absence of bias has received considerable attention due to its significant implications in microfluidic devices.

Recently, Daniel et al[1] have shown that liquid drops can be transported on a solid surface in the absence of external bias by applying asymmetric periodic vibrations with zero mean to the solid support. It has been well understood that, in order to

achieve directed motion in presence of periodic or stochastic forcing with zero mean there needs to be at least one symmetry breaking mechanism present in the system[23]. Daniel et al[1] argued that contact angle hysteresis is responsible for symmetry breaking in this case. In the context of rectification of motion of protein motors resulting in unidirectional motion, Mogilner et al[23] indicated that there is a requirement for symmetry breaking mechanism as the stochastic velocity fluctuations resulting from conformational changes of motor protein are of zero mean. They suggested that Coulombic type friction is responsible for unidirectional motion of motor proteins.

Recently, in theoretical analysis of motion of solid objects on a solid support, Fleishman et al[24,25] and Buguin et al[26] have also argued, similar to the arguments of Daniel et al[1], that Coulombic friction analogous to contact angle hysteresis in the case of liquid drop, is responsible symmetry breaking. Experimental demonstrations of the motion of a solid on another solid by asymmetric vibration and friction were provided by Mahadevan et al[27], Eglin et al[28] as well as by Buguin et al[26]. Recent experimental study of liquid drops subjected to simultaneous vertical and horizontal vibrations as carried out by Noblin et al[29] also supports the argument that the contact angle hysteresis is responsible for symmetry breaking resulting in the directed motion. In their experimental study, a sessile drop was subjected to horizontal and vertical vibrations simultaneously that resulted in the net motion of drop without any applied external bias. They proposed that the asymmetric forces acting on the contact line of drop brought about by the contact angle hysteresis are responsible for the ratcheting motion of drops. However, there have been several other arguments in the literature[30-32] as to which mechanism is responsible for directed motion of drops in the absence of bias. Brunet et al[30] used an

137

empirical non-linear friction model to describe the uphill motion of a drop subjected to strong symmetric vibrations. John and Thiele[31,32] argued that the vibration component of the drop perpendicular to the substrate leads to a strongly nonlinear lateral force-velocity relation that breaks the symmetry of the periodic forcing. They attributed the effect studied by Brunet et al[30] and Noblin et al[29] to such a non-linearity. Also, John and Thiele[31,32], Brunet et al[30] argued that the asymmetry in vibrations or contact angle hysteresis may not be necessary ingredients for directed motion of drops in the absence of external applied bias. Based upon such conflicting arguments in literature, it is very important to check whether hysteresis is at all the necessary non-linearity for the drop motion under asymmetric vibration in the types of experiments presented by Daniel et al[1]. John and Thiele[31,32], Brunet et al[30] also indicated that the applied external vibration helps only in depinning the drop from solid support hence resulting in the complete elimination of contact angle hysteresis.

However, in a recent experimental study[33] as already described in Chapter 4, we have shown that contact angle hysteresis is not completely eliminated during the relaxation of drop from non-equilibrium state to equilibrium state under the influence of external vibration[34-39]. In this experimental study a water drop, which is either stuck in advancing or receding state on a high hysteresis PDMS substrate, is subjected to white noise vibration in vertical direction. The drop that is initially stuck in a metastable-equilibrium state relaxes to equilibrium state due to externally applied white noise vibrations. We looked at the relaxation time of liquid drop from non-equilibrium state to equilibrium state. There are two relaxations times in presence of contact angle hysteresis on the surface. The first one is Langevin   relaxation time due to kinematic friction

and the second one being the relaxation time due to dissipation coming from contact angle hysteresis. If the contact angle hysteresis is completely eliminated due to external vibrations, we expect the dynamics of the relaxation of drop would be controlled only by kinematic friction hence relaxation time would be of the order of Langevin relaxation time. But the relaxation time of contact line of drop is found to be much higher than the Langevin relaxation time indicating that the contact angle hysteresis is not eliminated during the relaxation of the drop. It was also shown from numerical calculations that, in order to completely eliminate contact angle hysteresis, the drop has to be subjected to huge acceleration pulses which may not be easily achieved in laboratory. Also, the distribution of displacement fluctuation of contact line of drop would be Gaussian if the contact angle hysteresis is completely eliminated. However, the displacement fluctuations followed non-Gaussian distribution with exponential tails confirming that the contact angle hysteresis is present during the relaxation of drop.

As there seems to be no consensus on whether all or some of these non-linearities contribute to symmetry breaking resulting in rectification, there is a need to analyze the motion of drops systematically using experiments and theory. We wanted to elucidate the role of non-linearity in contact angle hysteresis that is responsible for symmetry breaking using experiments and theory. We designed an experiment in which the motion of drops is studied by systematically varying the amount of contact angle hysteresis on the surface. We also developed a non-linear contact angle hysteresis model that clarifies the uncertainties associated with role of contact angle hysteresis. Using experiments and simulations, we convincingly show for the first time that contact angle hysteresis is an essential factor that is responsible for symmetry breaking resulting directed

139

motion of drops.

(a)

(b)
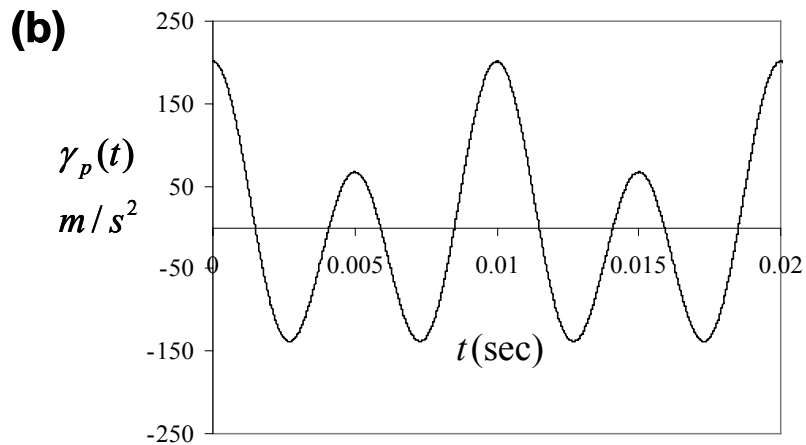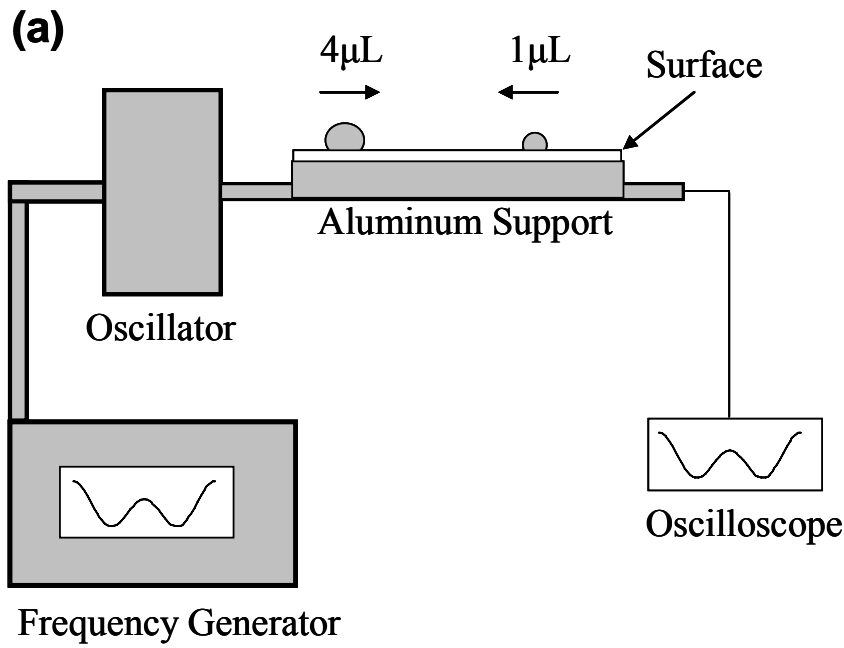
$$\gamma_P(t) = A_o(\cos(2\pi\omega t) + 2\cos(4\pi\omega t))$$

Figure 5.1. (a). Experimental set up (b) Typical asymmetric acceleration wave profile used to vibrate the solid support. $\gamma_P(t)$ is the acceleration of the plate with $A_o = 67m/s^2$ and $\omega = 100Hz$.

5.2. Experimental Procedure

Typical experiment (Figure 5.1(a)) is to place drops of deionized water of volumes 1 and $4\mu L$ on two ends of a solid surface that is attached to a solid support and then subject the solid support to lateral asymmetric vibrations of zero mean. The solid surface was attached on an aluminum platform that is connected to the stem of a mechanical oscillator (Pasco Scientific, Model SF-9324). The asymmetric wave generated in a wave form editor was sent through the wave form generator (Agilent, Model 33120A) to the mechanical oscillator after it was amplified by a power amplifier (Sherwood Model No: RX-4105). The entire setup was placed on a vibration isolation table (Micro-g, TMC) to eliminate the effect of ground vibration. The asymmetric acceleration profile that is used to vibrate the solid support is a combination of two cosine waves[24] given by $A_o(\cos(2\pi\omega t) + 2\cos(4\pi\omega t))$. Here, A_o is the amplitude of acceleration and ω is the fundamental frequency of oscillations. Typical asymmetric wave used to vibrate the solid support is shown in Figure 5.1(b) with $A_o = 67 m/s^2$ and $\omega = 100 Hz$. Accelerometer (PCB Peizotronics, Model No: 353B17) driven by a Signal Conditioner (PCB Peizotronics, Model No 482), and connected to an oscilloscope (Tektronix, Model No. TDS 3012B), was used to estimate the acceleration of the plate. Accelerometer reading showed that the above asymmetric wave was slightly distorted, when it passed though the oscillator (see Figure 5.3). However, as the displacement is periodic, its time average is zero. When subjected to asymmetric vibrations, 1 and $4\mu L$ drops move in opposite directions which are recorded from side view using a high speed camera (Redlake, MotionPro, Model 2000) operating at 2000 frames/sec and stored in computer

141

for analysis in leisure. Motion analysis software *MiDAS* was used to track the dynamics of contact line motion of drop.

We used surfaces of negligible hysteresis, intermediate hysteresis as well as strong hysteresis in order to systematically check the effect of amount of contact angle hysteresis on drop motion. The hysteresis force acting on the liquid drop depends not only on the difference between the cosine of advancing and receding angles, but also the perimeter of contact between the drop and the substrate. We used micro fibrillated PDMS (Dow Corning Sylgard 184) surfaces as surfaces with negligible hysteresis. We used hydrocarbon monolayer coated silicon wafer and PDMS monolayer (Trimethylsiloxy-terminated, Gelest Inc., Product Codes DMS-T22 and DMS-T12) coated silicon wafers as intermediate hysteresis surfaces. Fluorocarbon monolayer coated glass slide and polystyrene coated silicon wafer are used as surfaces with high hysteresis. Below, we describe the procedures used to prepare these surfaces.

5.3. Preparation of Micro Fibrillated PDMS Substrate

We prepared micro fibrillated PDMS substrates by a procedure previously used by Glassmaker et al[40]. The oligomeric component of the Sylgard 184 kit was thoroughly mixed with the crosslinker in a 10:1 ratio by weight followed by degassing using in house vacuum for 2hrs. The degassed mixture was then cast onto lithographically etched silicon master wafer. The silicon wafer is silanized with decyltrichlorosilane using vapor deposition method for easy removal of cured fibrillated PDMS sample. The cast PDMS was then cured at 80°C for two hours. The crosslinked PDMS was cooled in dry ice (-78.5^{o}C) for an hour followed by its removal from silicon master wafers manually. The PDMS surface thus prepared has square   fibrils of 10μm size with fibrillar spacing of

$95\mu m$. The fibrillar spacing here corresponds to the center to center distance between two adjacent fibrils. The height of the fibrils was $25\mu m$. The low hysteresis fibrillated PDMS surfaces were characterized using drop rolling method in which a $10\mu L$ drop was placed on a horizontal fibrillated PDMS surface and the angle of inclination of the surface was increased gradually until the drop started to move. The advancing and receding angles of the rolling drop were measured from their video images captured with a computer. These values were 162° and 160° respectively, with a hysteresis of 2°. The adhesion of water drops to this fibrillated PDMS surface was so low that it proved difficult to transfer the drops onto the surface as they stuck more to the microsyringe needle rather than to the fibrillated PDMS surface. Use of a very thin micro needle solved this problem.

5.4. Preparation of Hydrocarbon Monolayer Coated Silicon Wafer

The hydrocarbon monolayer was prepared by reacting plasma cleaned silicon wafer (Silicon Quest International) to the vapor of decyltrichlorosilane (CH_3-$(CH_2)_9$-$SiCl_3$, Gelest Inc.). Before the vapor deposition is carried out, the silicon wafers are thoroughly cleaned as described below. The silicon wafer was placed in Piranha solution (20% Hydrogen Peroxide and 80% Sulfuric Acid by volume) for 30 min followed by rinsing with copious amount of distilled deionized (DI) water. After drying with ultra purified nitrogen gas (Praxair Inc.), the silicon wafer was treated with oxygen plasma (model PDC-32G; Harrick Plasma) at 0.2Torr for 45s. Before the vapor deposition is carried out, the silane is degassed for two hours in vacuum to remove any trapped air bubbles. The plasma treated silicon was immediately transferred to a vapor deposition chamber containing decyltrichlorosilane. The vapor deposition of silane onto silicon wafer was carried for 1h in vacuum. After deposition, the silicon wafer was

baked in oven for 15 min at 75°C. After cooling the samples to room temperature, they are rinsed with DI water followed by drying with ultra purified nitrogen gas (Praxair Inc.). The advancing and receding contact angles of water on this hydrocarbon monolayer coated silicon wafer measured using drop inflation and deflation method are 107° and 99°, with a net hysteresis of 8°. The ellipsometric (V-Vase Ellipsometer, J. A. Woollam Co, Inc) thickness of hydrocarbon monolayer on silicon wafers is found to be ~1 *nm*. The root mean square (RMS) roughness of hydrocarbon monolayer coated silicon wafer is found to be 0.2 *nm* using Atomic Force Microscopy (Veeco NanoscopeV, Digital Instruments, Metrology Group) over an area of 1$\mu m \times 1\mu m$.

5.5. Preparation of Trimethylsiloxy Terminated PDMS Monolayer Coated Silicon Wafers

PDMS monolayer (Trimethylsiloxy-terminated, Gelest Inc., Product Codes DMS-T22 and DMS-T12) coated silicon wafers were used as intermediate hysteresis surfaces. The PDMS (Trimethylsiloxy-terminated) coated silicon wafers were prepared using a method similar to that is described earlier[41] with a slight modification. The silicon wafers (Silicon Quest International) were first cleaned with Piranha solution (20% Hydrogen Peroxide and 80% Sulfuric Acid by volume) for 30 min, followed by rinsing with copious amounts of distilled deionized (DI) water and drying it with ultra purified nitrogen gas (Praxair Inc). The silicon wafers were then further cleaned by oxygen plasma (Model PDC-32G; Harrick Plasma) at 0.2 Torr for 45s. Some of these oxygen plasma cleaned silicon wafers were immediately transferred to and immersed in trimethylsiloxy-terminated poly-dimethylsiloxane (PDMS) (Gelest Inc., DMS-T22, Viscosity of 200cSt, MW 9000-10000) in a cleaned glass Petri dish. The other remaining

oxygen plasma cleaned silicon wafers were immediately transferred to and immersed in a separate clean glass Petri dish containing a different trimethylsiloxy-terminated poly-dimethylsiloxane (PDMS, DMS-T12 (Viscosity of 20cSt, MW 1600-2400). These Petri dishes were covered and kept in an oven at 100^oC for 24*hrs*. The samples were then cooled to room temperature and dipped in toluene (99.9% pure, ACS grade) for 10*min*. Both the samples were rinsed with copious amounts of flowing toluene, after which they were dried with ultra pure nitrogen gas. The thicknesses of the grafted PDMS films were found to 1.7 *nm* for DMS-T12 and 5 *nm* for DMS-T22. The RMS roughness these surfaces were 0.3 *nm* for DMS-T12 and 0.4 *nm* for DMS-T22. The advancing and receding angles measured using drop inflation and deflation method on silicon wafer coated with PDMS (DMS-T12) were 106° and 95° respectively, whereas they were 112° and 104° on silicon wafer coated with PDMS (DMS-T22) respectively. The hysteresis (8°) on the latter surface is comparable to that of the hydrocarbon monolayer coated silicon wafer.

5.6. Preparation of Fluorocarbon Monolayer Coated Glass Slide

Self assembled monolayer of 1H, 1H, 2H, 2H-Perfluorodecyltricholorsilane was prepared on microscopic glass slides using vapor deposition method. The microscopic glass slides (Fisher Scientific) of dimensions of 75×25×1mm were placed in Piranha solution (20% Hydrogen Peroxide and 80% Sulfuric Acid by volume) for 30 min followed by rinsing with copious amount of distilled deionized (DI) water. After drying with ultra purified nitrogen gas, the glass slides were treated with oxygen plasma (model PDC-32G; Harrick Plasma) at 0.2Torr for 45s. Before the vapor deposition is carried out, the silane is degassed for two hours in   vacuum to remove any trapped air bubbles.

The plasma treated glass slides were immediately transferred to a vapor deposition chamber. The vapor deposition of silane onto glass slide was carried for 2h in vacuum. After deposition, the glass slides were baked in oven for 15 min at 75°C. After cooling the samples to room temperature they are rinsed with DI water followed by drying with nitrogen. The advancing and receding contact angles of water on this fluorocarbon surface measure using drop inflation and deflation method are 117° and 103° (hysteresis of 14°) respectively. The thickness of the grafted fluorocarbon layer on glass could not be estimated by ellipsometry due to its roughness and close match of the refractive indices of the glass and the grafted layer. The ellipsometric thickness of an equivalent layer on silicon wafers is found to be ~1.4 *nm*. The root mean square (RMS) roughness of the fluorocarbon coated glass slide is found to be 18 *nm*.

5.7. Preparation of Polystyrene Spin Coated Silicon Wafers

Polystyrene coated substrates were prepared by spin casting a 5% solution by weight of Polystyrene (MW~50,000, Aldrich Chemical Company Inc.) in Toluene on the silicon wafer and drying it for several days. The thickness of polystyrene film was 357*nm* with a RMS roughness of ~0.3 *nm*. Using the drop inflation and deflation methods, the advancing and receding angles were found to be 91° and 68° (hysteresis of 23°).
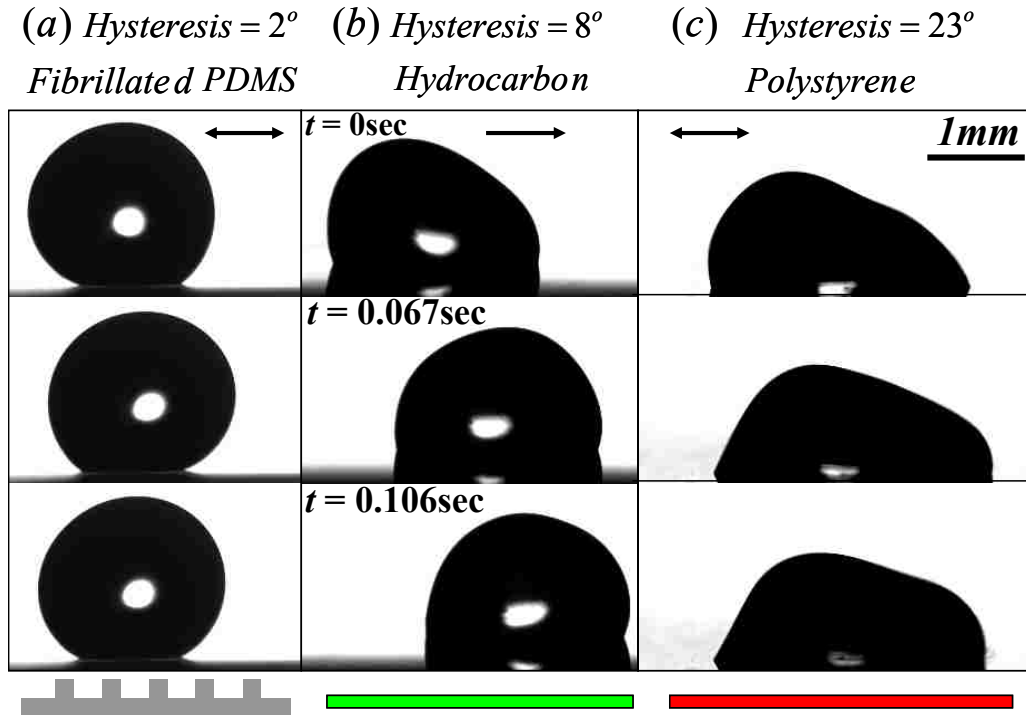
Figure 5.2. Shape fluctuations of a 4μL drop subjected to an asymmetric vibration ($A_o = 33m/s^2$, $\omega = 100Hz$) on surfaces of varying magnitude of contact angle hysteresis. (a) Fibrillated PDMS (Sylgard 184) (b) Hydrocarbon monolayer (Decyltrichlorosilane) coated silicon wafer and (c) Polystyrene coated silicon wafer. The amount of contact angle hysteresis increases from panel (a) to (c) as indicated by the magnitude of hysteresis on the top of each panel. The standard deviations in the measurement of the advancing and receding angles are about 1°. The time sequence shown on the middle panel also corresponds to the left and right panels. The drop does not show a net motion on low hysteresis (2°) fibrillated PDMS surface and on the high hysteresis (23°) polystyrene surface, whereas it drifts on the hydrocarbon monolayer coated silicon wafer that has intermediate hysteresis (8°).

5.8. Experimental Results

We show the shape fluctuations of a $4\mu L$ drop when subjected to asymmetric vibration ($A_o = 33 m/s^2, \omega = 100 Hz$) on surfaces possessing varying amount of contact angle hysteresis in Figure 5.2. As observed from the figure, the drop did not show any motion on low hysteresis (2°) micro fibrillated PDMS. This result is counterintuitive to the expectation that the drops would move with high velocity on low hysteresis surfaces. However, the drop drifts with high velocity on hydrocarbon monolayer coated silicon wafer that had intermediate hysteresis (8°). The drop again does not move on polystyrene coated silicon wafer that had very high hysteresis (23°). This counterintuitive experimental result clearly points out that some amount of contact angle hysteresis is required in order for the drop motion to get rectified resulting in directed motion when it is subjected asymmetric periodic vibrations. The same experimental results are observed when a $1\mu L$ drop is subjected to asymmetric vibration on surfaces with varying magnitudes of contact angle hysteresis. $1\mu L$ drop did not show net drift on low hysteresis micro fibrillated PDMS surfaces as well as on high hysteresis polystyrene coated silicon wafer, but it drifts with high velocity on intermediate hysteresis hydrocarbon monolayer coated silicon wafer. These experimental observations unequivocally support our hypothesis that hysteresis provides essential symmetry breaking mechanism resulting in directed motion of liquid drops when subjected to asymmetric vibrations.
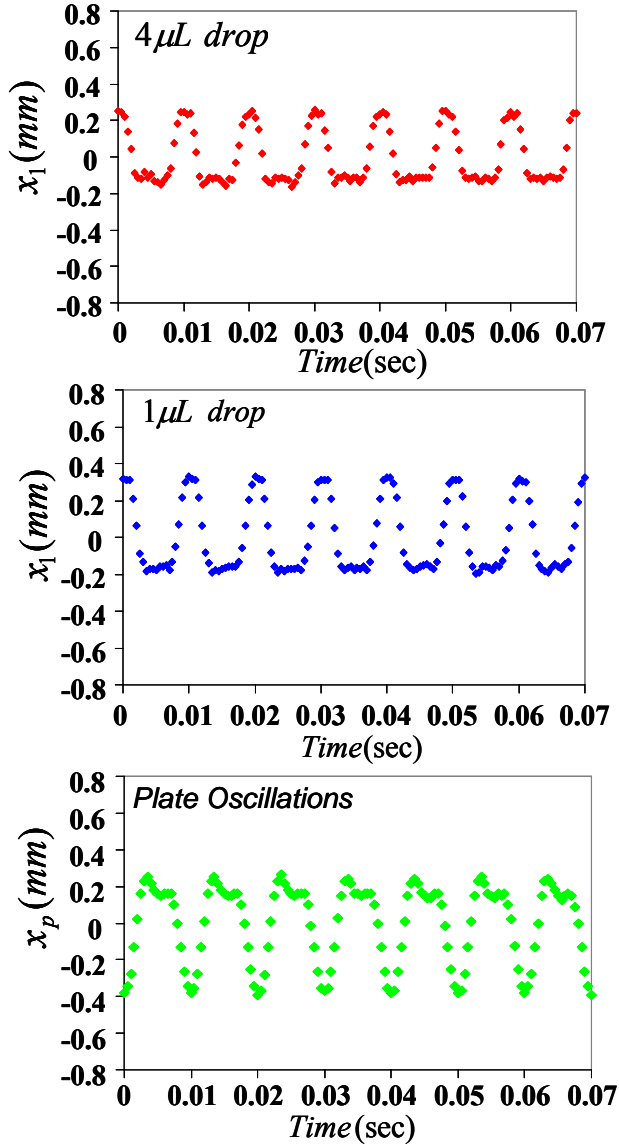
Figure 5.3. The dynamics of the contact lines of 4μL and 1μL water drops on low hysteresis (2°) fibrillated PDMS surface that is subjected to asymmetric vibrations of an amplitude of $A_o = 97m/s^2$. The plate oscillations are also shown. The drops do not exhibit any net drift. Here x_1 corresponds to displacement of contact line of the drop relative to the plate as shown in figure 5.9. x_p corresponds to the displacement of the plate with respect to the laboratory frame.

In order to show detailed contact line dynamics of 1 and 4μL drops oscillating on micro fibrillated PDMS surface, we carried out the experiments at a high amplitude of

vibration ($A_o = 97 m/s^2$, $\omega = 100 Hz$). We tracked the high resolution motion (2000 frames/s) of contact lines of 1 and $4\mu L$ drops and plotted the contact line dynamics in Figure 5.3. The contact lines of 1 and $4\mu L$ drops oscillate back and forth without showing any net motion over several cycles of oscillations. These experimental observations clearly show that there needs to be some amount of contact angle hysteresis on the solid surfaces in order to show directed motion of liquid drops. Here, contact angle hysteresis provides the essential symmetry breaking mechanism.
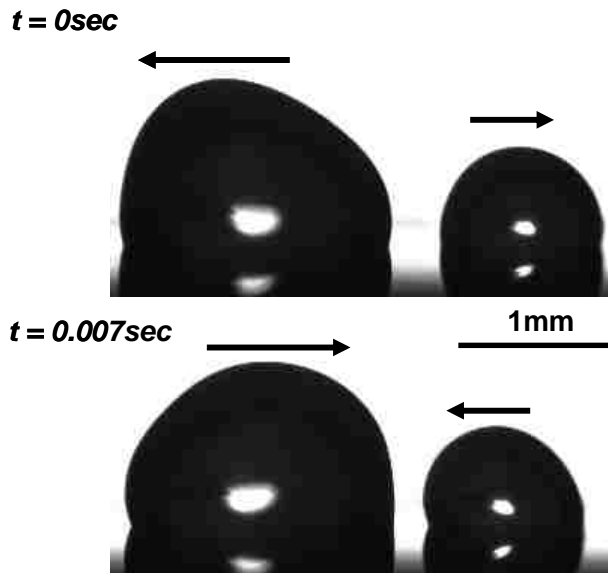
Figure 5.4. Oscillations of the center of masses of $4\mu L$ and $1\mu L$ water drops subjected to asymmetric vibration with $A_o = 33 m/s^2$ on a hydrocarbon monolayer coated horizontal silicon wafer. The directions of center mass oscillations are shown by arrows on top of each drop. At $t=0$ sec, the center of mass of the $4\mu L$ drop moves to the left whereas that of the $1\mu L$ moves to the right. At $t=0.007$ sec, the center of mass of the $4\mu L$ moves to the right whereas that of the $1\mu L$ drop moves to the left. These observations suggest that the oscillations of these drops are out of phase.
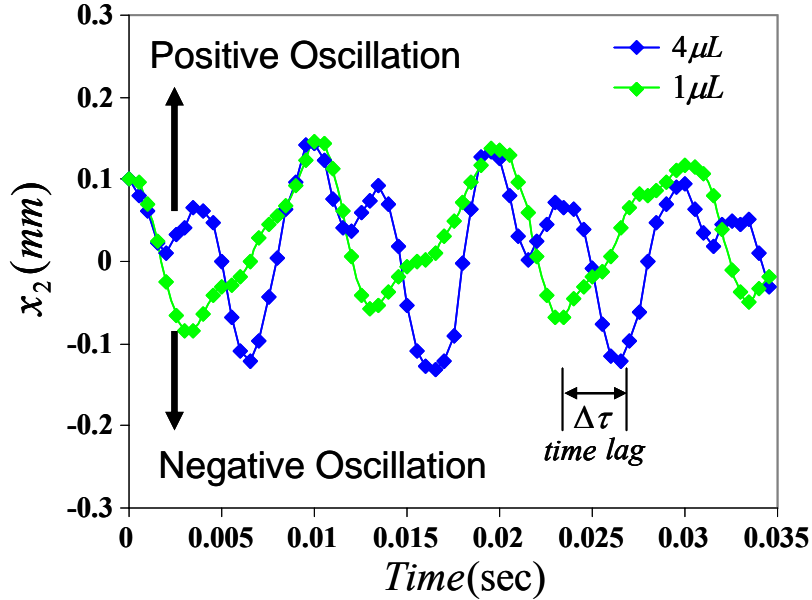
Figure 5.5. Oscillations of the center of masses of $4\mu L$ and $1\mu L$ water drops subjected to asymmetric vibration with $A_o = 33m/s^2$ on a hydrocarbon monolayer coated horizontal silicon wafer. The oscillations are shown in the reference frame of moving drops. As shown by arrows, the center of masses $4\mu L$ and $1\mu L$ water drops oscillate in opposite direction that result in time lag in the oscillations.

5.9. Flow Reversal

Recently, flow reversal of liquid drops was observed by Daniel et al[1], Dong et al[42] with a different kind of asymmetric vibration. Such a flow reversal was termed polarized ratchet. Here, 1 and $4\mu L$ drops moved in different directions when subjected to asymmetric vibrations of zero mean. The flow reversal has been attributed to the phase change in the oscillations of center of masses of drops of different volumes. The phase change in the oscillations results from the amount of viscous dissipation in the bulk of the drops that is volume dependent. The smaller drops have smaller dissipation in the bulk where as the larger drops have large dissipation. The liquid drops move in opposite directions due to opposite phase in the oscillations of center of masses which are

151

illustrated in Figure 5.4 and 5.5. Here the oscillations of the center of masses of $4\mu L$ and $1\mu L$ water drops are out of phase with each other. In order to show such details, the center of masses of $4\mu L$ and $1\mu L$ drops was tracked using a video recording with a high speed camera at 2000 frames/sec. The analysis of center of masses from the high speed video images is carried out using Moment Calculator plug-in available in ImageJ software[43]. The plug-in calculates spatial moment of order 1 that corresponds to the center of mass of 2-dimensional image. The oscillations of center of masses of $4\mu L$ and $1\mu L$ water drops thus determined are shown in Figure 5.5 in the reference frame of moving drop. The time lag (phase shift) between oscillations of center of masses of $4\mu L$ and $1\mu L$ water drops results in the drops moving in opposite directions when subjected to asymmetric vibrations. Another interesting observation is that for every one cycle of oscillation of center of mass of $1\mu L$ drop, there are two cycles of oscillations for $4\mu L$ drop. Benilov[44] recently analyzed situation of a drop moving uphill due to asymmetric vibrations whose acceleration profile has flat wide crests and narrow deep troughs with zero mean.

In order to dramatically show such an effect, we carried out an experiment with current asymmetric vibration on decyltrichlorosilane monolayer coated surface by inclining it 15° deg to the horizontal. The $1\mu L$ drop was placed on the upper side of the inclined surface where as $4\mu L$ drop was placed on the bottom side of the surface. When subjected to asymmetric vibration, contrary to the naïve expectation, the $1\mu L$ runs down the surface where as the $4\mu L$ moves up hill (Figure 5.6). These experiments are relevant to the recent experiments carried out by Noblin et al[29] and Brunet et al[30]. Here, Noblin et al[29] have subjected liquid drops to simultaneous vertical and horizontal

152

vibrations on horizontal substrate and showed that the direction of the drop motion can be reversed by tuning the phase difference between the vertical and horizontal vibrations. These experiments are in a sense similar to the experiments of Daniel et al[1] because the phase difference in the oscillations is tuned by changing the volume of drop in Daniel et al[1]'s experiments where as it is done by tuning the phase difference between the vertical and horizontal vibrations in Noblin et al's[29] experiment. Noblin et al[29] have also argued, similar to the arguments of Daniel et al[1], that the contact angle hysteresis is responsible for symmetry breaking resulting in the directed motion. They proposed that the asymmetric forces acting on the contact line of drop brought about by the contact angle hysteresis are responsible for the ratcheting motion of drops.

In a different experiment, Brunet et al[30] observed climbing of drops on an inclined surface when subjected to symmetric vibrations of high accelerations. They attributed this effect to the symmetry breaking mechanism resulting from inclination of substrate and to the non-linear friction force between the drop and the substrate. They indicated that the contact angle hysteresis is completely eliminated when the drops are moving; hence it plays no role in making the drops move uphill. However, this is in contrast to Daniel et al[1]'s theory that attributes such a climbing up of drops to contact angle hysteresis in absence of which the drops would simply run down without showing any upward motion. In order to show that the vibration component vertical to the substrate may not be required in moving the drops on horizontal substrate, we carried out an experiment by subjecting a $10\mu L$ water drop on PDMS DMS-T22 surface to symmetric sine vibrations at a frequency of 40 Hz and acceleration amplitude of 100 m/s^2(Figure 5.7, left panel). Here, the drop shows significant deformation of shape. Such a huge and

chaotic shape deformation might have been responsible for climbing of drop as observed by Brunet et al[30]. We also carried an experiment where a $10\mu L$ water drop on micro fibrillated PDMS substrate subjected symmetric sine vibration at a frequency of 40 Hz and acceleration amplitude of 90 m/s^2(Figure 5.7, right panel). The PDMS surface is the low hysteresis (2 deg) surface used in the asymmetric vibration experiments described above that has square fibrils of $10\mu m$ size with fibrillar spacing of 95 μm. Here, the drop detaches from surfaces due to low hysteresis, bounces off of the surface. It drops onto the surface to bounce of again. The drop repeats the process of bouncing off until it reaches the end of the substrate. Such a detachment of drop from superhydrophobic surfaces has been discussed in the literature in the context of vertical vibrations[45]. But, here we show that horizontal vibrations can also be used for detachment of water drops.

154
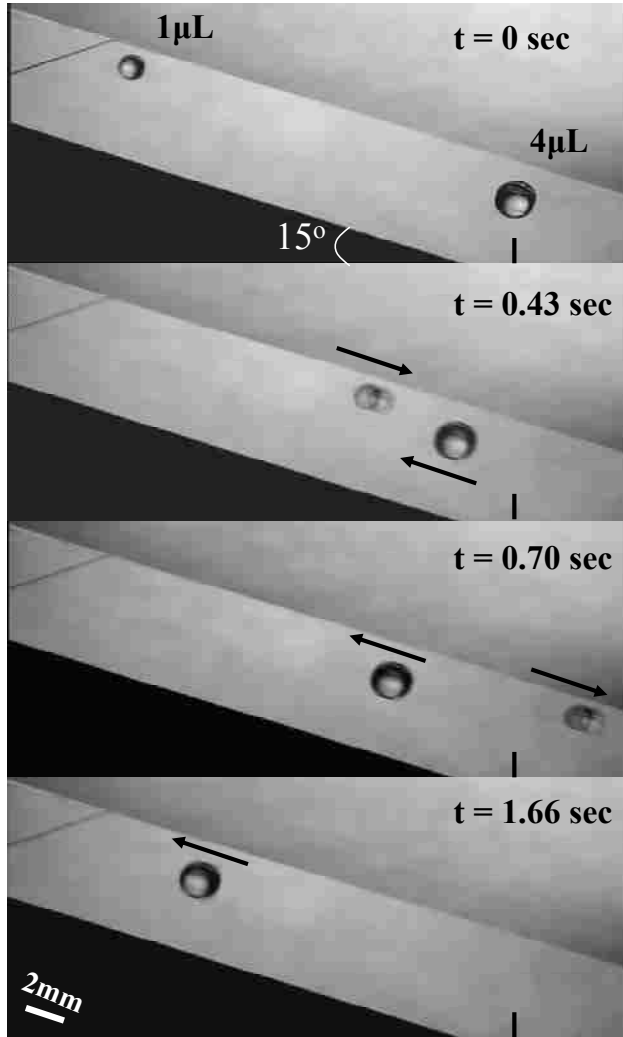
Figure 5.6. (a). Uphill motion of a $4\mu L$ drop and a downhill motion of a $1\mu L$ drop on an inclined hydrocarbon (decyltrichlorosilane) monolayer coated silicon wafer subjected to an asymmetric vibration ($A_o = 63m/s^2$ and $\omega = 100Hz$). The inclination of the plate is 15° from the horizontal plane.
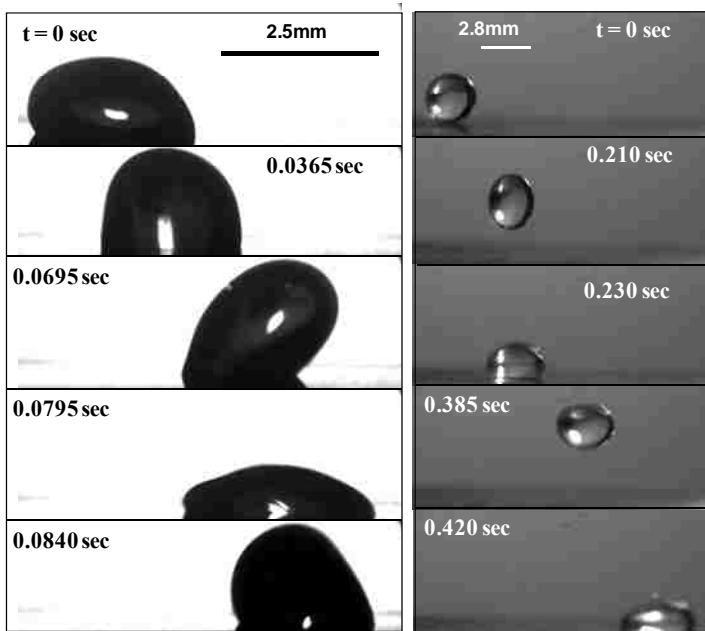
Figure 5.7. (Left panel) A 10μL drop of water moves on a PDMS (DMS T22) coated horizontal silicon wafer that is vibrated with a sinusoidal vibration parallel to the surface at a frequency of 40 Hz and acceleration amplitude of 100 m/s^2. Significant deformation of the drop shape is observed here. (Right panel) A 10μL drop of water moves on micro fibrillated PDMS substrate when it is vibrated with a sinusoidal vibration parallel to the surface at a frequency of 40 Hz and acceleration amplitude of 90 m/s^2. The PDMS surface is the low hysteresis (2 deg) surface used in the asymmetric vibration experiments described above that has square fibrils of 10μm size with fibrillar spacing of 95 μm. The drop flies in the air, falls on the surface -- only to fly off again. The repetition of this process leads to a net motion of the drop. A vibration induced detachment of a drop from a superhydrophobic surface was reported previously[36,54-56] with a vertical vibration. Here the vibration is horizontal to the surface.

John and Thiele[31,32] also indicated that the asymmetric shape fluctuations are responsible for the motion in the above experiments. However, we show that the flow reversal as observed in the case of liquid drops can also be observed when a solid object on a solid substrate is subjected to asymmetric vibrations. In order to show this, we carried out an experiment where a 4mm diameter solid steel ball on micro fibrillated PDMS substrate is subjected to asymmetric vibrations of various amplitudes (Figure 5.8). The PDMS surface has square fibrils of   10μm size with fibrillar spacing of 50 μm.

156

Here, the steel ball moves to the right when amplitude of acceleration of vibrations is 92 m/s^2 where as it moves to the left when it is 142 m/s^2. As the steel ball is rigid there are no shape fluctuations; hence the flow reversal might be the result of non-linear rolling friction force between the steel ball and fibrillated surface. Such a flow reversal is observed when friction force between the steel ball and fibrillated PDMS surface has an ascending and descending branch as a function of velocity. In a related theoretical analysis of a solid object on solid substrate subjected to asymmetric vibrations, Fleishman[24] et al observed a similar flow reversal that was attributed to non-linear friction force between the two solids.
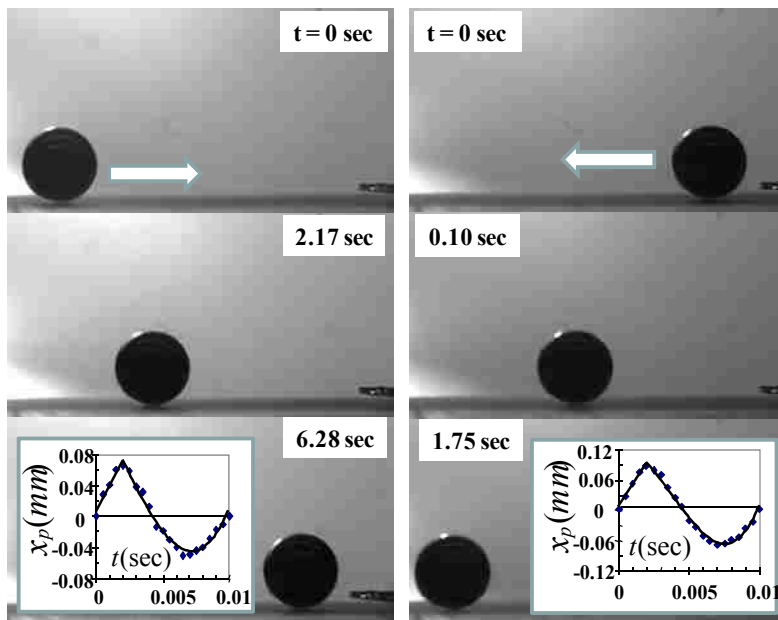
Figure 5.8. Motion of a steel ball (4 mm) on a horizontal fibrillated PDMS surface due to an asymmetric vibration. The PDMS surface has square fibrils of $10\mu m$ size with fibrillar spacing of 50 μm. The frequency of the vibration is 100 Hz. Left panel shows that the steel ball moves from left to right when the vibration amplitude is 92 m/s^2. The steel ball moves in the opposite direction (right panel) when the vibration amplitude is 142 m/s^2. A nonlinear rolling friction force between steel ball and surface, which has an ascending and descending branch as a function of velocity, seems to be responsible for the flow reversal. One cycle of the displacement of the plate as a function of time is shown in the insets. Previously, Fleishman[24] et al envisaged a similar flow reversal for the case of small solid object sliding on a   solid support.

5.10. Comparison of Experimental and Simulation Results

We describe the procedure used to theoretically explain the above experimental observations. In the previous model of contact angle hysteresis[1,3,26,,46,47,53], drop is approximated as a linear harmonic oscillator and magnitude of threshold hysteresis force that is acting to retard contact line motion of a drop is assumed to be constant. Even though previous model was able to qualitatively show that contact angle hysteresis is responsible for symmetry breaking, it could not quantitatively predict the role played by contact angle hysteresis. Therefore, we introduced modifications to the previous model by incorporating a non-linear contact angle hysteresis term that depends on velocity of contact line of drop. Since a liquid drop has two degrees of freedom (Figure 5.9), one at the base and the other at the center of mass, two coupled equations are required to describe its motion. In order to describe the equation of motion of the center of mass of the drop (x_2), an inertial force, a damping force, a spring force and the imposed oscillatory force are taken into account (eq 5.1). The inertial force is formally ignored in describing the dynamics of the contact line (x_1). Here, an additional force due to contact angle hysteresis is considered (eq. 5.2)[1].
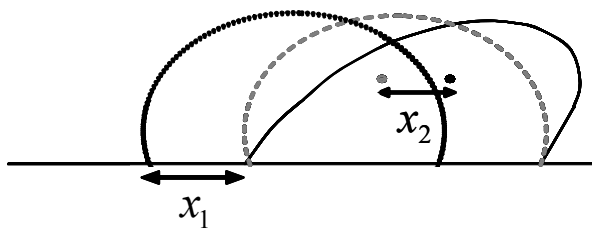
Figure 5.9.   Schematic of the oscillation of a drop on a surface. x_1 indicates the displacement of the contact line relative to the plate and x_2 indicates the displacement of center of mass relative to its undeformed state.

$$\frac{d^2x_2}{dt^2} + \frac{1}{\tau_B}\frac{dx_2}{dt} + \omega_o^2 x_2 = \gamma(t) \qquad\qquad (5.1)$$

$$\frac{1}{\tau_L}\frac{dx_1}{dt} = \omega_o^2 x_2 + \frac{1}{\tau_B}\frac{dx_2}{dt} - \Delta\tanh\left(\alpha\frac{dx_1}{dt}\right) \qquad\qquad (5.2)$$

Here, x_1 and x_2 are the displacements of contact line and center of mass of drop respectively. τ_B and τ_L are the relaxation times (the ratios of the mass of the drop and kinematic friction coefficient) due to viscous friction in the bulk and near the contact line of the drop. $\omega_o = \sqrt{k_s/M}$ is the resonance frequency of a drop with M being its mass. The spring constant ($k_s = 2\pi\gamma_{lv}$) is proportional to the surface tension of the liquid, γ_{lv}. $\gamma(t)$ is the imposed acceleration on drop: $-A_o(\cos(2\pi\omega t) + 2\cos(4\pi\omega t))$. The negative sign indicates that the acceleration of the drop is in opposite direction to that of the plate. $\Delta\tanh(\alpha V)$ is the hysteresis force divided by the mass of the drop, where $V = dx_1/dt$ is the velocity of the contact line. Usually, hysteresis term enters in the equation of motion as a jump discontinuity, $\sigma(V)\Delta$ with $\sigma(V) = V/|V|$ providing the sign of velocity of the contact line. $\sigma(V)$ takes the values of -1, 0, +1 when $V < 0$, $V = 0$, $V > 0$ respectively that ensures that the resistance due to contact angle hysteresis always acts against the motion of contact line of drop. The difficulty associated with this model is that the signum function is discontinuous at $V = 0$ which results in the discontinuity in force versus velocity relationship. Several approximations can be used to by-pass this discontinuity. One approximation is to use piecewise continuous functions[49-51] instead of the signum function. The second method is to replace the signum function with another non-linear function such as $\tanh(\alpha V)$, which is widely used in tribology literature[52]. Here,

Coulombic dry friction[48] that has a jump discontinuity similar to that of the wetting hysteresis at $V=0$. Here, α is a parameter that signifies how fast the resistive force (acceleration) due to contact angle hysteresis reaches the threshold force (acceleration, Δ) as a function of velocity of contact line as shown schematically in Figure 5.10. In the limit of $\alpha \to \infty$, hyperbolic tangent function is a good approximation to signum function. We numerically solve equations 5.1 and 5.2 to gain an understanding of how the drift velocity depends on the threshold value of the hysteresis Δ.
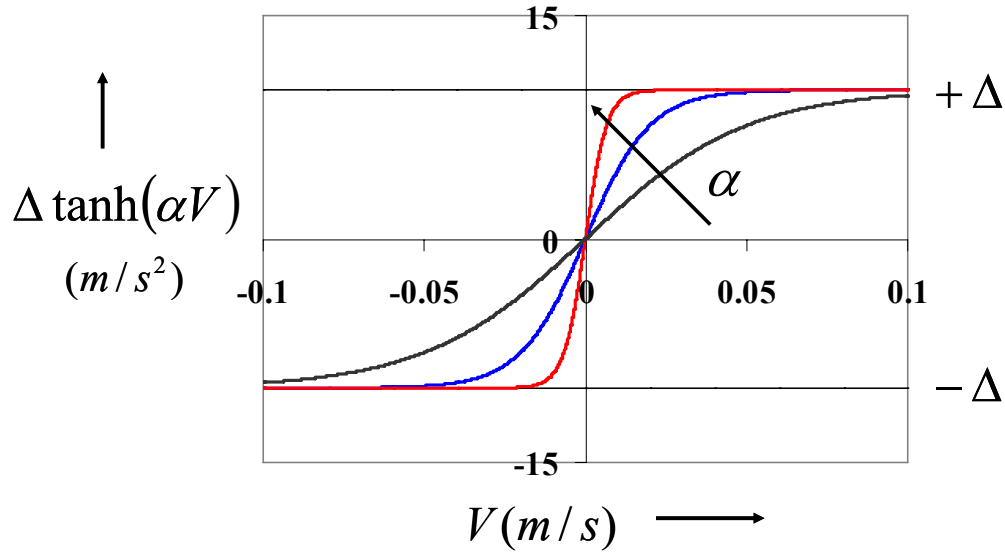
Figure 5.10. Schematic of variation of non-linear contact angle hysteresis as a function of velocity of contact line at various α values. Here, Δ is the threshold contact angle hysteresis. The force versus velocity relation is linear in the limit of small α and it is highly nonlinear in the limit of large α. In the limit of $\alpha \to \infty$, hyperbolic tangent function is a good approximation to signum function ($\sigma(V) = V/|V|$).

5.11. Estimation of Parameters for Numerical Simulations

The unknown parameters in the simulations are Δ, τ_L and τ_B. We found that it is very difficult to accurately estimate these physical parameters required to carry out numerical simulations. In order to approximately estimate these parameters,

we tracked the high resolution motion of the contact line of water drops (1μL and 4μL) on the hydrocarbon surface to match drift velocity, the direction of the drift, amplitude of oscillation and its phase in simulations to the experiments. We carried out numerical simulations of equations 5.1 and 5.2 in order to obtain displacement of contact line (x_1) of drop and thus the velocity of the drop which is compared with the experimental data. We used commercial software Mathematica$^{®}$ to numerically solve the simultaneous differential equations 5.1 and 5.2. The integration time step is $\Delta t = T/1000$ where $T = 0.01s$ is time period corresponding to fundamental frequency ($\omega = 100 Hz$) of oscillations. We show the comparison of experimental and simulation results corresponding to $A_o = 33 m/s^2$ in Figure 5.11. We are able to describe the magnitude and drift velocity as well as amplitude of contact line oscillations and its phase using the values of τ_L, τ_B and Δ as 0.003 sec, 0.002sec and $35 m/s^2$ respectively for the 1μL drop. These values are 0.01sec, 0.008 sec and $10 m/s^2$ for the 4μL drop. As seen from Figure 5.11, not only the amplitude of contact line motion but also the exact shape from simulations matches accurately with the contact line motion obtained from experiments. The simulation not only predicts the exact details of the contact line motion of 4μL and 1μL drops but also shows that the drops move in opposite direction. The simulation results are found to be insensitive to the value of α as long as it is large enough. We used a value of $\alpha = 50(s/m)$, although higher values of α (100 s/m to 200 s/m) produced similar numerical results as well.
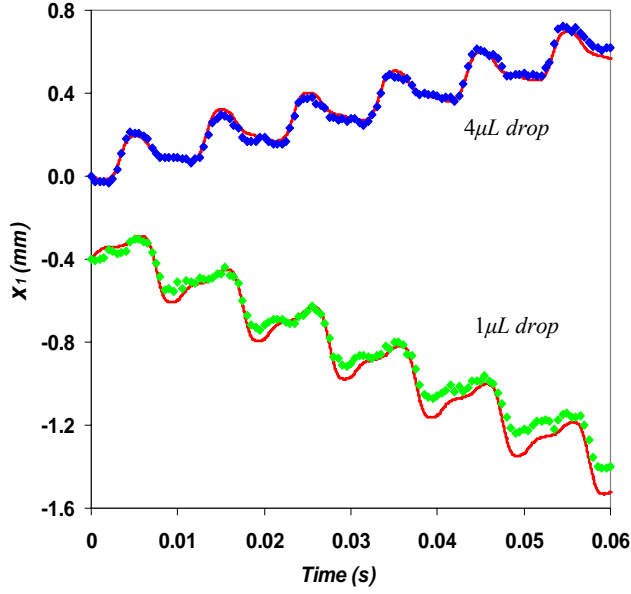
Figure 5.11. Displacements of the contact lines of $4\mu L$ and $1\mu L$ water drops on a hydrocarbon monolayer coated silicon wafer subjected to an asymmetric vibration with $A_o = 33m/s^2$. x_1 corresponds to the displacement of the contact line of the drop relative to the plate as shown schematically in Figure 5.9. The initial positions of the drops are shifted from zero for the clarity of presentation. The blue and green symbols represent the experimental data and the red lines represent the simulation results. We used commercial software Mathematica$^®$ to numerically solve the simultaneous differential equations 5.1 and 5.2. The integration time step is $\Delta t = T/1000$ where $T = 0.01s$ is time period corresponding to fundamental frequency ($\omega = 100Hz$) of oscillations.

We found that the values of the relaxation times and Δ are in the expected directions for the drops of two different sizes. The Langevin relaxation time (the ratio of the mass to kinematic friction coefficient) is $\tau_L = M/\zeta$; hence $\tau_L \sim R^3/R$ i.e. $\tau_L \sim V^{2/3}$ where R is the radius of drop and V is the volume of the drop. Thus τ_L scales with the volume (V) of the drop as $\tau_L \sim V^{2/3}$. Using this scaling law, τ_L for the larger drop is expected to be at least 2.5 times larger than that of the smaller drop. The value of τ_L that is used to describe the motion of the contact line for the larger drop is found to be about 3

times larger than that of the smaller drop. However, as $\Delta \sim R/M$; hence $\Delta \sim R/R^3$.

This results in $\Delta \sim V^{-2/3}$. Using this scaling law, we expect that Δ for the larger drop to

be at least 2.5 times smaller than that of the smaller drop. The value of Δ used in the

simulations to describe the motion of the contact line for the smaller drop is found to be

about 3.5 times larger than that of the larger drop. The bulk relaxation time for the larger

drop being greater than the smaller drop is also in the expected direction. The values of

the parameters τ_L, τ_B and Δ, as obtained by fitting the experimentally obtained motion

of contact lines, are further validated by simulation of drift velocities of the two different

size drops on two chemically different surfaces (PDMS coated and hydrocarbon coated

silicon wafers) but with similar hysteresis at different amplitudes (Figure 5.12). Here, the

drift velocities are calculated as function of amplitude of vibration.
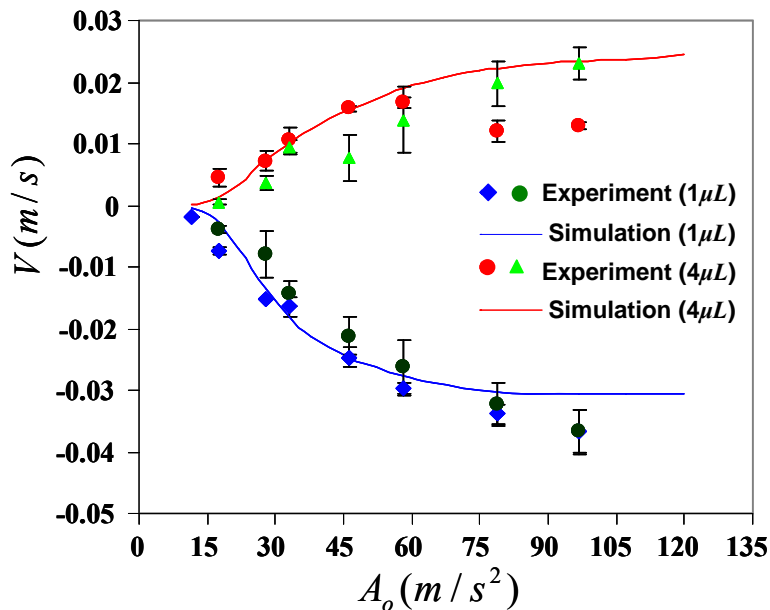
Figure 5.12. Drift velocities of 1 and $4\mu L$ water drops subjected to asymmetric vibration as a function of amplitude of acceleration (A_o). These experiments are carried out on two different surfaces of similar hysteresis. Blue diamonds and red circles correspond to the data obtained on a hydrocarbon monolayer coated silicon wafer whereas the dark green circles and the light green triangles correspond to the data obtained on a PDMS monolayer (Trimethylsiloxy-terminated, Gelest Inc., product code: DMS-T22)

coated silicon wafer. As indicated in the text, both of the surfaces used in these experiments have similar hysteresis (8°). The solid blue and red lines correspond to the simulation results.

The simulation results show that there exists threshold amplitude of acceleration for each drop ($A_o \sim 11.5 m/s^2$ for 1μL drop and $A_o \sim 17 m/s^2$ 4μL for drop), below which no drift occurs. The drift velocity increases non-linearly as the amplitudes of acceleration becomes greater than the threshold. The drift velocity of drops saturates at higher amplitude of vibrations. Later, we describe the reasons for such a saturation observed at high amplitudes. The simulation results are in good agreement with the experimental observations of drop motion as shown in Figure 5.12.

After such a thorough validation of the new contact angle hysteresis model as done by matching the detailed contact line motion, magnitude and direction of drift velocity as well as the drift velocities on two different surfaces as a function amplitude of vibration, we were convinced that the model is reasonably accurate. We then numerically estimated the drift velocities of the drops of different sizes as a function of the threshold hysteresis Δ using equations 5.1 and 5.2. The values of the parameters τ_L and τ_B used for this simulation are same as those used for the hydrocarbon monolayer. In reality τ_L and Δ values are dependent on the chemical and physical nature of the surface. In ideal numerical simulation τ_L should be estimated approximately for each surface. However, we used constant τ_L in the numerical simulations by varying Δ in order to observe the effect of contact angle hysteresis alone on the drift velocity of drops. The value of τ_L is initially estimated for drop motion of hydrocarbon monolayer coated silicon wafer. For fluorocarbon and PDMS coated silicon wafers τ_L estimated as above is reasonable since

164

the average contact angles on these surfaces are in the range 103-110. These angles are in the range of contact angles for hydrocarbon monolayer coated silicon wafer. However, for fibrillated PDMS surface and polystyrene coated silicon wafer the average angles are 161 and 80 for which τ_L may be very different. As we were only interested in trend of drift velocity as a function of Δ, we carried the numerical simulations by keeping τ_L constant and varying Δ. The simulation results (Figure 5.13) thus obtained are in semi-quantitative agreement with the experimental results that show that the drift velocity vanishes as Δ goes to zero; it increases with Δ, reaching a maximum value, and then it decreases as the hysteresis increases further.
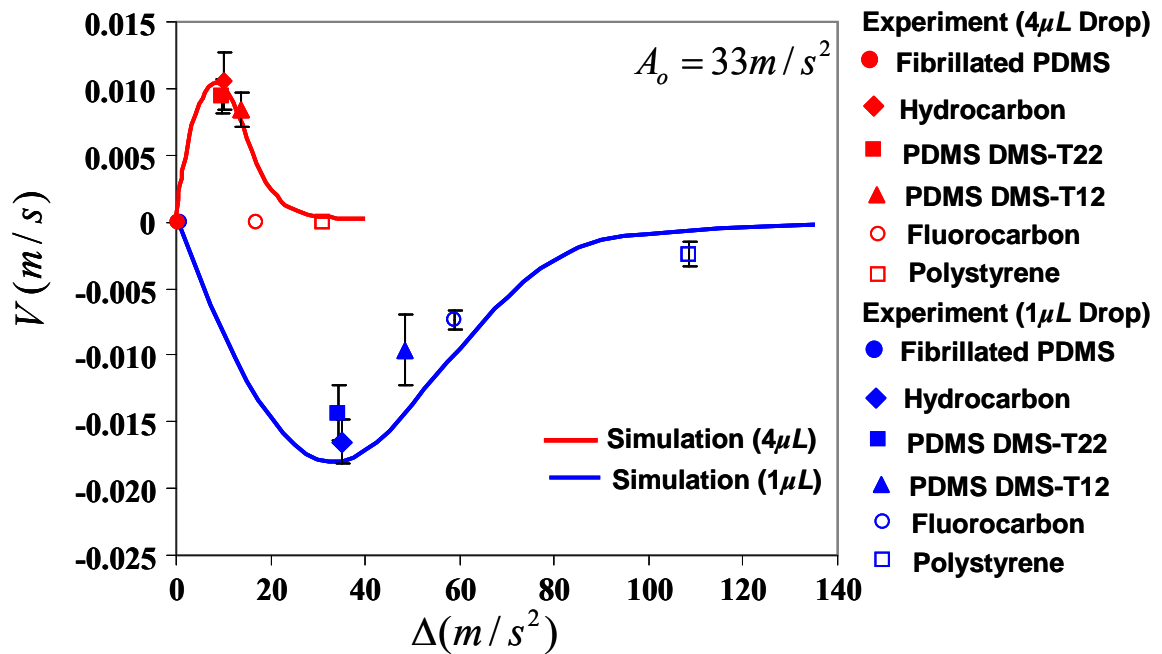
Figure 5.13. Effect of contact angle hysteresis (Δ) on the drift velocities of 1μL and 4μL drops subjected to an asymmetric vibration ($A_o = 33m/s^2, \omega = 100Hz$). The solid blue and red lines correspond to the simulation results.

When Δ is zero, the drops do not show any net motion due to the absence of the required non-linearity to break the periodic symmetry of external vibrations. On the other hand, with intermediate hysteresis the drop drifts with high velocity. At very high hysteresis, the applied vibration is not able to de-pin the contact line from the surface defects; hence the drift velocity is zero. The simulation results are compared with the threshold hysteresis for various surfaces obtained using equation 5.3 and using the measured contact angles[53].

$$\Delta = \frac{2\pi a \gamma_{lv}(\cos\theta_r - \cos\theta_a)}{M} \qquad (5.3)$$

where a is contact radius of drop, θ_a and θ_r are the advancing and receding contact angles respectively, M is the mass of the drop and γ_{lv} is the surface tension of the liquid. The trend of the simulation results is in good agreement with the experimental data in which the drift velocity varies non-monotonically with Δ, exhibiting maximum at intermediate values of the hysteresis. As observed from the Figure 5.13, the simulations results deviate from experimental data. This is due to approximate nature of the model used in the simulation. In order to accurately simulate the drop motion, we need to solve full hydrodynamic equations along with taking into effect of details of contact angle hysteresis phenomena. In spite of these deviations, the main result is clear in that neither vanishing hysteresis nor large hysteresis is conducive to the drop motion. Some finite, but, small hysteresis is needed for drop to move on a surface in the presence of an asymmetric vibration.

5.12. Drift Velocity Saturation at High Amplitudes

In this section we explain why the drift velocities of drops show a plateau at higher amplitudes of acceleration (Figure 5.12). Here, we provide an explanation based on our numerical simulations and show that the velocity saturation at higher amplitudes of acceleration is a manifestation on non-linearity in contact angle hysteresis. Ignoring the initial transients in the solution of center of mass from equation 5.1, the response of center of mass (x_2) of drop to asymmetric vibrations is periodic. Assuming x_2 to be a periodic function of time, equation 5.2 can be integrated over one cycle of asymmetric vibration as below

$$\frac{1}{\tau_L}\int_0^T\left(\frac{dx}{dt}\right)dt = \omega_o^2\int_0^T x_2 dt + \frac{1}{\tau_B}\int_0^T\left(\frac{dx_2}{dt}\right)dt - \int_0^T \Delta\tanh\left(\alpha\frac{dx}{dt}\right)dt \qquad (5.4)$$

Here T is the time period of vibration. The contributions of first two terms on the right hand side of equation 5.4 to the net drift are zero as x_2 and $\dfrac{dx_2}{dt}$ are periodic functions (here also ignoring the initial transients). Therefore, net drift in one cycle of vibration is given by the area under the curve of non-linear contact angle hysteresis as a function of time as given below.

$$\frac{\overline{X}}{\tau_L} = -\int_0^T \Delta\tanh\left(\alpha\frac{dx}{dt}\right)dt \qquad (5.5)$$

We have carried out numerical simulation of equations 5.1 and 5.2 for a 1μL water drop subjected to asymmetric vibrations of various amplitudes in order to see whether the area under the curve of non-linear contact angle hysteresis as a function of time shows saturation at higher amplitudes. As seen from Figure 5.14 that shows non-linear contact angle hysteresis at various amplitudes of accelerations for a 1μL water

drop, the area under the curve increases as the amplitude of acceleration increases showing saturation at very high amplitudes of acceleration.
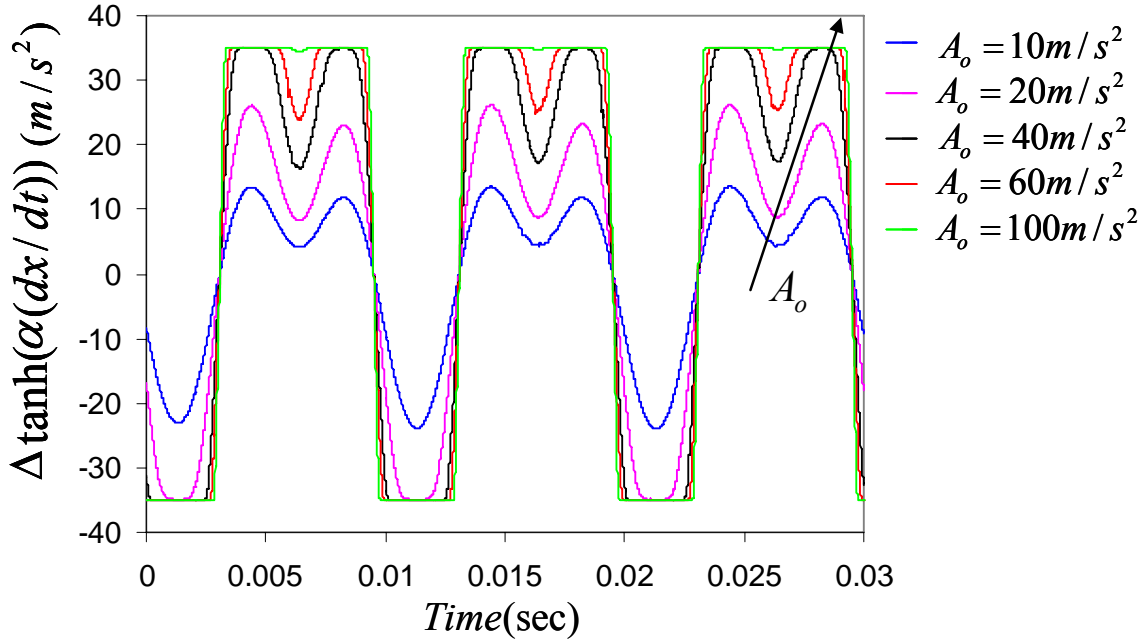
Figure 5.14. Variation of non-linear contact angle hysteresis as a function of time at various amplitudes of acceleration of asymmetric vibrations for a $1\mu L$ water drop. As the amplitude of acceleration increases, area under the curve $\left(\dfrac{\overline{X}}{\tau_L} = -\displaystyle\int_0^T \Delta\tanh\left(\alpha\dfrac{dx}{dt}\right)dt\right)$ i.e. the net drift over one cycle of vibration saturates resulting in the saturation of drift velocity at higher amplitudes of vibration as observed in Figure 5.12.

5.13. Conclusions

We experimentally demonstrated that for drop motion to occur in presence of asymmetry vibrations there needs to be a symmetry breaking mechanism. We showed that the contact angle hysteresis provides necessary non-linearity that breaks the symmetry. We successfully developed a non-linear contact angle hysteresis model to elucidate the critical role played by contact angle hysteresis in this case. Systematic experiments are also carried out to elucidate the nature of velocity amplitude

relation for drops subjected to asymmetric vibration. The non-linear contact angle hysteresis model predicts magnitude and direction of velocities of drops of various masses. The model also accurately predicts the minute details of contact line motion. The drift velocity increases non-linearly with amplitude reaching a plateau at higher amplitudes.

We think that the role played by non-linear hysteresis required for drop motion to occur on an asymmetrically vibrated surface that is proposed earlier by Daniel et al[1] is very similar to the non-linear friction model put forward by Brunet et al[30] to explain the motion of drops due to an oblique vibration. However, the current experiments confirm the definitive role played by contact angle hysteresis in the rectification. The absence of any net motion of the drops on the fibrillated PDMS with negligible hysteresis, but its high drift on the hydrocarbon coated wafer clearly shows that there needs to be some amount of contact angle hysteresis in order to break periodic symmetry resulting in rectification. However, on surfaces with very high hysteresis the drops do not show any motion due to contact line pinning that is not overcome by a moderate amount of external vibration. It is worth noting here that the shape of the oscillating drop on the fibrillated PDMS as well on the polystyrene surface exhibit some noticeable asymmetry, but it does not lead to a net motion of the drop. This observation suggests that asymmetric shape fluctuation may not have a strong role to play in these experiments, although it is quite plausible that its role would be significant for larger size drops experiencing much stronger vibrations (Figure 5.7). In the problem studied here, a first order non-linear force due to hysteresis is responsible for breaking the periodic symmetry. The Coulombic friction that is analogous to contact angle   hysteresis can also lead to motion of solid

objects under periodic or stochastic settings. It is to be noted that there is no shape fluctuations with a solid object. Hence, the only mechanism that is responsible for symmetry breaking is non-linear friction force between solid object and solid surface (Figure 5.8).

5.14. References:

1. Daniel, S.; Chaudhury, M. K.; De Gennes, P.-G. *Langmuir* **2005**, *21*, 4240.

2. Daniel, S.; Chaudhury, M. K. *Langmuir* **2002**, *18*, 3404.

3. Daniel, S.; Sircar, S.; Gliem, J.; Chaudhury, M. K. *Langmuir* **2004**, *20*, 4085.

4. Ouellette, J. *Ind. Phys*. **2003**, *9*, 14.

5. Wu, H.; Wheeler, A.; Zare, R. N. *Proc. Natl. Acad. Sci. U.S.A.* **2004**, *101*, 12809.

6. Northrup, M. A. *Anal. Chem* **1998**, *70*, 918.

7. Darhuber, A. A.; Davis, J. M.; Troian, S. M.; Reisner, W. W. *Phys. Fluids* **2003**, *15*, 1295.

8. Darhuber, A. A.; Valentino, J. P.; Davis, J. M.; Troian, S. M.; Wagner, S. *Appl. Phys. Lett*. **2003**, *82*, 657.

9. Darhuber, A. A.; Troian, S. M. *Annu. Rev. Fluid Mech.* **2005**, *37*,425.

10. Daniel, S.; Chaudhury, M. K.; Chen, J. C. *Science* **2001**, *291*, 633.

11. De Gennes, P.-G. *Rev. Mod. Phys.* **1985**, *57*, 827.

12. Leger, L.; Joanny, J. F. *Rep. Prog. Phys* **1992**, *55*, 431

13. Bonn, D.; Eggers, J.; Indekeu, J.; Meunier, J.; Rolley, E. *Rev. Mod. Phys*. **2009,** *81*, 739.

14. Sandre, O.; Gore-Talini, L.; Ajdari, A.; Prost, J.; Silberzan, P. Phys. Rev. E 1999, 60, 2964.

15. Buguin, A.; Talini, L.; Silberzan, P. *Appl. Phys. A* **2002**, *75*, 207.

16. Marquet, C. ; Buguin, A.; Talini, L.; Silberzan, P. *Phys. Rev. Lett.* **2002**, *88*, 168301.

17. Gorre, L.; Ioannidis, E.; Silberzan, P. *Eur. Phys. Lett* **1996**, *33*, 267.

18. Ajdari, A.; Prost, J. ; Mukamel, D.; Peliti, L. ; *J. Phys. I France* **1994**, *4*, 1551.

19. Julicher, F .; Ajdari, A.; Prost, J. *Rev. Mod. Phys.* **1997**, *69*, 1269.

20. Kettner, C.; Reimann, P.; Hanggi, P.; Muller, F. *Phys. Rev. E* **2000**, 61, 312.

21. Cebiroglu, G.; Weber, C.; Schimansky-G, L. *Chem. Phys.* **2010**, *375*, 439.

22. Hanggi, P.; Marchesoni, F. *Rev. Mod. Phys*. **2009**, *81*, 387.

23. Mogilner, A.; Mange1, M.; Baskin, R. J. *Phys. Lett. A.* **1998**, *237*, 297.

24. Fleishman, D.; Asscher, Y.; Urbakh, M. *J. Phys.: Condens. Matter*. **2007**, *19*, 096004.

25. Fleishman, D.; Klafter, J.; Porto, M.; Urbakh, M. *Nano Lett*. **2007**, *7*, 837.

26. Buguin, A.; Brochard, F.; De Gennes, P.-G. *Eur. Phys. J.E* **2006**, *19*, 31.

27. Mahadevan, L.; Daniel, S.; Chaudhury, M. K. *PNAS* **2004**, *101*, 23 (see also the supporting movie 1)

28. Eglin, M.; Eriksson M, A.; Carpick R, W. *J. Appl. Phys* **2006**, *88*, 091913.

29. Noblin, X.; Kofman, R.; Celestini, F. *Phys. Rev. Lett.* **2009**, *102*, 194504.

30. Brunnet, P.; Eggers, J.; Deegan, R. D. *Phys. Rev. Lett.* **2007**, *99*, 144501.

31. John, K.; Thiele, U. *Phys. Rev. Lett.* **2010**, *104*, 107801.

32. Thiele, U.; John, K. *Chem. Phys.* **2010**, *375*, 578.

33. Mettu, S.; Chaudhury, M. K. *Langmuir* **2010**, *26*, 8131.

34. Smith, T.; Lindberg, G.; *J. Colloid Interface Sci.* **1978**, *66*, 363.

35. Andrieu, C.; Sykes, C.; Brochard, F. *Langmuir* **1994**, *10*, 2077.

36. Nadkarni, G. D.; Garoff, S. *Langmuir* **1994**, *10*, 1618.

37. Decker, E. L.; Garoff, S. *Langmuir* **1996**, *12*, 2100.

38. Meiron, T.S.; Marmur, A.; Saguy, I.S. *J. Colloid Interface Sci.* **2004**, *274*, 637.

39. Marinescu, M.; Urbakh, M.; Barnea, T.; Kucernak, A. R.; Kornyshev, A. A. *J. Phys. Chem. C* **2010**, *114*, 22558.

40. Glassmaker, N. J.; Jagota, A.; Hui, C. Y.; Noderer, W. L.; Chaudhury, M. K. *PNAS* **2007**, *104*, 10786.

41. Krumpfer, J. W.; McCarthy, T. J. *Faraday Discuss.* **2010**, *146*, 103.

42. Dong, L.; Chaudhury, A.; Chaudhury, M. K. *Eur. Phys. J.E* **2006**, *21*, 231.

43. ImajeJ Software, NIH, USA. http://rsbweb.nih.gov/ij/.

44. Benilov, E. S. *Phys. Rev. E* **2010**, *82*, 026320.

45. Boreyko, J.B.; Chen, C-H. *Phys. Rev. Lett.* **2009**, *103*, 174502.

46. De Gennes, P. -G. *J. Stat. Phy*s. **2005,** *119*, 953.

47. Mettu, S.; Chaudhury, M. K. *Langmuir* **2008**, *24*, 10833.

48. Caughey, T. K.; Diennes, J, K.; *J. Appl. Phys* **1961**, *32*, 2476.

49. Makkar, C.; Dixon, W. E.; Sawyer, W. G. ; Hu, G. Proceedings of the 2005 IEEE/ASME International Conference on Advanced Intelligent Mechatronics, Monterey, California, USA, 24-28 July, 2005

50. Cull, S. J.; Tucker, R. W. *J. Phys. A: Math. Gen.* **1999**, 32, 2103.

51. Karnopp, D. *ASME J. Dyn. Syst .Measurement and Control* **1985**, *107*, 100.

52. Andersson, S.; Soderberg, A.;   Bjorklund, S. *Tribology*

International **2007**, 40, 580.

53. Noblin, X.; Buguin, A.; Brochard, F. *Eur. Phys. J. E* **2004**, *14*, 395.

54. Shastry, A ; Case, M.J ; Bohringer, K.F. *Langmuir*, **2006**, *22*, 6161.

55. Reyssat, M ; Pardo F ; Quere, D. *Euro. Phys. Lett*. **2009**, *87*, 36003.

56. Malvadkar, N.A ; Hancock, M.J, Sekeroglu, K ; Dressick, W.J, Demirel, M.C. *Nat. Mat*. **2010**, *9*, 1023.

Chapter 6: Resonance Modes of the Surface and the Slipping Contact Line of a Sessile Liquid Drop Subjected to Random Vibration

6. 1. Introduction:

It is well known from the works of Kelvin[1], Rayleigh[2], Lamb[3] and Chandrasekhar[4] that a vibrating liquid drop exhibits multiple resonance modes that depend on mass, and surface tension of liquid. The viscosity of liquid also has an effect on resonance frequencies which is minor compared the effect of mass and surface tension. The resonant properties of liquid drops are crucial to many technological processes such as crystallization[5,6], spray coating[7], inkjet printing[8], vibration induced motion of drops on surfaces[9-13] and microscale heat transfer involving drop wise condensation[12]. Estimation of multiple resonance modes of liquid drops would greatly enhance the design of microfluidic devices. Also, from the fundamental point of view, oscillating bubbles and drops are useful in estimating surface tension of liquids[14-16].

Recently, there have been many techniques developed for measuring resonant properties of liquid drops[5,6,10,11,17-35]. The first method involves subjecting liquid drops to external harmonic vibration and recording high speed videos of oscillating drops with a high speed camera[5,6,10,11,17-24,35]. Vibrating drops show maximum displacements when excited close to resonance frequencies. Here, the shape fluctuations of drops or displacements measured from high speed videos are used to estimate resonance frequencies. The second method involves subjecting the drops to external vibration and measuring the deformation of interface using laser beam deflection from the surface of drop[25-29] or displacement of particle trapped inside the drop using optical tweezers[30]. Third

method developed recently uses an AFM probe to disturb interface of a liquid drop and measures response of AFM cantilever to interface oscillations in order to deduce the information of resonance properties[31]. Another class of technique used for measuring resonance properties is electrowetting of liquid drops that uses response of an electrowetting liquid subjected to oscillating electric field[34]. Recently, significant advances have also taken place in characterizing the internal flow of a vibrating drop using particle velocimetry[36, 37] that may be potentially used for resonance frequency identification. All of above mentioned experimental methods, except the experiments by Noblin et al[25], require frequency sweep to estimate multiple resonance modes. Frequency sweep involves time consuming experiments of subjecting the liquid drops to harmonic vibrations of various frequencies at regular intervals. These techniques also suffer due to errors resulting from the selection of interval for frequency sweep.

There have been few attempts by Sharp et al[26,27], Jonas et al[28], Vukasinovic et al[29], McGuiggan et al[31] and Hill and Eaves[32,33] to estimate multiple resonance frequencies using a single experimental run. For example, Hill and Eaves[32,33] measured response of a magnetically levitated water drop that is disturbed by air injection in order to identify resonance frequencies. This technique is very complex and requires highly sensitive equipment and the presence of magnetic potential slightly alters the resonance frequencies. Also, this technique is more applicable towards vibration of free drops that are not in contact with a solid boundary whereas in practical applications like microfluidics drops move on surfaces rather than levitate in air.

Noblin et al[25] used a much simpler method to measure multiple resonance frequencies where a loud speaker supplied with white noise is used to excite

175

large liquid drops. The deformation of interface of oscillating drop is measured using laser beam deflection from surface of the drop. When the deflection of the laser beam was Fourier-transformed, multiple resonance frequencies were readily obtained from a single run. Unlike previous estimation methods, this technique ideally requires only one experimental run to measure multiple resonance frequencies. While Noblin et al[25] mentioned this experiment in their paper, they did not report any related experimental data, other than pointing out that these were essentially same as those obtained using frequency sweeps.

In recent years, we have been using computer generated Gaussian white noise vibration to induce shape fluctuation in a liquid drop[38, 39] in the context of generating a rectified motion on a surface. Here, we did observe that a drop excited by a white noise vibration exhibits shape fluctuations that resembled resonance modes (figure 6. 1). A saw-tooth wave or a sinusoidal wave composed of multiple harmonics can also be used to excite multiple resonance modes but it does not cover full spectrum of frequencies as an experiment with a white noise that has equal power at each frequency within the bandwidth of the vibration. Hence, in our experiments, we used white noise vibration to excite liquid drops in the spirit of experiments by Noblin et al[25]. Noblin et al[25] used larger drop volumes ranging from $100\mu L$ to $3000\mu L$ that were flattened by gravity, in order to facilitate the comparison of experimental data with 1-D capillary-gravity wave theory for a large liquid bath of uniform height. However, in our experiments, we subjected small drops of volume ranging from $1\mu L$ to $20\mu L$ to a controlled white noise vibration. Equilibrium shape of these small drops is dominated by surface tension rather than gravity. We were

interested in small drop volumes owing to their ubiquitous presence in microfluidic devices. Our experiment involves recording the height fluctuation of a drop with a high speed camera and then calculating its power spectrum.

The aim of our experiments is many folds, the first is aim being simultaneous estimation of multiple resonance frequencies of small volume drops that are dominated by surface tension force, second aim being to test 1-D capillary wave theory for small drops with pinned contact lines (on polystyrene) as well as on superhydrophobic surface (micro-fibrillar PDMS or polydimethylsixolane) with very large contact angles ($\sim 162^{\circ}$) where the contact line of drop shows substantial slippage. Third aim is to measure the resonance frequencies of liquid drop by studying the contact line fluctuations. Here, the comparison of contact line fluctuations with that of height fluctuations provides insights into the effect of contact line slippage on each resonance mode. Fourth aim is to understand the effects of viscosity on the variance of height fluctuations of drops that may be potentially used to measure the viscosity of liquids using very small drops.

6. 2. Experiment:

Figure 6. 1(a) shows the schematic of the experimental procedure. Two types of supports were used for the sessile drop of water. One was a polystyrene coated silicon wafer and the other was a micro-fibrillar PDMS (polydimethylsiloxane or silicone) rubber, the details of which have been described in a previous publication[13]. The microfibrillar PDMS rubber had square fibrils of $10\mu m$ in size and $25\mu m$ in height with a fibrillar spacing of $50\mu m$. The advancing and receding angles on the polystyrene surface were 91° and 68° (hysteresis of 23°) respectively. This surface, owing to high contact angle hysteresis, pins a liquid drop on the   surface. By contrast, the advancing and

receding contact angles on the micro-fibrillar surface were 170° and 157° respectively, with a cosine average contact angle of ~ 162°. When vibrated, the contact line contracted and expanded rather freely on this surface.
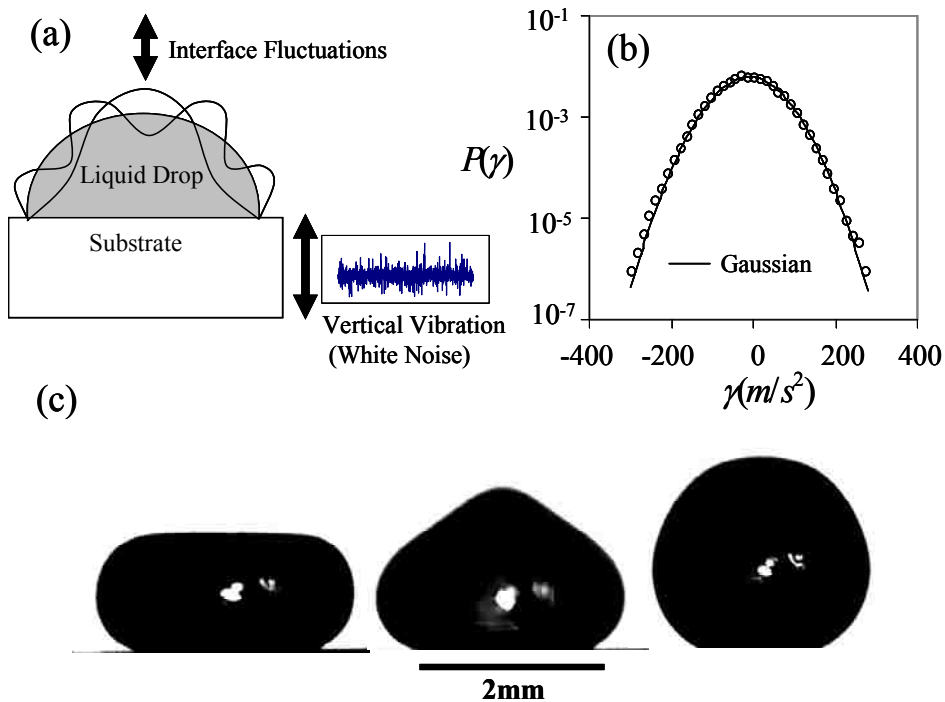
Figure 6. 1. (a) Schematic of a liquid drop on a solid substrate subjected to white noise vibration perpendicular to the plate. **(b)** Gaussian distribution of acceleration of plate. **(c)** A few randomly selected frames of a $20\mu L$ water drop vibrating on a micro-fibrillar PDMS surface show some of the resonance modes.

The substrate was firmly attached to an aluminum platform which was fixed on a mechanical oscillator (Pasco Scientific, Model No: SF-9324). De-ionized water drops of volumes ranging from 1 to $20\mu L$ are placed on the substrate and subjected to white noise vibration generated by a signal generator (Agilent, Model 33120A). The details of the experimental set up are not repeated here as they have been presented in previous chapters. The distribution of plate acceleration as measured with an

accelerometer was found to be Gaussian as shown in figure 6. 1(b). With these random accelerations (γ), the nominal strength of the noise was estimated as, $K = \langle \gamma^2 \rangle \tau_c$, τ_c is the time duration (40 μs) of the pulse. This is a fairly accurate definition of K if the noise is ideally white. However, a mechanical transducer produces a colored white noise in which there is a certain correlation of the noise pulses.

For most part of the paper, we use the above nominal definition of K. However, towards the end this value of K was corrected with a numerical factor as was discussed in reference 40. For most experiments, white noise of (nominal) strength $K = 0.17 m^2/s^3$ was used. The vibrating interface of liquid drops were recorded with a high speed camera (Redlake, MotionPro, Model 2000) operating either at 1000 or 2000 frames/sec. The high speed videos were stored in a computer for analysis in leisure. Motion analysis software MIDAS (Xcitex Inc, USA) was used to automatically track the interface fluctuations of drops.

6. 3. Results and discussion:

It is well known that power spectrum of an ideal white noise has equal power for all frequencies. Hence, it is theoretically possible to excite all resonance modes of liquid drops when subjected to a true white noise vibration. However, in laboratory experiments, due to limitations of mechanical systems, it is not possible to achieve an ideal white noise vibration. The mechanical oscillator that we used in our experiments had a total bandwidth of 10KHz. Here the vibration is considered as an ideal white noise

vibration below the frequency of 5*KHz*. With the highest frame speed of 2000 fps for the video camera in our lab, the highest frequency that could be measured was 1 kHz. The side view (figure 6. 1c) of the recorded image of a vibrating drop was analyzed with an automatic motion tracking MIDAS software (Xcitex Inc, USA) to measure height of drop as a function time. The height fluctuations of the drops were fast Fourier transformed (FFT) using OriginLab® Software in order to indentify resonance modes. Several power spectra (five or more) were added together before de-noising in order to improve the clarity of the resonance peaks (figure 6. 2). The noisy power spectrum (not shown) is denoised using wavelet transform to show a clean power spectrum that facilitates in easy identification of resonance frequencies (figure 6. 2). MATLAB® was used to carry out 1-dimensional automatic denosing of noisy power spectrum using wavelet transformation method. Heuristic threshold with level 4 wavelet decomposition was used for denoising. (Command: PS_denoised=wden(PS_original, 'heursure', 's', 'one', 4, 'sym8'). We observe some satellite peaks apart from the main resonance peaks (figure 6. 2a), the origin of which is not understood at present.

6. 4. Resonance Modes:

A few randomly selected frames of the vibrating drop (Figure 6. 1c) show some of the resonance modes. Figures 6. 2 and 6. 3 demonstrate the typical vibration spectra that can be obtained from the measurements of the height fluctuations. As shown in figure 6. 2a, where we compared power spectrum of $10\mu L$ water drop on two substrates, the resonance frequencies shift significantly to lower values for a given mode on fibrillar PDMS surface compared to Polystyrene surface due to the effect of contact angle.

However, we note that the positions of the resonant peaks on either the polystyrene ($j = 2$ to 6) or the fibrillar PDMS surface ($j = 2$ to 5) are rather independent of the strength of the noise (figure 6. 3). The resonance peaks corresponding to $j = 6$, 7 and 8 on fibrillar PDMS are damped out (figure 6. 3b) at low power of $K \sim 0.006 \ m^2/s^3$ compared to higher powers. However, the position of peaks corresponding to $j = 2$ to 5 on fibrillar PDMS are independent of the strength of the noise. The observation that resonance frequencies are independent of strength of noise coupled with the fact that the height fluctuations are Gaussian (figure 6. 2b) suggest that there are no overwhelming non-linearities[38, 39] associated with these drop dynamics.
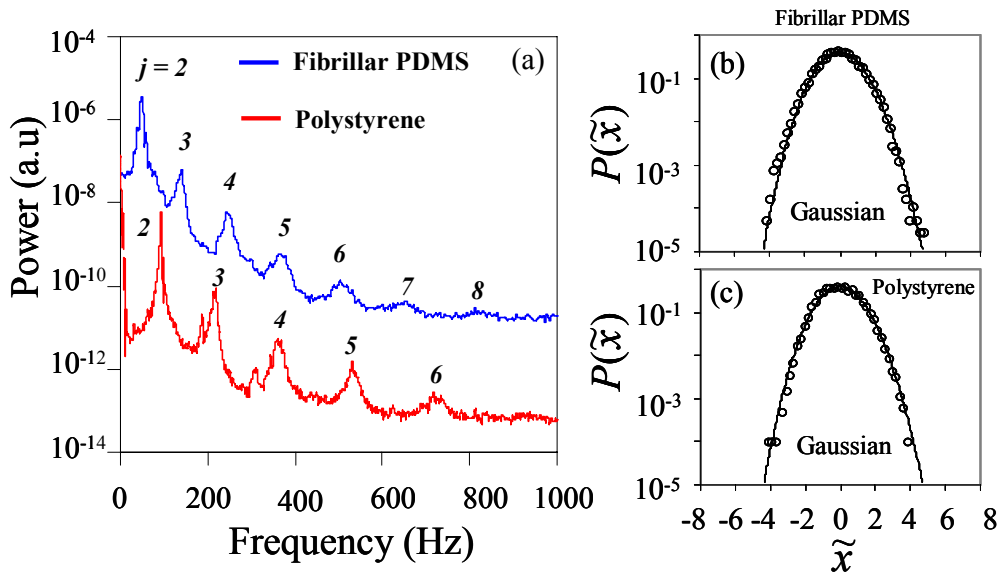
Figure 6. 2. (a) Comparison of de-noised power spectra of a $10\mu L$ water drop vibrating on a fibrillar PDMS and a polystyrene surface. The mode numbers are shown on the spectra. Gaussian probability distribution of height fluctuations of the same size drop on a fibrillar PDMS (b) and a polystyrene surface (c) corresponding to an observation time of 0.001s. Here $\tilde{x}$ is the non-dimensional height fluctuation $\tilde{x} = (x - x_p)/\sigma_x$ expressed in terms of the position of the peak (x_p) and the standard deviation (σ_x) of the height fluctuations. White noise of strength $K = 0.17 m^2/s^3$ was used to vibrate the drop, which was recorded with a video camera at 2000 frames/s.
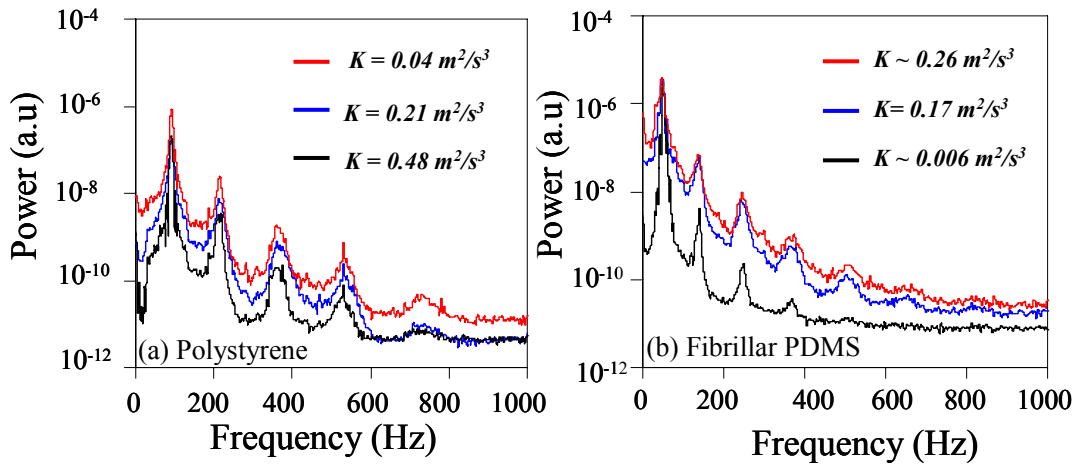
Figure 6. 3. Effect of the strength of white noise vibration on resonance frequencies of a $10\mu L$ water drop on Polystyrene (a) and Micro-fibrillar PDMS surface (b). The strength of vibration has no effect on the peak positions.

6. 5. Comparison of experimental resonance frequencies with theory:

In this section, we compare our experimental results for resonance frequencies with theoretical calculations. Here, we also provide a brief summary of theoretical efforts in the literature for prediction of resonance frequencies of oscillating liquid drops. The earlier theoretical studies by Kelvin[1], Rayleigh[2], and Lamb[3] focused on oscillations of free spherical drop for which resonance frequency of jth mode of vibration for $j \geq 2$ is given by.

$$\omega_o = \sqrt{\frac{\gamma_{lv}}{3\pi m} j(j-1)(j+2)} \tag{6. 1}$$

Here j corresponds to the number of lobes (protrusions) present on the surface of drop as schematically shown in figure 6. 1(a). γ_{lv} is surface tension of the liquid, m is mass of drop. Later Strani and Sabetta[6] numerically computed resonance

182

frequencies for liquid drop in partial contact with a solid support as a function of contact angle and showed that solid support increases the resonance frequencies compared to free drop. In a recent theoretical study, Lyubimov et al[41] analyzed lateral oscillations of drop in partial contact with solid substrate. Celestin and Kofman[24] studied low frequency bending vibration mode of liquid drop in partial contact with a solid support by experiments and theory. They derived a semi-analytical expression for resonance frequency of rocking vibration mode as a function of contact angle of drop. Recently, Dong et al[22] carried out 3D numerical simulations of Navier-Stokes equations using computational fluid dynamics software FLUENT for a laterally vibrating liquid drop on a solid support. They were able identify vibration modes of drop that were in excellent agreement with experiments of Daniel et al[10,11].

Recently, Lyubimov et al[42] have extended their theoretical study on lateral vibration[41] of drop to normal vibration of hemispherical drop ($\theta = 90^o$) accounting for contact line dynamics. They derived expression for resonance frequencies of drop which was given in simplified form by McGuiggan et al[31] as follows

$$f_j^2 = \frac{\gamma_{lv}\tilde{\omega}_j^2}{6\pi m}$$

(6.2)

where γ_{lv} is the surface tension of the drop and m is mass and $\tilde{\omega}_j$ are roots of equation

$$F(\tilde{\omega}_j) = \sum_{l=1}^{\infty} \frac{l(4l+1)}{\tilde{\omega}_j^2 - 4l(2l-1)(l+1)}\left(\frac{(2l-1)!!}{2^l l!}\right)^2 = 0$$

(6.3)

As mentioned earlier, McGuiggan et al[31] measured resonance frequencies corresponding to modes $j = 2$ and 3 for water drops volumes ranging from 5 to $200\mu L$ by disturbing the interface of a liquid drop   by AFM probe. They numerically solved

183

equation 6.3 for modes corresponding to $j = 2$ and 3 and calculated first two roots to be

$\tilde{\omega}_2 = 4.4171$ and $\tilde{\omega}_3 = 10.5706$ by using 1000 terms in the summation while solving for $\tilde{\omega}_j$.

In order to compare our experimental data with theoretical predictions of equation 6.2, we

numerically solved equation 6.3 for modes corresponding to $j = 2$ and 6. We got very

good agreement with $\tilde{\omega}_j$ values for $j = 2$ and 3 as calculated by McGuiggan et al[31] even

though we only used 150 terms in the summation of equation 6.3. The roots of the equation

6.3 that we calculated are $\tilde{\omega}_2 = 4.4268$, $\tilde{\omega}_3 = 10.5920$, $\tilde{\omega}_4 = 18.0377$, $\tilde{\omega}_5 = 26.5954$,

$\tilde{\omega}_6 = 36.1426$. We used above roots in equation 6.2 to calculate resonance frequencies

corresponding to modes $j = 2$ and 6 for water drops of various volumes. The data

summarized in figure 6. 4a for resonance frequencies on polystyrene and the corresponding

Table 6. 1 comparing the slopes of the lines suggest that the agreement between the theory

and experiment is very good.
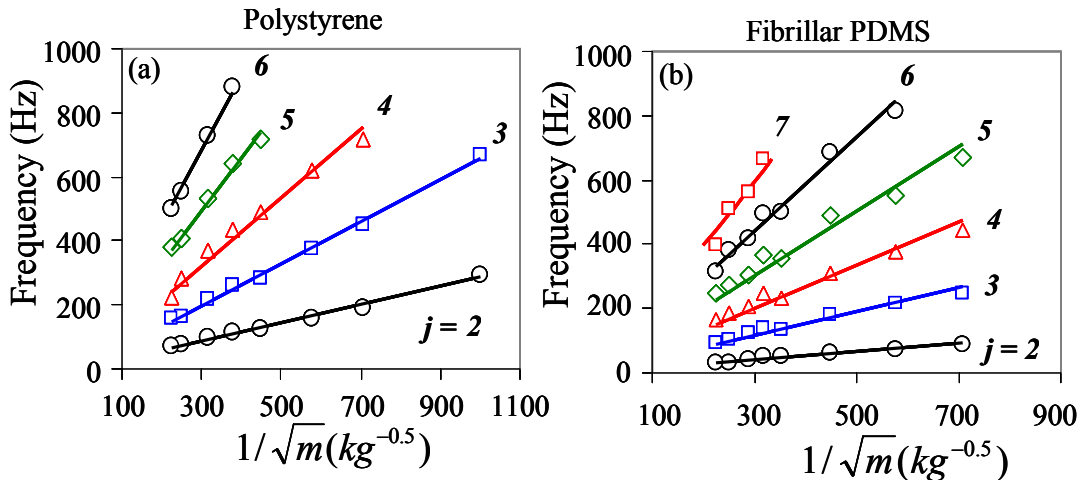
Figure 6. 4. (a) Resonance frequencies of water drops as a function of mass on a polystyrene coated silicon wafer (a) and a micro-fibrillar PDMS surface (b). Open symbols are the experimental data whereas the solid lines are the linear fits through the data by forcing the lines to meet at (0, 0). The slopes of these lines are compared with the theoretical predictions in tables 6. 1 and 6. 2 (see below).

Table 6. 1. Comparisons of the slopes of linear fits through the experimental data of the drop vibrating on the polystyrene surface with those calculated from Equation 6.2 (Lyubimov et al[42]) and Equation 6.4 (Noblin et al[25]). All the lines were forced to pass thorough the origin.

Mode (j)	Slope ($kg^{0.5} s^{-1}$)		
		Theory	
	Experiment	Noblin et al[25]	Lyubimov et al[42]
2	0.28±0.01	0.32	0.27
3	0.66±0.01	0.69	0.66
4	1.06±0.02	1.15	1.12
5	1.65±0.02	1.68	1.65
6	2.29±0.02	2.27	2.24

Table 6. 2. Comparisons of the slopes of linear fits through the experimental data of the drop vibrating on the micro fibrillar PDMS surface with those calculated from Equation 6.4 (Noblin et al[25]) taking slip and no-slip of contact line into account. All the lines were forced to pass thorough the origin.

Mode (j)	Slope ($kg^{0.5} s^{-1}$)		
		Theory	
	Experiment	Noblin et al[25] (No Slip)	Noblin et al[25] (Slip)
2	0.13±0.01	0.19	0.11
3	0.38±0.01	0.41	0.29
4	0.67±0.02	0.68	0.54
5	1.00±0.03	0.98	0.83
6	1.46±0.02	1.33	1.15
7	1.99±0.07	1.71	1.51

For the drop on the fibrillar surface ($\theta \sim 162^o$), the equation of Lyubimov et al[42] could not be used as it was not meant to apply for contact angle larger than 90°. Here, we

used the approximate analysis by Noblin et al[25] that is an improvised version of 1-D gravity-capillary wave vector relation of Landau and Lifshitz[43]. Landau-Lifshitz equation predicts the resonance frequency (f_j) for a thin layer of liquid on a surface as follows:

$$f_j^2 = \left(\frac{1}{4\pi^2}\right)\left(gq_j + \frac{\gamma_{lv}}{\rho}q_j^3\right)\tanh(q_j h)$$ (6.4)

Here g is gravitational acceleration, q_j is the wave vector for j^{th} mode, γ_{lv} and ρ are surface tension and density of liquid and h is the mean height of the drop. The first term in equation 6.4 accounts for effect of gravitational acceleration and second term for effect of capillary force contribution to normal vibration modes. Ideally this equation is valid for a liquid bath of uniform height h or for large volume drops that are flattened by gravity but nor for a sessile liquid drops whose equilibrium curved shape is dominated by surface tension force rather than gravity. However, as we show in later part of the chapter, indeed this approximate equation works well even for small drops. Noblin et al[25] have modified this equation in order to apply it to drops by modifying the wave vector relation to meridian (side view) perimeter of liquid drop. Here the wave vector for j^{th} mode is given by $q_j = \pi(j - 1/2)/p$ when contact line of drop is pinned whereas $q_j = \pi(j - 1)/p$ when the contact line slips. These wave vector relations are derived by expressing meridian perimeter of drop in terms of wavelength of normal modes. Here $p = R\theta$ is half of meridian perimeter of liquid drop where R is the radius circle of which the drop is spherical cap with contact angle θ. Such a radius is given as a function of volume (V) and contact angle (θ) of drop by the following expression.

$$R = \left(\frac{3V}{\pi} \frac{1}{(2 - 3\cos\theta + \cos^3\theta)} \right)^{1/3} \qquad (6.5)$$

Mean height of drop is given by $h = V / \pi R^2$.

For the polystyrene surface, we used $\theta = 90^o$ in calculating the resonance modes assuming that the drop is deposited onto the surface in an advancing mode. Numerical calculation, however, shows that even if we use the average contact angle of 80°, instead of 90°, the calculated resonance frequencies increase by $< 3\%$. We present the results based on $\theta = 90^o$ in order make a fair comparison with the calculations based on the model of Lyubimov et al[42]. On the polystyrene surface with pinned contact line, the model of Noblin et al[25] practically makes the same prediction (figure 6. 4a and Table 6. 1) as that of Lyubimov et al[42], although the later prediction is slightly better than the former.
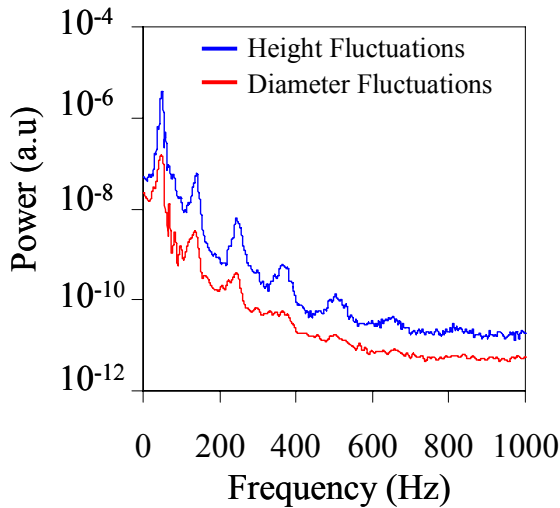
Figure 6. 5. Comparison of the power spectra of the height and the contact diameter fluctuations of a $10\mu L$ water drop on fibrillar PDMS surface. White noise of strength $K = 0.17 m^2/s^3$ was used to vibrate the drop, which was recorded with a video camera at 2000 frames/s.

The calculations on the fibrillar PDMS surface were carried out with a contact

angle of 162º using the model Noblin et al[25]. Figure 6. 4b summarizes the resonance frequencies calculated from equation 6.4 with those measured experimentally for a total of six modes. As mentioned earlier, unlike the case of drops oscillating on polystyrene surface where the contact line was pinned, contact line of drops shows significant slip on the fibrillar PDMS surface. The contact line slip affects the wavelength of capillary waves on surface of drop hence affecting the resonance frequencies calculated from equation 6.4. The slopes of the lines (figure 6. 4b, Table 6. 2) obtained from resonance frequency versus $1/\sqrt{m}$ plot shows that the agreement between experiments and theory is good for lowest mode when contact line slip is taken into account whereas for higher modes, the agreement is good when no slip model is used. In order to understand how the contact line slip affects power spectrum, we measured the fluctuation of contact diameter of drop on fibrillar PDMS surface. Liquid drop contour oscillations (top view of drop diameter oscillations) when subjected to high amplitude harmonic vibrations were studied by Noblin et al[44] in the context of parametric resonance. Here, the authors analyzed the stability of drop contour that changes from circular shape (harmonic mode) to non-circular shape (subharmonic modes) as the amplitude of harmonic vibration is gradually increased. In reference 25, Noblin et al[25] measured the oscillations of contact radius of drop that is subjected to harmonic vibrations. Here, authors measured radius oscillations in frequency sweep in order to identify shift in resonance frequencies as the amplitude of harmonic vibration is increased. However, in our experiment, we measured the fluctuation of the contact diameter of drop when it is subjected to white noise vibration, power spectrum of which shows multiple resonance modes simultaneously. As shown in figure 6. 5, the contact line modes corresponding to $j = 2, 3,$ and 4 are prominent and agree with the resonance

188

modes obtained from height fluctuations. However, the higher modes corresponding to $j =$ 5, 6, and 7 are damped out but they are weakly noticeable at the same locations as observed with height fluctuations. This observation indicates that the contact line slip is mode dependent explaining the fact that lower mode resonance frequency agrees well with slip model where as the higher modes agree with no slip model. The power spectrum of a water drop on a fibrillar surface is independent of the noise strength and peak position do not change with the strength of the noise even when the rms fluctuation of the contact diameter was increased from 2.5 % of the drop diameter to 9 %.

6. 6. Effects of viscosity on resonance spectra:

In order to study the effects of viscosity on the resonance spectra, we carried out experiments with $10\mu L$ liquid drops of various glycerol-water solutions as per the previous studies of Sharp[27]. The viscosities of these solutions as measured using a rotating spindle viscometer (Model: Anton Paar Physica MCR301) were 1 , 2, 3.9, 6.2, and 10.9 cP (centiPoise) respectively for pure water, and 20, 40, 50 and 60 volume percent of glycerol in water respectively. The corresponding surface tensions (du Nouy ring method, FDS Dataphysics, Germany) were found to be 72.5, 70.8, 69.4, 69.1, 67.9 mN/m respectively. Though there is a small change in the surface tension of the solution with the increase amount of the glycerol concentration, the change in viscosity is more pronounced as it varies from 1 cP (water) to 10.9 cP (60% glycerol).

189
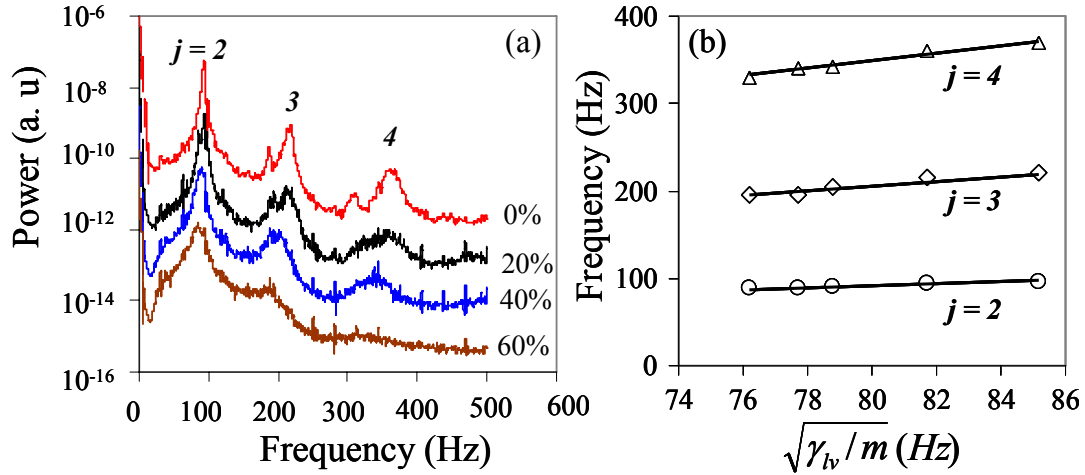
Figure 6. 6. (a) Resonance spectra of glycerol-water solutions. Composition of the glycerol-water solution is stamped beside each spectrum. **(b)** Resonance frequency is proportional to $\sqrt{\gamma_{lv}/m}$ as expected from equation 6.2. The slopes of $j = 2$, 3 and 4 are 1.14, 2.57 and 4.36 respectively.

The first theoretical studies that studied the effect of viscosity on vibrating liquid drops are by Lamb[3] and Chandrasekhar[4] which pointed out that apart from dampening resonance modes, viscosity also affects the resonance frequencies. The effect of viscosity is taken into account by adding viscous stress contribution to the Laplace pressure difference at the interface of drop. There have been extensive numerical studies in the literature that studied this problem[14,15,45-53]. Recently Sharp[27] has used water-glycerol mixtures to study the effects of viscous damping on resonance peak. However, he did not report any shift in resonance frequencies as a function of viscosity.

Recently, Behroozi et al[53-56] have developed an experimental technique where damping of capillary waves is used to simultaneously measure surface tension and viscosity of water-glycerol mixtures. They presented viscosity correction term as derived by Lamb[3] which indicates that the reduction in resonance frequencies due to

190

viscosity is proportional to $\left(\mu^3 f_j / \gamma_{lv}^2 \rho\right)^{1/2}$ in high viscosity limit. The viscosity correction is frequency dependent hence higher modes are affected significantly than lower modes. As we show later, the viscosity correction is negligible for most of the modes that we observed in experiments. In our study, we observed (figure 6. 6a), as did Sharp[27], that the height of the peak decreases and its width increases with the viscosity. We also noted that the variance of the interfacial fluctuation decreases with viscosity that can be accounted for in a semi-quantitative manner using Langevin dynamics simulations (not shown here). The main observation here is that the resonance peak undergoes a red shift as the concentration of glycerol increases (figure 6. 6a). Figure 6. 6b shows that the resonance frequency varies linearly with $\sqrt{\gamma_{lv}/m}$ for each of the three modes studied here. The slopes of these lines (1.14, 2.57, 4.35) for the three modes ($j = 2$, 3 and 4) are in good agreement with their values (1.00, 2.45, 4.16) estimated from the theory of Lyubimov et al[42], which strongly favors the view that the observed red-shifts are mainly due to capillarity.
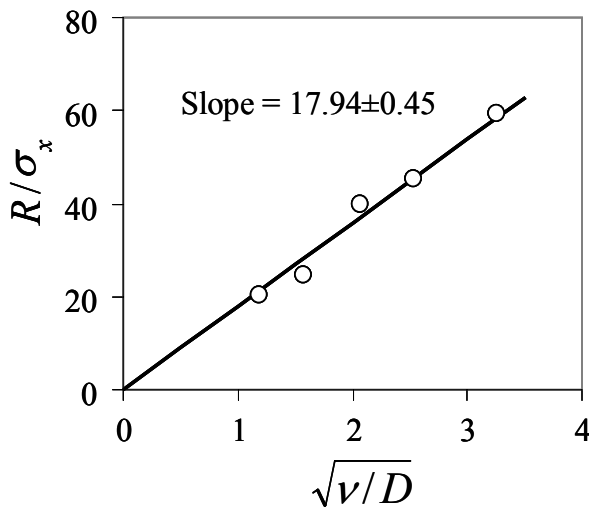
Figure 6. 7. R/σ_x varies linearly with $\sqrt{v/D}$.

Here we discuss how viscosity of liquid affects the variance of fluctuation of the interface. It is expected that the variance of the interfacial fluctuation would increase with the noise strength (K), the mass of the liquid, and decrease with the friction factor ($\xi \sim \mu$) and the surface tension. A simple dimensional analysis shows that, ($\sigma_x^2 \sim mK\tau_L / \gamma$) where τ_L is the Langevin relaxation time and $mK\tau_L$ is an effective temperature (T_{eff}) of the system. Further re-arrangements ($\sigma_x^2 \sim D\tau_L \sim \dfrac{Dm}{\xi} \sim \dfrac{DR^3\rho}{\mu R} \sim \dfrac{DR^2}{\nu}$) of the appropriate terms lead to $R/\sigma_x \sim \sqrt{\nu/D}$, where R is the radius of the drop, ν is the momentum diffusivity (or kinematic viscosity) and D is the index of spatial dispersion $D \sim mK/\gamma \sim K/f^2$. Figure 6. 7 shows that R/σ_x is fairly linear with $\sqrt{\nu/D}$. As D varies very little with the glycerol concentration, the observation of figure 6. 7 shows that the interfacial roughness induced by the noise is strongly correlated with the kinematic viscosity of the liquid.

6. 7. Conclusions

We show that white noise vibration can be used to successfully identify the multiple vibration modes of micro liter drops on Polystyrene surface and mircofibrillar PDMS surface. The power spectrum plots of height fluctuations of the water drops show peaks at the corresponding resonance frequencies. Experimentally identified resonance frequencies of drops on Polystyrene surface agree well with the theoretical model of Lyubimov et al[42]. Also, model of Noblin et al[25] that is an improvised version of capillary wave vector relation

of Landau and Lifshitz[43] predicts the resonance frequencies on Polystyrene surface where contact angle is close to 90°, but also when the contact angle is as high as 162°. The contact line of drop is pinned on Polystyrene surface where as it shows significant slippage on fibrillar PDMS surface. We observed that contact line slippage is mode dependent. The contact line slip affects lower resonance more than higher resonance modes. Hence, the resonance frequencies predicted by slip model agree well with experimental resonance frequency for low modes, where as the no slip model predicts higher modes accurately. We also measured the power spectrum of contact line fluctuations. Higher resonance modes of contact line are damped where as the lower modes agree well with that of resonance modes observed with height fluctuations. The observation that the resonance frequencies are independent of strength of vibration signifies that the dynamics are linear. The effect viscosity on the resonance spectra of drops of various water-glycerol mixtures was studied. The height of the resonance peaks decreases where as the width increases with increase in the viscosity. The shift in resonance frequencies is accounted by surface tension where as the decrease in variance of interface fluctuations is accounted by viscosity. The variance of interface fluctuations correlates well with kinematic viscosity that results in possibility of using our experiments not only to estimate the surface tension of drops but also the viscosity using micro liter volume liquid drops.

6. 8. References:

1. Lord Kelvin, Mathematical and Physical Papers **1890**, *3*, 384 ,

2. Lord Rayleigh, The Theory of Sound (Macmillan, **1894**).

3. Lamb, H. Hydrodynamics; Cambridge University Press: Cambridge,

U.K., **1932**.

4. Chandrasekhar, S. *Proc. London Math. Soc.* **1959**,*9*,141. Chandrasekhar, S. Hydrodynamic and Hydromagnetic Stability; Clarendon: Oxford, **1961**. Page: 466.

5. Rodot, H.; Bisch, C.; Lasek. A. *Acta Astronaut*. **1979**, *6*, 1083

6. Strani, M.; Sabetta, F, *J. Fluid Mech*. **1984**, *14*, 23.

7. Harris, M. T.; Scott, T. C.; Byers, C. H. U.S. Patent 5,122,360 (June 16, l992).

8. Chaudhary, K.C.; Maxworthy, T. *J. Fluid Mech*., **1980**, *96*, 275.

9. Sekeroglu, K.; Gurkan, U. A.; Demirci, U.; Demirel, M. C. *Appl. Phys. Lett.* **2011**, *99*, 063703.

10. Daniel, S.; Sircar, S.; Gliem, J.; Chaudhury, M. K. *Langmuir* **2004**, *20*, 4085.

11. Daniel, S.; Chaudhury, M. K.; De Gennes, P.-G. *Langmuir* **2005**, *21*, 4240.

12. Daniel, S.; Chaudhury, M. K.; Chen, J. C. *Science* **2001**, *291*, 633.

13. Mettu, S.; Chaudhury, M. K. *Langmuir* **2011**, *27*, 10327.

14. Basaran, O. A.; DePaoli, D. W. *Phys. Fluids* **1994**, *6*, 2923.

15. Wilkes, E. D.; Basaran, O. A. *Phys. Fluids* **1997**, *9*, 1512.

16. Chang, C. H.; Coltharp, K. A.; Park, S. Y.; Franses, E. I. *Colloid Sur A*. **1996**, *114*, 185.

17. Perez, M.; Brechet, Y.; Salvo1, L.; Papoular, M.; Suery, M. *Euro. Phys. Lett.* **1999**, *47*,189.

18. Trinh, E. H.; Wang, T. *J. Fluid Mech*. **1982**, *122*, 315.

19. Trinh, E. H.; Thiessen, D. B.; Holt, R. G. *J. Fluid Mech*. **1998**, *364*, 253.

20. Smithwick, R. W.; Boulet, J. A. M. *J. Colloid Interface Sci*., **1989**, *130*, 588.

21. Yoshiyasu, N.; Matsuda, K.; Takaki,   R. *J. Phys. Soc. Jpn.* **1996**, 65, 7.

22. Dong, L.; Chaudhury, A.; Chaudhury, M. K. *Eur. Phys. J.E* **2006**, *21*, 231.

23. Moon, J. H.; Kang, B. H.; Kim, H. Y. *Phys. Fluids* **2006**, *18*, 021702.

24. Celestini, F.; Kofman, R. *Phys. Rev. E*, **2006**, 73, 041602.

25. Noblin, X.; Buguin, A.; Brochard, F. *Eur. Phys. J. E* **2004**, *14*, 395.

26. Sharp, J. S.; Farmer, D. J.; Kelly, J. *Langmuir*, **2011**, *27*, 9367.

27. Sharp, J. S. *Soft Matter*, **2012**, *8*,399.

28. Jonas, A.; Karadag, Y.; Tasaltin, N.; Kucukkara, I.; Kiraz, A. *Langmuir* **2011**, *27*, 2150.

29. Vukasinovic, B.; Smith, M. K.; Glezer, A. *J. Fluid Mech*., **2007**, *587*, 395.

30. Ghosh, S.; Sharma, P.; Bhattacharya, S. *Rev. Sci. Instrum*, **2007**, *78*, 115110.

31. McGuiggan, P. M.; Daniel A. G.; Wallace, J. S.; Cheng, S.; Prosperetti, A.; Robbins, M. O. *Langmuir*, **2011**, *27*, 11966.

32. Hill, R. J. A.; Eaves, L. *Phys. Rev. E* **2010**, *81*, 056312.

33. Hill, R. J. A.; Eaves, L. *Appl. Phys. Lett*. **2012**, *100*, 114106.

34. McHale, G.; Elliot, S. J.; Newton, M. I.; Herbertson, D. L.; Esmer, K. *Langmuir*, **2009**, *25*, 529.

35. Bormashenko, E.; Pogreb, R.; Whyman, G.; Erlich, M. *Langmuir* **2007**, *23*, 12217.

36. Palero, V.; Lobera, J.; Brunet, P.; Arroyo, M. P. in the proceedings of the 16th Int Symp on Applications of Laser Techniques to Fluid Mechanics Lisbon, Portugal, 09-12 July, 2012, pages 1-12.

37. Mugele, F.; Staicu, A.; Rina Bakker,R.; van den Ende, D. *Lab Chip*. **2011**, *11*,2011.

38. Chaudhury, M. K.; Mettu, S. *Langmuir* **2008**, *24*, 6128.

39. Mettu   S.;   Chaudhury,   M.   K.   *Langmuir* **2010**, *26*, 8131.

40. Goohpattader, P. S.; Mettu, S.; Chaudhury, M. K. *Eur. Phys. J.E* **2011**, *34*,120.

41. Lyubimov, D.V. Lyubimova, T. P. Shklyaev, S.V. *Fluid Dynamics*, **2004**, *39*, 851.

42. Lyubimov, D.V. Lyubimova, T. P. Shklyaev, S.V, *Phys. Fluids*, **2006**, *18*, 012101.

43. L. D. Landau and E. M. Lifshitz, Fluid Mechanics, 2nd ed. Butterworth- Heinemann, Oxford, 1984. Page: 247

44. Noblin, X.; Buguin, A.; Brochard, F. *Phy. Rev. Lett.* **2005**, *94*, 166102.

45. Basaran, O. A. *J. Fluid Mech.* **1992**, *241*,169.

46. Reid, W.H. *Quart. Appl. Math.* **1960**, *18*, 86.

47. Tang, H. H. K.; Wong, C. Y. *J. Phys. A: Math. Nucl. Gen.* **1974**, *7*, 1038.

48. Prosperetti, A. *J. Fluid Mech.* **1980**, *100*, 333.

49. Lundgren, T. S.; Mansour, N. N. *J. Fluid Mech.* **1988**, *194*, 479.

50. Becker, E.; Hiller, W. J.; Kowalewski, T. A. *J. Fluid Mech.* **1991**, *231*,189.

51. Padrino, J. C.; Funada, T.; Joseph, D. D. *Int. J. Multiphase Flow* **2008**, *34*, 61.

52. Meradji, S.; Lyubimova, T. P.; Lyubimov, D. V.; Roux, B. *Cryst. Res. Technol.* **2001**, *36*, 7.

53. Priede, J. *J. Fluid Mech.* **2011**, *671*, 399.

54. Behroozi, F.; Smith, J.; Even, W. *Wave Motion* **2011**, *48*, 176.

55. Behroozi, F.; Perkins, A. *Am. J. Phys.* **2006**, *74*, 957.

56. Behroozi, F.; Smith, J.; Even, W. *Am. J. Phys.* **2010**, *78*, 1165.

57. Behroozi, F.; Lambert, B.; Buhrow, B. *Appl. Phys. Lett.* **2001**, *78*, 2399.

Chapter 7: Summary of Doctoral Research and Recommendations for Future Work

7. 1. Summary of doctoral research

The main goal of my doctoral research has been to elucidate the role played by contact angle hysteresis during the motion of liquid drops on a solid surface. The topic of contact angle hysteresis for research emanated from previous findings of our group about liquid drops motion on surfaces. Here, the drop motion was induced by external vibration and surface energy gradients. The main result that led to the current topic is the observation of random motion of water drops condensing on a silicon wafer having surface energy gradient. It was observed that the condensing water drops coalesced randomly on the surface and drifted away from hydrophobic end of the substrate towards hydrophilic end. Here, drifted random motion of liquid drops looked similar to the Brownian motion of colloidal particle in a solvent. We simulated the above situation by subjecting a liquid drop on a solid substrate to external white noise vibration in presence of a bias. Here, the external vibration mimics the effect of random coalescence and fluctuations of contact line of liquid drops. The bias mimics the effect of surface energy gradient. We focused on the effect of extra dissipation resulting from threshold contact angle hysteresis force that is not present in the classical Brownian motion of colloidal particle. We also focused on another aspect of contact angle hysteresis that is elimination of it when liquid drop is subjected to vibration. We have drawn analogy between Brownian motion of colloidal particle in a solvent and liquid drop undergoing Brownian like motion. Unlike the drift velocity of colloidal particle which is independent of strength of the noise, the drift velocity of   drop is found to be a non-linear function of

strength of noise. The drift velocity of did not saturate to Stokes-Einstein limit in the range of experimental powers used. This observation provides solid evidence to our hypothesis that the contact angle hysteresis is not eliminated when the drops are moving under the influence of external vibration. We also studied the detailed contact line fluctuations of drop using high time resolution video recording. Here, we looked at the probability distribution of displacement of liquid drop. Unlike the case of colloidal particle where displacement PDF is Gaussian due to linear nature of kinematic friction, we have shown that the displacement distribution of liquid drop is non-Gaussian following exponential distribution. The observed non-Gaussianity is the result of non-linearity in contact angle hysteresis. We also looked at the work done by gravity on the drop in order to check whether the work distribution follows recently developed non-equilibrium work fluctuation theorem. We showed that the work distribution does not follow conventional fluctuation theorem due to the presence of contact angle hysteresis.

We also addressed the effect of contact angle hysteresis during the contact line motion of liquid drop in a different experiment. Here, contact line of liquid drop in non-equilibrium is subjected to external white noise vibration. In this case, the drop does not translate as whole on surface but contact line of drop relaxes from non-equilibrium to equilibrium. In this study, we have drawn analogy between a harmonically bound colloidal particle undergoing Brownian motion and contact line of liquid drop. The retracting force due to surface tension of liquid induces harmonic potential where as external vibration mimics the thermal fluctuations. We focused on the relaxation of the contact of drop in order to draw some definitive conclusions about elimination of contact angle hysteresis. The overall relaxation   behavior of contact line of drop is found to

be exponential with significant stick-slip motion. The stick-slip relaxation behavior is attributed to the presence of metastable equilibrium states in the corrugated parabolic free energy of the drop. The displacement distribution of contact line of drop is found to be non-Gaussian following exponential distribution. This observation emphasizes the role played by contact angle hysteresis during the relaxation process. The relaxation time of contact line was found to be much higher than Langevin relaxation time. This indicates that even though the drop relaxes to equilibrium, the contact angle hysteresis is not eliminated. It plays crucial role during the relaxation. We determined that the power required to completely eliminate contact angle hysteresis is so high that it is not easily achieved in usual laboratory conditions.

We also studied another important aspect of contact angle hysteresis that is its role in symmetry breaking resulting rectification of drop motion when subjected external asymmetric periodic vibrations of zero mean. We hypothesized that non-linearity in contact angle hysteresis is the mechanism for symmetry breaking in this case. In order to verify this, we carried out systematic drop motion experiments on solid surfaces possessing varying amount of contact angle hysteresis. Contrary to the intuition that drops move with high velocities on low hysteresis surfaces, the drops did not show any net motion on surfaces with very low contact angle hysteresis. However, the drops moved with high velocities on surfaces with intermediate hysteresis. Again, the drops did not show any motion on very high hysteresis surfaces. Here, the contact line of drop is pinned due to large hysteresis. These observations clearly indicates that there needs to be some amount of contact angle hysteresis present on the solid surface in order to achieve net motion with asymmetric periodic vibrations. We developed a non-linear

contact angle hysteresis model to explain such a counterintuitive observation. We could predict magnitude and direction of velocities of drops of various masses accurately using the non-linear contact angle hysteresis model. We could also accurately predict the minute details of contact line motion. We found that the drift velocity increases non-linearly with amplitude of external vibrations reaching a plateau at higher amplitudes. We showed that such a saturation of drift velocities is also a result of non-linearity in contact angle hysteresis.

On the practical application side of the work, we demonstrated the combined effect of thermal gradient and vibration on liquid drops motion on a solid surface. We showed that application of external energy through vibration of solid surface overcomes the limitation of high temperature gradients required for high surface tension liquids in microfluidic devices. Very high temperature gradients are impractical especially when dealing with temperature sensitive reactants. The liquid drops remain stationary on thermal energy gradient surface due to the resistive force due to contact angle hysteresis. However, the drops show drifted motion when subjected to periodic vibrations. The velocity amplification shown by moving liquid drops corresponds to the resonance frequencies predicted by Rayleigh's equation. Using a simple model we could explain the velocity amplification when the frequency of oscillations is close to the resonance frequency of liquid drops. Approximate numerical simulations predict the detailed contact line motions reasonably well. However, they predict complete sticking of the drop that is contrary to the experimental observation. Such a velocity dependent slipping of contact line observed in experiments is reproduced by simulations incorporating recently developed non-linear contact   angle hysteresis model. In order to get a

detailed understanding of the dynamics of the flow phenomena and to analyze the development of temperature, velocity and pressure profiles inside the drop, we carried out numerical simulations of 3-D Navier-Stokes equations. We used the commercial Computational Fluid Dynamics (CFD) software code FLUENT. We looked at CFD simulations in a qualitative way as they have not been conclusive. This is due to the fact that we did not take the details of dynamic contact angles as well as contact angle hysteresis phenomenon into account.

We showed that white noise vibration can be used to successfully identify the multiple vibration modes of micro liter drops on Polystyrene surface and mircofibrillar PDMS surface. The power spectrum plots of height fluctuations of water drops show peaks at the corresponding resonance frequencies. Experimentally identified resonance frequencies of drops on Polystyrene surface and fibrillar PDMS surface. agree well with the theoretical models available in literature. The contact line shows huge slippage on fibrillar PDMS surface. We also measured the power spectrum of contact line fluctuations of drops. The lower modes are prominent in the power spectrum of contact line where as higher modes are damped out. The prominent lower modes in contact line power spectrum is in agreement with the modes observed in height fluctuations. We found that the slippage of contact line is mode dependent. The lower modes are affected by contact slip more than higher modes. This is explained by taking slip and no slip of contact line into account in the model. We also studied the effect of viscosity on resonance power spectra using water-glycerol mixtures. The heights of resonance peaks are found decrease with viscosity where as the width increased. The shift in resonance frequencies is accounted by surface tension. The variance of interface

fluctuations is found to decrease with increase in viscosity.

7. 2. Recommendations for Future Work

7.2.1 Future work on CFD simulations

1. As described earlier in Chapter 2 in CFD simulations, the drops with $\theta_e > 90^o$ are moving towards hotter side and drops with $\theta_e \leq 90^o$ moving towards colder side there may be a range of contact angles where the drops remain stationary. Such a discrepancy in the simulation may be a result of an artifact of boundaries. The drop may be in transient state which may move in right direction at steady state. We need to carry out numerical simulations with large domain size for long time to observe the steady state behavior of drop.

2. The change of dynamic contact angles during the motion of drop has not been accounted in the simulations which if taken into account may predict the experimental results accurately.

3. We did not take the details of contact angle hysteresis phenomenon into account. In order for the liquid drop to move on a solid surface, it has to overcome threshold resistive force due to contact angle hysteresis. However, in the current simulations we specified only one equilibrium contact angle on the surface. This results in the drop moving instantaneously when supplied with external force of any magnitude. In reality, the contact line of liquid drop moves only when the contact angle on the advancing side of the drop is greater than the advancing angle. Also, the contact angle of drop lies always between advancing and receding angles. The contact line of drop moves whenever the

contact angle of drop deviates above and below these angles. There have been few attempts in recent literature[1-4] to incorporate these dynamic contact angles and contact angle hysteresis phenomenon into CFD simulations of drop motion using VOF method. However, there is a tremendous scope to improve these simulations to predict contact line motion behavior accurately.

7.2.2 Future work on Brownian like motion of drop

There is also a tremendous scope for the future work on the Brownian like motion of liquid drops on a solid surface. In the current experiments, we subjected the liquid drops to uncorrelated white noise vibration. In the following section we describe how the correlation of noise affects the drop motion.

7.2.3. Motion of Liquid Drops on a Surface Subjected to Simultaneous Colored Noise and a Weak Periodic Vibration

The main goal of this experiment is to understand the role of nonlinearity in the contact angle hysteresis. The nonlinearity might induce a stochastic resonance when a liquid drop is subjected simultaneously to a weak periodic vibration along with colored noise vibration. Stochastic resonance is observed, whenever there is nonlinearity in the system and the system is subjected to a weak periodic signal in presence of noise[23, 47]. The response of the system when plotted as a function of intensity of noise shows resonance behavior. It would be very interesting to test this idea by subjecting a liquid drop or a solid block on a solid substrate to simultaneous periodic and color noise vibration.

7.2. 4. Relaxation Behavior of Contact Line of a Liquid Drop on Soft Substrates of Various Elastic Moduli

In the current experiments, we looked at the relaxation behavior of contact line of drop on flat PDMS substrate that is elastic in nature (elastic modulus ~3MPa). However, it would be very interesting to systematically vary the modulus of PDMS and study the relaxation behavior of contact line of drop when subjected to white noise vibration. In this experiment bulk viscoelastic effects on the relaxation of contact line can be studied.

7.2. 5. Computational Fluid Dynamics Simulations of Liquid Drop Subjected to White Noise, Symmetric and Asymmetric Periodic Vibration

It would be very interesting to carry out CFD Simulation of drops subjected to white noise, asymmetric, symmetric vibration after introducing contact angle hysteresis into FLUENT. Here, the details of velocity and pressure profiles would give rich information about the dynamics. Also, there is an added advantage of switching on or off of the effect of contact angle hysteresis that is not easily achieved in the experiments.

7.3. References

1. Nichita, B. A.; Zun, I.; Thome, J. R. 7th Int. Conf. on Multi Phase Flow. **2010**, Tampa, FL, USA.
2. Fang, C.; Hidrovo, C.; Wang, F. M.; Eaton, J.; Good, K. Int. J. of Multiphase Flow **2008**, *34*, 690.
3. Sikalo, S.; Wilhelm, H. D.; Roisman, I. V.; Jakirlic, S.; Tropea, C. *Physics of Fluids* **2005**, *17*, 062103.

4. Chris Miller, Bachelors of Engineering Thesis, University of Victoria, **2007** ([Thesis Miller](#))

5. Stroock, A. D.; Dertinger, S. K. W.; Ajdari, A.; Mezic, I.; Stone, H. A.; Whitesides, G. M. *Science* **2002**, *295*, 647.

6. Grigoriev, R. O.; Schatza,M. F.; Sharma, V. *Lab Chip* **2006**,*6*,1369.

7. Burns, M. A.; Mastrangelo, C. H.; Sammarco, T. S.; Man, F. P.; Webster, J. R.; Johnson, B. N.; Foerster, B.; Jones, D.; Fields, Y.; Kaiser, A. R.; Burke, D. T. *Proc. Natl. Acad. Sci. USA* **1996**, *93*, 5556.

8. Sammarco T. S.; Burns, M. A. *AIChE. J* **1999**,*45*,350.

9. Darhuber, A. A.; Valentino, J. P.; Davis, J. M.; Troian, S. M.; Wagner, S. *Appl. Phys. Lett*. **2003**, *82*, 657.

10. Stone, J. B.; Stone, H. A. *Phys. Fluids* **2005**, *17*,063103.

11. Muradoglu, M.; Stone, H. A. *Phys. Fluids* **2005**, *17*,073305.

12. Stone, H. A.; Stroock, A. D.; Ajdari, A. *Annu. Rev. Fluid Mech*. **2004**, *36*, 381.

13. Khakhar, D. V.; McCarthy, J. J.; Gilchrist, J. F.; Ottino, J. M. *Chaos* **1999**, *9*, 195.

14. Ottino, J. M. *Annu. Rev. Fluid Mech.* **1990**, *22*, 207.

15. Mazzino, A.; Castiglione, P. *Eur. Phys. Lett.* **1999**, *45*, 476.

16. Sancho, J. M.; Miguel, S. M.; Katz, S. L.; Gunton, J. D. *Phys. Rev. A* **1982**, *26*, 1589.

17. Hanggi, P.; Marchesoni, F.; Grigolini, P. *Z. Phys. B-Cond. Matt* **1984**, *56*, 333.

18. Hanggi, P.; Mroczkowski, T. J.; Moss, F.; McClintock, P. V. E. *Phys. Rev. A* **1985**, *32*, 695.

19. Hanggi, P. *J. Stat. Phys* **1986**, *42*, 105.

20. James, M.; Moss, F.; Hanggi, P.; Van den Broeck, C. *Phys. Rev. A* **1988**, *38*, 4690.

21. Hanggi, P.; Jung, P.; Marchesoni, F. *J. Stat. Phys* **1989**, *54*, 1367.

22. Hanggi, P.; Talkner. P.; Borkovec. M. *Rev. Mod. Phys*. **1990**, *62*, 251.

23. Gammaitoni. L.; Hanggi, P.; Jung. P.; Marchesoni. F. *Rev. Mod. Phys*. **1998**, *70*, 223.

24. Luzka, J. *Phys. Lett. A* **1989**, 1*39*, 29.

25. Luzka, J. *Chaos* **2005**, *15*, 026107.

26. Leiber, T.; Marchesoni, F. ; Risken, H. *Phys. Rev. Lett.* **1987**, *59*, 1381.

27. Marchesoni, F. *Phys. Rev. A* **1987**, *36*, 4050.

28. Leiber, T.; Marchesoni, F. ; Risken, H. *Phys. Rev. A* **1988**, *38*, 983.

29. Sen, M. K.; Bag, B. C. *Eur. Phys. J. B* **2009**, *68*, 253.

30. Bag, B. C.; Hu, C. K. *J. Stat. Mech. Theo Exp.* **2009**, *2*, 1.

31. Nozaki, D.; Mar, D. J.; Grigg, P.; Collins, J. J. *Phys. Rev. Lett.* **1999**, *82*, 2402.

32. Siegle, P. ; Goychuk, I.; Talkner, P.; Hänggi, P. *Phys. Rev. E.* **2010**, *81*, 011136.

33. Ai, B. Q.; Wang, X. J.; Liu, G. T.; Liu, L. G. *Phys. Rev. E.* **2003**, *67*, 022903.

34. Chaudhury, S.; Cherayil, B. J. *J. Chem. Phys* **2006**,*125*,184505.

35. Min, W.; Luo, G.; Cherayil, B. J.; Kou, S. C.; Xie, X. S. *Phys. Rev. Lett.* **2005**, *94*, 198302.

36. Chaudhury, S.; Chatterjee, D.; Cherayil, B. J. *J. Chem. Phys* **2008**,*129*, 075104.

37. Chatterjee, D.; Cherayil, B. J. *Phys. Rev. E.* **2003**, *80*, 011118.

38. Chechkin, A. V.; Hofmann, M.; Sokolov, I. M. *Phys. Rev. E.* **2009**, *80*, 031112.

39. Farias, R. L. S.; Ramos, R. O.; da Silva, L. A. *Braz. J. Phys* **2008**, *38* ,499.

40. Qian, H. *Bio. Phys. J* **2000**, *79*, 137.

41. J. Boussinesq, *C. R. Acad. Sci. Paris*, **1885**, *100*, 935.

42. Lisy, V.; Tothova, J.; arXiv:1006.1060v1

43. Lukic, B.; Jeney, S.; Tischer, C.; Kulik, A. J.; Forro, L.; Florin, E.L. *Phys. Rev. Lett.* **2005**, *95*, 160601.

44. Jeney, S.; Lukic, B.; Kraus, J. A.; Franosch, T.; Forro, L. *Phys. Rev. Lett.* **2008**, *100*, 240604.

45. Franosch, T.; Jeney, S. *Phys. Rev. E.* **2009**, *79*, 031402.

46. Waigh, T. A. *Rep. Prog. Phys* **2005**, *68*, 685.

47. R. Benzi, A. Sutera and A. Vulpiani, *J. Phys*. **1981**, *A14*, L453.

Biography

Srinivas Mettu was born on 24th June of 1981 to Siddi Ramulu and Yashodha, in Ramayampet of Andhra Pradesh state in India. He attended high school at Andhra Pradesh Residential School in Lingampally. He finished his Bachelors degree in Chemical Engineering from Osmania University in Hyderabad in 2003. After finishing bachelors he enrolled for masters program in Chemical Engineering at Indian Institute of Technology, Kanpur in India in 2003. After defending master's thesis in 2005, he joined IBM India as a software engineer in Bangalore. He worked as a software engineer for a year and then enrolled in PhD program in Chemical Engineering at Lehigh University in 2006.

EDUCATION:
Ph.D. Chemical Engineering
Graduation Date: **Sep 2012**
Lehigh University, Bethlehem, PA, GPA: 3.71/4.00

M. Tech. Chemical Engineering
Graduation Date: **June 2005**
Indian Institute of Technology, Kanpur, India, GPA 9.33/10.00

B.Tech. Chemical Engineering
Graduation Date: **June 2003**
Osmania University, Hyderabad, India

RESEARCH EXPERIENCE:

Post Doctoral Research Scientist, Xerox Research Center at Webster, NY. from Oct 2011

Graduate Research Assistant, Chemical Engineering, Lehigh University, Dec 2006 – Oct 2011

Graduate Research Assistant, Indian Institute of Technology, Kanpur, India,
   Fall 2003- Summer2005

OTHER WORK EXPERIENCE:
- Worked as a **Software Engineer** in IBM India from July 2005-Aug 2006.

JOURNAL PUBLICATIONS:

1. P. S. Goohpattader, **Srinivas Mettu**, M. K. Chaudhury, "Stochastic Rolling of a Rigid Sphere in Weak Adhesive Contact with a Soft Substrate", *Eur. Physical. Journal E*, *34*,120, **2011**.

2. **Srinivas Mettu**, M. K. Chaudhury, "Motion of Liquid Drops on Surfaces Induced by Asymmetric Vibrations: Role of Contact Angle Hysteresis" *Langmuir, 27* (16), 10327-10333, **2011**.

3. **Srinivas Mettu**, M. K. Chaudhury, "Stochastic Relaxation of the Contact Line of a Water Drop on a Solid Substrate Subjected to White Noise Vibration: Roles of Hysteresis", *Langmuir, 26* (11), 8131–8140, **2010**.

4. P. S. Goohpattader, **Srinivas Mettu**, M. K. Chaudhury, "Experimental Investigation of the Drift and Diffusion of Small Objects on a Surface Subjected to a Bias and an External White Noise: Roles of Coulombic Friction and Hysteresis", *Langmuir, 25* (17), 9969–9979, **2009**. (Equal contribution as the first author)

5. **Srinivas Mettu**, M. K. Chaudhury, "Motion of Drops on a Surface Induced by Thermal Gradient and Vibration", *Langmuir, 24* (12), 10833–10837, **2008.**

6. M. K. Chaudhury, **Srinivas Mettu**, "Brownian Motion of a Drop with Hysteresis Dissipation", *Langmuir, 24* (12), 6128–6132, **2008.**

7. **Srinivas Mettu**, N. Verma, and R. P. Chhabra, "Momentum and Heat Transfer from an Asymmetrically Confined Circular Cylinder in a Plane Channel", *Heat and Mass Transfer, 42*, 1037-1048, **2006.**

8. **Srinivas Mettu**, M. K. Chaudhury, "Resonance Modes of the Surface and the Slipping Contact Line of a Sessile Liquid Drop Subjected to Random Vibration", Submitted to *Langmuir.*

ORAL PRESENTATIONS:

1. **Srinivas Mettu** , R. P Chhabra, Nishith Verma, " Computational Fluid Dynamics study of unsteady flow past a circular cylinder confined in a plane channel" **AICHE/IICHE-2004 (Indo-US) International Conference,** Mumbai, 28-30th Dec 2004.

2. *Invited Presentation*: **Srinivas Mettu**, M. K. Chaudhury "Stochastic Relaxation of the Contact Line of a Water Drop on a Solid Substrate Subjected to White Noise Vibration: Roles of Hysteresis", SEVENTH INTERNATIONAL SYMPOSIUM ON CONTACT ANGLE, WETTABILITY AND ADHESION; June 23-25, 2010, Danbury, Connecticut, USA.

3. *Invited Presentation*: **Srinivas Mettu**, M. K. Chaudhury, "Motion of Liquid Drops on Surfaces Induced by Asymmetric Vibrations: Role of Contact Angle Hysteresis", **Gordon-Kenan Research Seminar on Science of Adhesion**, July 2011, Bates College, Lewiston, ME, USA.

POSTER PRESENTATIONS:

1. P. S. Goohpattader, **Srinivas Mettu**, M. K. Chaudhury, "Drift and Diffusion of Small Objects on a Surface Subjected to a Bias and an External White Noise", **Gordon Research Conference on Science of Adhesion**, July 2009.

2. **Srinivas Mettu**, M. K. Chaudhury, "Motion of Liquid Drops on Surfaces Induced by Asymmetric Vibrations: Role of Contact Angle Hysteresis", **Gordon Research Conference on Science of Adhesion**, July 2011, Bates College, Lewiston, ME, USA.